HUMAN HEALTH BENEFITS OF STRATOSPHERIC OZONE PROTECTION

Peer Reviewed Report

Prepared for:

Global Programs Division
Office of Air and Radiation
U.S. Environmental Protection Agency
Washington, DC 20460

Prepared by:

ICF Consulting
1725 Eye Street NW, Suite 1000
Washington, DC 20006

April 24, 2006

Preface and Peer Review Summary

This report was prepared by the U.S. Environmental Protection Agency (EPA) with the support of its contractor, ICF Consulting, Inc. (ICF). This report describes the analytical and empirical methodologies used by the Atmospheric Health Effects Framework (AHEF), a model used to predict changes in human health effects that result from changes in the use and release of ozone-depleting substances (ODS).

The authors of this report consulted with experts from government, industry, and academia in the fields of atmospheric chemistry and dynamics, health effects of ultraviolet radiation atmospheric modeling, and health effects modeling (see Acknowledgments section). In August and September of 2003, the draft final document was peer reviewed for its technical content by Dr. Edward De Fabo of The George Washington University in Washington, DC, and by Mr. Archie McCulloch of Marbury Technical Consulting in Cheshire, United Kingdom, and visiting research fellow at the School of Chemistry, University of Bristol. The peer reviewers were asked to draw upon their expertise in ultraviolet (UV) radiation biological effects assessment and atmospheric science, respectively, to comment on whether the methods, tools, and approach used in the study reflect sound scientific practice and adequately address the questions at hand.

Written comments were received from peer reviewers. In these comments, the reviewers stated that the methodology used in this model represents a sound, state-of-the-art approach to assessing ozone-related health effects. A number of comments identified areas for clarification of specific technical items, all of which have been considered by the authors. The reviewers stated that the report provides solid analysis and discussion of results, given the scope of the work and the uncertainties that currently exist in the areas of ozone depletion and UV radiation health impacts estimation.

Several areas were highlighted during peer review of this report. Dr. De Fabo highlighted the fact that one of the greatest sources of uncertainty in estimating UV radiation-induced health impacts is the lack of adequate experimental data from which a biological action spectrum for cutaneous malignant melanoma (CMM) can be developed. Due to this lack of information, the AHEF predicts cases of malignant melanoma based on the SCUP-h action spectrum for squamous cell carcinoma (SCC). Dr. De Fabo agreed that the SCUP-h spectrum is the most appropriate action spectrum available to model CMM at this time. He noted that the action spectrum for CMM still remains to be determined, and that use of the SCUP-h in modeling CMM should be reconsidered if future research reveals that the shape of the action spectrum for CMM is not congruent with the SCUP-h action spectrum. EPA acknowledges that further scientific research in these and other areas could complement and significantly enhance the information presented in this report.

Dr. De Fabo also agreed that the removal of cataract incidence from the AHEF's health effects modeling reflects a sound decision, in light of recent analyses that suggest a weak correlation between UV exposure and cataract incidence in the United States. Dr. De Fabo also affirmed that the paper's discussion on immunosuppression accurately reflects the current state of the science.

Mr. McCulloch suggested several revisions to the original text to remove ambiguity, and provided additional information on the methodologies and assumptions used by WMO in their 1999 and 2003 reports, to allow for a more accurate and thorough comparison of the projected ozone concentrations predicted by WMO and by the AHEF. Mr. McCulloch also commented on the need to clearly justify the selection of 55 as the bromine efficiency factor—or *alpha factor*—for use in the AHEF instead of 45, which is the value recommended by WMO (WMO 2003). The selection of an alpha factor of 55 is based on the results of state-of-the-art atmospheric models, and is also the value used in a recent report prepared for the U.S. Department of Defense (Independent Review Panel 2002, Wuebbles 2003). In general, Mr. McCulloch affirmed that the atmospheric science module of the paper provides clear descriptions of the methodology and model parameters used, which allow the reader to reach conclusions about the way the methods have been applied and how they relate to "mainstream" atmospheric science (e.g., WMO Ozone Assessments).

All comments of the reviewers were considered, and the document was modified appropriately.

EPA wishes to acknowledge everyone involved in this report and thank reviewers for their extensive time, effort, and expert guidance. The involvement of peer reviewers and other scientific contacts greatly enhanced the technical soundness of this report. EPA accepts responsibility for all information presented and any errors contained in this document.

Global Programs Division (6205J)
Office of Atmospheric Programs
U.S. Environmental Protection Agency
Washington, DC 20460

TABLE OF CONTENTS

Executive Summary

Stratospheric ozone protects the biosphere from potentially damaging doses of ultraviolet (UV) radiation. Depletion of stratospheric ozone, caused by the release of man-made ozone-depleting substances (ODS)—such as chlorofluorocarbons (CFCs), halons, methyl bromide, and hydrochlorofluorocarbons (HCFCs)—could lead to significant increases in UV radiation reaching the Earth's surface, which could in turn lead to adverse human and animal health effects, as well as ecosystem impacts.

The Montreal Protocol on Substances That Deplete the Ozone Layer (Montreal Protocol) is a landmark international agreement designed to protect the stratospheric ozone layer. The treaty was originally signed in 1987 and substantially amended in 1990, 1992, and 1997. The Montreal Protocol stipulates phaseout schedules for the production and consumption of compounds that deplete ozone in the stratosphere.

The United States Environmental Protection Agency (EPA) uses its Atmospheric and Health Effects Framework (AHEF) to evaluate certain human health impacts associated with reduced emissions of ODS under the Montreal Protocol and associated amendments. Specifically, the AHEF estimates the probable increases in skin cancer mortality and incidence in the United States that result from ODS emission scenarios relative to the baseline. The baseline is defined as the health effects that would have occurred if ozone concentrations that existed in 1979-1980 had been maintained through the time period modeled. The 1979-1980 concentrations of ozone are used as the baseline because at this date minimal ozone depletion had occurred. Differences in health effects can be compared across broad policy scenarios to estimate potential benefits of alternative ODS controls.

The accuracy of the AHEF's predictions depends upon continual updating of its inputs and methodologies to reflect on-going scientific advances since the AHEF's creation in the mid 1980s. Significant new research results that have been incorporated into the revised version of the AHEF include the following:

- Recalibration and refinement of stratospheric ozone concentration measurements;
- Updated ODS emission data;
- Improved forecasts of the impact of emissions of ODS on stratospheric ozone concentrations;
- New predictions of the impact of changing ozone concentrations on UV radiation intensity at the Earth's surface;
- Updated information on the biological effects of UV radiation of different wavelengths (action spectra), and how age and year of birth affect the induction of skin cancers and other human health effects;
- Improved estimation of projected skin cancer mortality rates, based on more recent and reliable epidemiological data;
- Revised health effects modeled by the AHEF, to more accurately predict only those health effects for which an agreed upon dose-response relationship is available; and
- Updated population data.

While each of these model updates has affected the AHEF output to varying degrees—either slightly or significantly increasing or decreasing total projected health effects—each has contributed to more accurate modeling results. In addition to these model updates, several other changes have been made to enhance model resolution and flexibility. Appendix A details all of the model updates and changes that

have been made to the AHEF since its inception, and provides explanations and justifications for why each one was performed, and its implication on modeling results.

Despite these model updates, no model or set of results quantifying health effects impacts can be considered final, given that research on the atmospherics of ozone depletion and health effects of UV exposure is ongoing. Many important issues must continue to be investigated and, as significant new findings are incorporated into the AHEF, the accuracy of predictions and the implications for protecting stratospheric ozone will be enhanced. For example:

- Additional research on the effects of UV radiation on darker-skinned populations would enable the AHEF to predict the incremental health effects for all populations;

- Further disaggregation of cataract incidence data by state, and the generation of a population-weighted, geographically distributed dose-response relationship for cataract incidence and UV exposure would allow for appropriate modeling of cataract incidence changes in the AHEF;

- Additional scientific research into the impacts of UV exposure on immune suppression would allow for the inclusion of this health endpoint into the model;

- Improved ground-level UV monitoring would allow the AHEF to incorporate the effects of cloud-cover and pollution on UV radiation at ground-level; and

- Additional research on the effects of UV radiation on non-human endpoints (e.g., aquatic systems, agriculture) would allow the AHEF to predict the broader impacts associated with ODS emission scenarios.

The AHEF is a living model, designed with the ability to accept changes in any model input or assumption based on new scientific findings, and/or to incorporate any new information as it becomes available. As the science on stratospheric ozone depletion and its associated impacts continues to evolve, so too will the AHEF.

1. Introduction

Stratospheric ozone protects the biosphere from potentially damaging doses of ultraviolet (UV) radiation. Recent depletion of stratospheric ozone, caused by the release of man-made ozone-depleting substances (ODS)—such as chlorofluorocarbons (CFCs), halons, methyl bromide, and hydrochlorofluorocarbons (HCFCs)—could lead to significant increases in UV radiation reaching the Earth's surface, which could in turn lead to increased adverse human and animal health effects, in addition to potential ecosystem impacts.

UV radiation-induced health effects are primarily related to the skin, eyes, and immune system. Skin effects include erythema (sunburn), aging of the skin, and various forms of skin cancer—melanoma, squamous cell carcinoma (SCC), and basal cell carcinoma (BCC). Eye effects can include cataracts, squamous cell cancer of the cornea, conjunctiva, and other damage to the cornea (UNEP 1998, Anduze 1993). Sunlight exposure also reduces immunological defenses, impeding resistance to infectious diseases and skin tumors, and diminishing the effectiveness of vaccines (CIESIN website 2003). Of the human health effects from sun exposure, melanoma is the most lethal, causing more than 7,000 deaths annually in the United States and showing an alarming rate of increase worldwide (Kannan *et al*. 2003).

In addition to human and animal health effects, increased UV exposure can also damage ecological and agricultural systems. For example, sunlight is a key ingredient in the formation of photochemical smog, and can lower the immunity of vegetation to pest infestation, disrupt nutrient cycles, and cause bacterioplankton stress in water, which can lead to the reduction of amphibian and fish populations in aquatic ecosystems. Further, UV radiation can damage some plastic materials (Tang *et al*. 1998, Caldwell *et al*. 1998, Häder *et al*. 1998, Andrady *et al*. 1998).

To protect stratospheric ozone and avoid negative health and environmental impacts, the Montreal Protocol on Substances That Deplete the Ozone Layer (Montreal Protocol) was signed in 1987, a landmark international agreement designed to reduce production and consumption of compounds that deplete ozone in the stratosphere. The Montreal Protocol, now signed by more than 180 countries, was amended in 1990, 1992, and 1997, further tightening controls, and ultimately requiring phase out of ozone-depleting substances (ODS) listed by the Protocol. However, recovery of stratospheric ozone remains uncertain and depends on continued international commitment to limit ODS emissions.

The United States Environmental Protection Agency (EPA) uses its Atmospheric and Health Effects Framework (AHEF) to evaluate certain human health impacts associated with reduced emissions of ODS under the Montreal Protocol and associated amendments. Specifically, the AHEF estimates the probable increases in skin cancer mortality and incidence in the United States that result from ODS emission scenarios. Modeling of cataract incidence, although included in earlier versions of the AHEF, has been removed because of the uncertain link between UV exposure and cataract incidence in the United States (see text box on next page).

The increase in skin cancer mortality and incidence for all ODS emission scenarios are estimated relative to the baseline, which is defined as the health effects that would have occurred if ozone concentrations that existed in 1979-1980 had been maintained through the time period modeled. These differences can be compared across policy and control scenarios to estimate the additional benefits of scenarios with increasingly stringent ODS controls. The major scenarios are the four presented in this paper (see Section 4.3). The AHEF can also be used to look at the effect of other emission scenarios resulting from potential future ODS control policies. This paper reviews the AHEF's inputs, assumptions, and computational methods for estimating future human health effects and reports the estimated benefits of four policy/emission scenarios: the Montreal Protocol (1987), the London Amendments (1990), the

Copenhagen Amendments (1992), and the Montreal Adjustments (1997).[1] The remainder of the paper is organized as follows:[2]

- **Section 2** provides an overview of how the AHEF works;
- **Section 3** explains how the baseline estimates of incidence and mortality were obtained and projected into the future for the health effects examined;
- **Sections 4** present the methods used for projecting ozone depletion under various policy scenarios;
- **Section 5** explains the methods used for estimating changes in ground-level solar UV irradiance associated with ozone depletion, as well as the resulting changes in health effects, derived using dose-response relationships between UV exposure and health effect incidence/mortality;
- **Section 7** presents the modeling results for each of the four policy scenarios examined;
- **Section 8** presents a sensitivity analysis for action spectra and exposure/dose metrics;
- **Section 9** presents quantitative and qualitative analyses of the uncertainties in the AHEF; and
- **Section 10** suggests topics for future research.

Justification for Omission of Cataract Incidence Reporting in the AHEF Model

While cataract incidence historically has been assessed in the AHEF model, this health effect is not currently modeled. This is a result of a recent analysis that has revealed a weak correlation between UV exposure and cataract incidence in the United States.

Specifically, in an effort to determine the statistical correlation between UV exposure and age on the development of cataract incidence, state-by-state average annual UV exposures were correlated with cataract incidence data reported by the National Eye Institute/Prevent Blindness America (NEI/PBA) (2002)—the most recent and comprehensive cataract incidence data available—of populations aged 40 and above. The results of this analysis suggest that cataract incidence is directly correlated with age. However, it was not possible to develop a good correlation between the intensity of UV exposure and cataract incidence using this data.

One reason for the lack of correlation may be that the state-averaged UV values currently available may be too aggregated to discern differences in population-based effects. It may be possible to develop a dose response curve using data that is further disaggregated. Therefore, if additional data or research becomes available on the dose-response relationship for cataracts, this health effect will be reconsidered for inclusion in the AHEF. (See Appendix E for more information on modeling cataract incidence.)

Human behavior can complicate the development of a dose response curve for UV. For example, many people in the United States wear protective sunglasses when in the sun, or may engage in sun avoiding behaviors. These behaviors, while beneficial to human health, tend to confound analysis of cataract incidence versus UV exposure.

[1] The Vienna Amendments (1995) and the Beijing Amendments (1999) are not presented in this paper because the ODS phaseout schedules are very similar to that of the Montreal Adjustments.

[2] A glossary defining terms used in this paper appears at the end of this document.

2. Model Overview

The AHEF has five main computational steps that lead to estimated changes in incidence and mortality for various UV-related health effects for a given ODS emission scenario. These computational steps are as follows:

1. Projecting baseline incidence and mortality of health effects;
2. Projecting impacts of future ODS emissions on stratospheric ozone;
3. Modeling the resulting changes in ground-level UV radiation;
4. Deriving dose-response relationships for health effect incidence and mortality; and
5. Projecting future health effects incidence and mortality.

These steps are described in detail below.

Step 1. Projections of baseline incidence and mortality are computed based on historical rates assuming column ozone concentrations remained constant at 1979-1980 levels.

The AHEF defines the "baseline" incidence and/or mortality for skin cancer as what would be expected to occur in the future if the concentration of stratospheric ozone remained fixed at 1979-1980 levels. This baseline provides a standard against which to evaluate increases in mortality and/or incidence for these health effects from future ODS emissions and ozone depletion and, under most scenarios, future recovery of the ozone layer to 1979-1980 levels.[3] The following data and calculations form the baseline estimate of current and future incidence and mortality:

- Historical data on skin cancer incidence and mortality were used to derive rates (per 100,000 people) for UV-related health effects in the U.S. population. Rates are based on age, sex, and in some cases, birth year.
- Historical U.S. population estimates (up to 1990) were obtained from the U.S. Census Bureau, and national population estimates for 1991-2050 were derived by age and sex groupings from U.S. Census Bureau projections. Population projections by state, age, sex, and race—based on national population projections for year 2050 and state population projections through 2025[4]—were grouped by latitude-based regions. (Population was assumed to be constant from 2050 to 2100.)
- The number of individuals in each age and sex group was multiplied by the appropriate historical incidence and/or mortality rate to produce an estimated baseline number of future skin cancer cases and deaths per year.

[3] The AHEF assumes that changes in behavior that might confound the establishment of an accurate baseline do not occur. For example, a population that becomes less sun-seeking could theoretically have a lower baseline risk than the earlier cohort that provided the baseline data, and an increase in cloudiness or rainfall could reduce the number of hours spent outdoors, thereby reducing baseline exposures.

[4] State population projections through 2025 were computed as the sum of the totals for the states in each region, and then regional populations (by age, sex, and race) were projected to 2050 based on the national Census projections for 2050—under the assumption that the 2025 regional age, sex, and race proportions of the total U.S. population will remain unchanged through 2050. In this way, population estimates for 1990-2025 were based on state population projections, while population estimates for 2025-2050 were based on national population projections. See Section 3.5 for more details.

Because skin cancer and solar UV irradiance vary by latitude, the baseline U.S. health effects data were stratified into three latitude regions (i.e., 20 to 30°N, 30 to 40°N, and 40 to 50°N), to correspond with satellite data on ozone concentrations. Because skin cancer incidence and mortality among darker-skinned populations are not well understood in terms of rates of responsiveness to increased UV exposures, these health effects are only modeled for light-skinned populations. Once the required information becomes available, data for darker-skinned U.S. populations may be included.

Step 2. Impacts of future emissions of ODS on stratospheric ozone concentrations are modeled.

Since 1978, satellites have provided measurements of stratospheric ozone concentrations using a latitudinal grid. Data from the first of these satellites, the Nimbus-7, indicate that during the satellite's lifespan from 1978 to 1993, ozone concentrations declined in a manner that corresponds to an increase in the concentration of stratospheric chlorine and bromine released from the dissociation of ODS molecules. Using this relationship, the AHEF can use estimated ODS emissions to predict future decreases in stratospheric ozone. First, the framework uses regression coefficients to quantify the relationship between past ODS emissions and past changes in ozone concentrations. These regression coefficients were derived as follows:

- Historical information on the concentrations of stratospheric ozone by latitude and month was obtained from satellite data.

- Estimates of emissions of ODS were obtained for past time periods that could affect ozone during the years for which satellite data were available. These ODS emissions estimates were then combined with information on each ODS species' degree of dissociation and rate of transport to the stratosphere. Using this information, total ODS emissions were converted to equivalent effective stratospheric chlorine (EESC) for each year and month for which ozone measurements were available from the Nimbus-7 satellite.

- Statistical linear regressions were performed using the 1978-1993 annual EESC estimates and stratospheric ozone concentrations, as measured by the Nimbus-7, to estimate the impact of ODS on ozone concentrations. These regressions were estimated by month and by latitudinal band.[5]

- Future changes in ozone associated with projected emissions for each ODS emission scenario were converted to EESC estimates which were then multiplied by the estimated regression coefficients to predict future ozone concentrations by month and latitude band.

Step 3. Changes in ground-level UV radiation are estimated.

Based on projections of stratospheric ozone concentration, UV radiation intensities at the Earth's surface were estimated by latitude, month, year, and time of day using the Tropospheric Ultraviolet-Visible radiation model (TUV, v3.9a, as described in Madronich 1993a, Madronich 1993b). The TUV model generates look-up tables[6] (see Section 5.1 for more detail) of weighted solar UV irradiance at sea level as a function of solar zenith angle and projected total column ozone based on the following assumptions: obstruction-free and cloud-free skies; standard profiles of air density, temperature, and tropospheric ozone (USSA 1976); typical continental aerosols (Elterman 1968); and 10 percent isotropic ground reflectivity.

[5] A similar procedure has been used in WMO assessments, which also use the Nimbus-7 satellite data (WMO 1995, WMO 1999). See Appendix D: Comparison of AHEF and WMO Predicted Ozone Concentrations for more information on how AHEF and WMO column ozone estimates compare.

[6] The axes of these look-up tables are solar zenith angle and column ozone concentrations.

Once solar UV irradiance at the Earth's surface is calculated, estimates of UV exposure experienced by humans can be computed. Peak hour or daily dose on any day of the year, or cumulative doses for a set of months or for an entire year are examples of possible dose metrics. The AHEF estimates UV exposures for both the entire day of June 21st (i.e., peak day) and the cumulative dose for the entire year (calculated as the dose on the 15th day of each month multiplied by 30 days per month summed across months) for selected action spectra.[7]

Step 4. Dose-response relationships for skin cancer incidence and mortality are selected.

Determining the health effects caused by UV exposure first requires information on the relative weights to be placed on each discrete UV wavelength to reflect the degree to which each wavelength causes biologic damage. Such a weighting function is called an action spectrum—an experimentally derived function that describes the relative effectiveness of each UV wavelength in the induction of skin cancers. Action spectra are normally developed by scientists by exposing a test animal to different UV wavelengths and then verifying the effectiveness of each wavelength at inducing a specific health effect. For each health effect, an available action spectrum must be selected for use in the AHEF.

Once the action spectrum for each health effect is selected, it is then possible to explore the relationship between those health effects and the intensity of UV exposure. These dose-response relationships are typically derived by correlating measurements or estimates of UV exposure received for a specific action spectrum and given health effect at various locations, and the level of incidence or mortality for that health effect at those same locations.

For example, the incidence of SCC decreases with distance from the equator (i.e., increasing latitude). It is also the case that UV irradiance decreases with distance from the equator. A dose-response relationship can thus be derived statistically by correlating the incidence of SCC measured at various locations at a variety of latitudes with the UV radiation doses measured or estimated for those same locations, as shown in Figure 1.

Step 5. All inputs are combined to project future skin cancer incidence and mortality.

The final step in the modeling framework incorporates the inputs from Steps 1-4 to project future additional skin cancers generated under a particular emission scenario compared to 1979-1980 baseline ozone conditions. This includes two calculations by the AHEF. First, the AHEF projects future baseline skin cancer incidence and mortality. Then the AHEF calculates the future annual percentage change in UV radiation dose for a given action spectrum across the three latitudinal bands of the United States for the specific ODS emission scenario. Multiplying the percentage change in UV exposure in a future year by the appropriate dose-response relationship yields the percentage change in future skin cancer incidence/mortality attributable to the future change in ozone concentrations. These percentages are then multiplied by the baseline incidence and/or mortality for that health effect to compute the absolute number of additional future cases or deaths attributable to ozone depletion under various ODS emission scenarios relative to the 1979-1980 baseline ozone levels.[8]

[7] It is important to note that this analysis does not include a comprehensive listing of all published action spectra that may be applicable to the prediction of skin care and cataracts in humans. For example, the derivation of new action spectra for UV-mediated health effects not considered in this report (e.g., immunosuppression) is an active field of research. The AHEF's modular structure, described in detail below, enables new action spectra or new information on other UV-mediated human health endpoints to be easily incorporated into the modeling framework.

[8] This method of multiplying the changes in UV exposure by the BAF and the underlying baseline incidence or mortality is the same as that used by other researchers to estimate changes in health effects based on changes in ozone concentrations (e.g., Madronich and de Gruijl 1994, Pitcher and Longstreth 1991).

Figure 1. Dose-response relationship (BAF) and derivation for UV exposure and SCC in light-skinned males.

(Scotto et al. 1983)

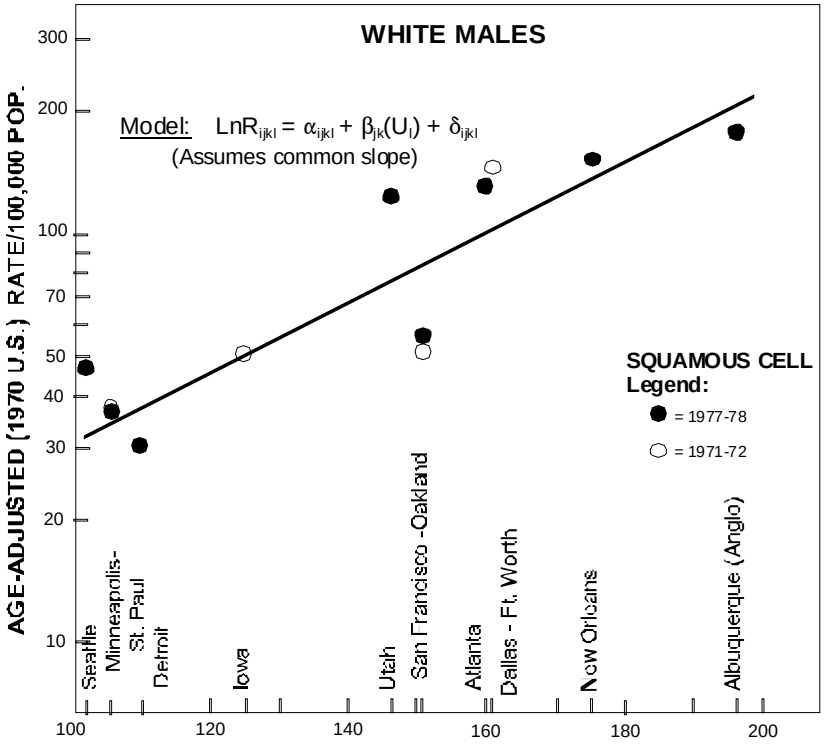

The remainder of this paper describes the steps above in greater detail. Specifically, Section 3 on Baseline Incidence and Mortality Projections elaborates on Step 1; Section 4 on Stratospheric Ozone Depletion Modeling provides more information about Step 2; Section 5 on Modeling Changes in UV Exposure and Health Effects further explains Steps 3 and 4; and Section 6 on Projecting Future Health Effects Under ODS Control Policies describes Step 5 in more detail.

3. Baseline Incidence and Mortality Projections

Baseline incidence and mortality rates for skin cancer were estimated using data on historical incidence and/or mortality for these health effects among the relevant U.S. populations. These rates were then applied to annual U.S. population estimates to project future skin cancer incidence and mortality in the absence of further stratospheric ozone depletion. A number of different data sources were used to calculate historical incidence and mortality rates for cutaneous malignant melanoma (CMM) and non-melanoma skin cancer (NMSC). The sections below review the historical information for each of the health effects rates used and present the data sources and methods for projecting the U.S. populations at risk.

3.1 CMM Mortality Rates

Baseline CMM mortality data for the years 1950 through 1984 were obtained from the EPA/National Cancer Institute (EPA/NCI) data set, which is described in Scotto et al. (1991) and Pitcher and Longstreth (1991). The data set used in Scotto et al. (1991) reports deaths from CMM in individuals for 18 age groups (birth cohorts), by sex and race, covering every county in the United States during the 35-year period.

To generate CMM mortality rates per 100,000 people per county, the CMM mortality information was combined with population data by county. Because the raw mortality data from NCI cover 5-year, rather than 1-year, intervals, the five-year mortality total was then divided by the five-year population total. For each year in the five-year period, this fraction was multiplied by 100,000 to produce the CMM mortality rate per 100,000 people per county (Pitcher and Longstreth 1991).

Once the mortality rate for each county and time period was calculated, the counties in the EPA/NCI CMM mortality data set were aggregated into three geographical regions based on latitude. The three geographical regions were formed out of entire states and roughly correspond to latitude bands 20°N to 30°N, 30°N to 40°N, and 40°N to 50°N (except for California, which was split in half and assigned to the 30°N to 40°N and 20°N to 30°N geographical regions). Table B-1 of Appendix B lists the states included in these geographical regions. The resulting CMM mortality rates by age, birth cohort, sex, and geographical region across the United States are also presented in Appendix B.

This regionally-aggregated data set contains baseline CMM mortality rates for 24 five-year birth cohorts (i.e., people born within five years of each other) beginning in 1863 and ending in 1982 observed over the 35-year history of the underlying data set (see Tables B-2 and B-3 and Appendix B). The shaded areas in Table 1 and Table 2 represent actual information from the original EPA/NCI data.

In order for the AHEF to project future baseline mortality rates, it was necessary to estimate mortality rates for populations alive at the time of collection of the NCI data as well as to estimate the future mortality rates for those yet to be born. To project future mortality rates for people in the EPA/NCI data set, the mortality rates for different age groups and their years of birth for each of the three geographical regions were examined using econometric analysis[9] to determine the quantitative influence of age and cohort on those mortality rates. In other words, these regressions correlate CMM mortality rates with age and year of birth. It should be noted that, in the case of CMM, mortality at any given age appears to have

[9] As it is used in this document, the term “econometric” refers to a statistical technique that enables analysts to determine to what degree one specific variable (e.g., UV exposure) may be responsible for a specific effect (e.g., skin cancer) thought to be caused by the interaction of several related variables. For example, it is hypothesized that age, birth year, and UV exposure all play a role in the etiology of CMM. Because ODS control policies can only reduce one of these risk factors (i.e., the amount of UV-B reaching the ground can be reduced by a thicker ozone layer), econometric estimation is used to isolate and quantify the contribution of UV exposure to CMM.

increased from the early 1900s to the mid-1950s, and then gradually declined. Because of this, age-specific mortality rates depend on birth year, especially for people born between approximately the 1920s to the 1960s. This effect, known as a 'cohort effect,' is included in the regression analyses. The precise reasons for this phenomenon are not known, but various factors, including behavior (e.g., use of sunscreen, selection of clothing that exposes or covers skin) are believed to play a role.[10]

Finally, the actual and predicted mortality rates for each age group in the 1960, 1965, and 1970 birth cohorts were averaged for purposes of projecting future cohorts' mortality rates. These three cohort groups were selected because they represent the most recent birth cohorts with statistically robust mortality data. Table 1 depicts a portion of the baseline mortality rates derived for CMM using the methods described above.

3.2 CMM Incidence Rates

A limited set of data on CMM incidence and mortality was extracted from the Surveillance, Epidemiology, and End Results (SEER) Program, based within the Cancer Control Research Program at NCI. Nine reporting areas were included in the resulting SEER CMM data extract (see Appendix B), covering individual cases diagnosed between the years 1973 and 1994 (Ries et al. 1999). This data set was aggregated into eighteen age groups by sex, race ("all races," light-skinned, and darker-skinned), and the three latitudinal U.S. regions described in Section 3.1. Again, because of data limitations, only light-skinned populations were included in the analysis.

Because of the small size of the SEER data set, a different method for projecting future incidence was necessary. To do so, the ratio of the SEER-based CMM incidence to mortality was calculated and averaged over ten years, 1984 to 1994, for each of the three regions and for each sex. (Results of these calculations are provided in Appendix B.) Then, incidence-to-mortality ratios were applied to the EPA/NCI CMM mortality rates to generate comprehensive CMM incidence rates by age, cohort, and sex, as reported in Appendix B. The results of this process for selected cohort mid-birth years are reported in Table 2 for latitudes 40ºN- 50ºN. Age-, sex-, region-, and cohort- specific rates do not change after 1990. The results for additional regions are reported in Appendix B. For very young age groups, incidence and mortality information were quite sparse and thus it was assumed that incidence was at least equal to mortality. Hence, cohorts and age groups for which the EPA/NCI data set reported positive CMM mortality but for which the SEER data set reported zero, the SEER data set was adjusted to report an identical percentage of CMM incidence.

As discussed in Section 3.1, CMM incidence rates exhibit a cohort effect, possibly due to behavioral factors (e.g., use of sunscreen, selection of clothing that exposes or covers skin).

[10] CMM is the only health effect modeled in the AHEF for which there is a statistical age-linked component, known as a cohort effect.

Table 1. CMM Mortality Baseline Cohort Tables by Sex (per 100,000)

°N to 50°Cohort Mi		Age Group															
	Birth Yea	0-4	5-9	10-14	15-19	20-24	25-29	30-34	35-39	40-44	45-49	50-54	55-59	60-64	65-69	70-74	75-79
'hite Male	1865																
	1870																
	1875																**4.713**
	1880															**3.519**	**4.398**
	1885														**2.882**	**3.673**	**5.148**
	1890													**2.484**	**4.091**	**4.913**	**7.729**
	1895												**1.725**	**2.604**	**4.954**	**5.176**	**9.091**
	1900											**1.441**	**2.332**	**3.206**	**4.487**	**6.029**	**9.376**
	1905										**1.683**	**2.212**	**2.844**	**3.544**	**6.150**	**8.273**	**11.701**
	1910									**1.313**	**1.834**	**2.802**	**3.451**	**5.148**	**7.092**	**9.598**	11.400
	1915								**1.190**	**1.456**	**2.153**	**3.402**	**4.049**	**6.427**	**9.362**	9.590	12.200
	1920							**0.937**	**1.326**	**1.982**	**2.749**	**4.095**	**5.549**	**7.342**	8.890	10.200	12.800
	1925						**0.676**	**1.214**	**1.721**	**2.664**	**3.183**	**4.843**	**6.916**	7.320	9.440	10.800	13.400
	1930					**0.406**	**0.724**	**1.350**	**1.907**	**2.428**	**4.158**	**5.166**	6.060	7.420	9.540	10.900	13.500
	1935				**0.113**	**0.318**	**0.805**	**1.191**	**1.611**	**2.621**	**3.898**	4.900	5.970	7.330	9.450	10.800	13.400
	1940			**0.038**	**0.103**	**0.425**	**0.689**	**1.235**	**1.704**	**3.309**	3.820	5.010	6.080	7.440	9.560	10.900	13.500
	1945		**0.000**	**0.020**	**0.122**	**0.337**	**0.815**	**1.084**	**2.319**	2.890	3.840	5.030	6.110	7.460	9.580	10.900	13.500
	1950	**0.018**	**0.009**	**0.000**	**0.166**	**0.573**	**0.937**	**1.741**	2.140	3.000	3.950	5.140	6.220	7.580	9.700	11.000	13.600
	1955	**0.000**	**0.008**	**0.000**	**0.126**	**0.444**	**0.873**	1.420	2.060	2.920	3.870	5.060	6.140	7.500	9.620	10.900	13.500
	1960	**0.008**	**0.008**	**0.024**	**0.142**	**0.282**	0.824	1.400	2.040	2.890	3.850	5.040	6.110	7.470	9.590	10.900	13.500
	1965	**0.009**	**0.000**	**0.027**	**0.080**	0.415	0.836	1.410	2.050	2.910	3.860	5.050	6.130	7.480	9.600	10.900	13.500
	1970	**0.009**	**0.006**	**0.024**	0.124	0.376	0.838	1.410	2.050	2.910	3.860	5.050	6.130	7.480	9.600	10.900	13.500
	1975	**0.000**	**0.000**	0.024	0.124	0.376	0.838	1.410	2.050	2.910	3.860	5.050	6.130	7.480	9.600	10.900	13.500
	1980	**0.000**	0.006	0.024	0.124	0.376	0.838	1.410	2.050	2.910	3.860	5.050	6.130	7.480	9.600	10.900	13.500
ite Fema	1865																
	1870																
	1875																**2.800**
	1880															**3.294**	**3.589**
	1885														**1.890**	**2.947**	**3.750**
	1890													**1.950**	**2.367**	**3.718**	**4.244**
	1895												**1.492**	**2.609**	**3.248**	**3.957**	**4.884**
	1900											**1.087**	**1.800**	**2.349**	**2.814**	**3.713**	**5.987**
	1905										**1.036**	**1.454**	**1.957**	**2.410**	**3.673**	**5.195**	**5.840**
	1910									**0.999**	**1.688**	**1.658**	**2.160**	**2.965**	**5.041**	**5.505**	6.320
	1915								**0.826**	**1.176**	**1.840**	**2.109**	**2.678**	**3.498**	**4.028**	5.540	6.500
	1920							**0.709**	**0.944**	**1.471**	**1.683**	**2.530**	**2.863**	**4.078**	4.700	5.850	6.800
	1925						**0.548**	**0.929**	**1.342**	**2.010**	**2.006**	**2.833**	**3.113**	4.120	5.020	6.160	7.120
	1930					**0.344**	**0.617**	**1.129**	**1.219**	**2.042**	**2.622**	**3.234**	3.430	4.330	5.230	6.370	7.330
	1935				**0.028**	**0.310**	**0.591**	**0.955**	**1.256**	**1.871**	**2.552**	2.870	3.320	4.220	5.110	6.260	7.220
	1940			**0.000**	**0.050**	**0.208**	**0.498**	**0.794**	**1.469**	**2.124**	2.400	2.880	3.320	4.220	5.120	6.260	7.220
	1945		**0.000**	**0.011**	**0.131**	**0.253**	**0.555**	**0.948**	**1.373**	1.980	2.420	2.900	3.340	4.240	5.140	6.280	7.240
	1950	**0.019**	**0.038**	**0.018**	**0.092**	**0.250**	**0.634**	**1.184**	1.440	2.030	2.470	2.950	3.390	4.300	5.190	6.340	7.290
	1955	**0.017**	**0.009**	**0.017**	**0.094**	**0.376**	**0.663**	1.080	1.440	2.040	2.480	2.950	3.400	4.300	5.190	6.340	7.300
	1960	**0.017**	**0.008**	**0.008**	**0.077**	**0.329**	0.619	1.060	1.420	2.020	2.460	2.930	3.380	4.280	5.170	6.320	7.280
	1965	**0.000**	**0.000**	**0.009**	**0.073**	0.292	0.607	1.040	1.410	2.000	2.450	2.920	3.360	4.270	5.160	6.310	7.260
	1970	**0.006**	**0.003**	**0.009**	0.078	0.306	0.612	1.050	1.420	2.010	2.450	2.930	3.370	4.270	5.170	6.310	7.270
	1975	**0.023**	0.003	0.009	0.078	0.306	0.612	1.050	1.420	2.010	2.450	2.930	3.370	4.270	5.170	6.310	7.270
	1980	**0.011**	0.003	0.009	0.078	0.306	0.612	1.050	1.420	2.010	2.450	2.930	3.370	4.270	5.170	6.310	7.270

Note: The shaded areas represent actual information from the original EPA/NCI data. Unshaded areas represent projected mortality rates. This table can be read in two ways. First, the increase in mortality for the cohort born in a given year (e.g., 1960) can be read horizontally as the individuals in that cohort age. For example, a female born in 1950 would have a baseline mortality rate of 0.018 in 1962 (12 years old) and a 0.092 mortality rate in 1969 (19 years old). Second, mortality rates for a single age group can be tracked across birth cohorts by reading vertically from the selected age group (e.g., 20-24). Baseline mortality rates for males aged 65-69 can be observed to increase from 2.882 to 9.600 for individuals born in 1885 and 1980, respectively. It is important to note that the rows for these tables are presented in terms of "birth cohort mid-year." For example, "1980" represents birth years 1978, 1979, 1980, 1981, and 1982. Similarly, "1985" represents birth years 1983, 1984, 1985, 1986, and 1987.

Table 2: Estimated CMM Incidence Rates for Selected Years by Region, Sex, Cohort, and Age Group (per 100,000)

40° N to 50° N	Cohort Mid Birth Year	Age Group												
		0-4	5-9	10-14	15-19	20-24	25-29	30-34	35-39	40-44	45-49	50-54	55-59	60-64
White Males	**1890**	0.0	0.0	0.0	0.0	0.0	0.0	0.0	0.0	0.0	0.0	0.0	2.5	18.2
	1940	0.0	0.0	0.0	0.1	6.5	5.7	13.0	14.2	26.9	35.4	36.6	39.4	54.6
	1990	0.0	0.0	0.0	0.1	5.8	6.9	14.9	17.1	23.6	35.8	36.9	39.7	55.0
	2040	0.0	0.0	0.0	0.1	5.8	6.9	14.9	17.1	23.6	35.8	36.9	39.7	55.0
	2090	0.0	0.0	0.0	0.1	5.8	6.9	14.9	17.1	23.6	35.8	36.9	39.7	55.0
White Females	**1890**	0.0	0.0	0.0	0.0	0.0	0.0	0.0	0.0	0.0	0.0	2.7	7.3	22.1
	1940	0.0	0.0	0.0	0.1	13.9	18.9	16.2	19.6	36.4	31.6	31.6	35.0	47.8
	1990	0.0	0.0	0.0	0.1	20.4	23.2	21.5	18.9	34.4	32.2	32.1	35.5	48.3
	2040	0.0	0.0	0.0	0.1	20.4	23.2	21.5	18.9	34.4	32.2	32.1	35.5	48.3
	2090	0.0	0.0	0.0	0.1	20.4	23.2	21.5	18.9	34.4	32.2	32.1	35.5	48.3

3.3 NMSC Mortality Rates

The baseline mortality data by county for basal cell carcinoma (BCC) and squamous cell carcinoma (SCC), both forms of non-melanoma skin cancer (NMSC), were obtained from the EPA/NCI data set following the same regional aggregation and regression extrapolation procedures described in Section 3.1 for CMM mortality. Because the underlying data set does not provide disaggregated information by tumor type (i.e., BCC is not reported separately from SCC), Table 3 reports all NMSC fatalities. Unlike melanoma mortality rates, no cohort-by-cohort historical tabulation is necessary for calculating NMSC mortality because NMSC mortality data do not display a cohort trend. NMSC mortality rates for the three latitudinal regions by age, sex, and birth cohort are reported in Appendix B. It is possible that the number of deaths included in this data set is somewhat uncertain, due to ambiguities in the reporting and recording of information on death certificates. It is expected that deaths would generally be under-reported, for example, if complications resulting from non-melanoma skin cancer hospitalizations (e.g., infections, pneumonia) are erroneously listed as the cause of death on death certificates. Nevertheless, this data set is far more comprehensive than any other for non-melanoma mortality and therefore is used in the AHEF.

3.4 NMSC Incidence Rates

The AHEF uses baseline BCC and SCC incidence rates derived from incidence data for the three latitude bands of interest (e.g., 20°N to 30°N, 30°N to 40°N, and 40°N to 50°N). Incidence rates for light-skinned males and females, by region and age group, as reported in U.S. EPA (1987) and Fears and Scotto (1983), are shown in Table 4 and Table 5. These estimates were originally derived from Scotto et al. (1983) and are based on a nation-wide survey in eight cities across the United States during the one-year period from June 1, 1977, through May 31, 1978. As the data in the tables indicate, the incidence of both SCC and BCC is skewed toward the older age groups, and a strong latitude gradient is apparent.

Unlike melanoma incidence rates, no cohort-by-cohort historical tabulation is necessary for NMSC incidence because non-melanoma skin cancers do not display a cohort trend. Hence, the age-specific incidence rates for NMSC by sex and region, as shown in Table 4 and Table 5, were applied to all cohorts.

Table 3: NMSC Mortality Baseline Cohort Tables by Sex (per 100,000)

°N to 50°; Cohort Mi — Age Group

	Birth Yea	0-4	5-9	10-14	15-19	20-24	25-29	30-34	35-39	40-44	45-49	50-54	55-59	60-64	65-69	70-74	75-79
'hite Male	1865																
	1870																
	1875																**13.698**
	1880															**7.766**	**9.950**
	1885														**4.813**	**6.011**	**10.695**
	1890													**3.684**	**4.773**	**5.915**	**8.153**
	1895												**1.901**	**3.048**	**3.240**	**5.587**	**4.704**
	1900											**1.125**	**1.762**	**2.893**	**3.222**	**3.232**	**6.368**
	1905										**0.626**	**1.237**	**1.673**	**2.508**	**2.104**	**4.494**	**6.371**
	1910									**0.249**	**0.697**	**0.914**	**1.509**	**1.899**	**2.613**	**4.479**	5.860
	1915								**0.157**	**0.404**	**0.411**	**0.912**	**1.121**	**1.882**	**3.596**	3.990	5.850
	1920							**0.052**	**0.129**	**0.293**	**0.458**	**0.661**	**1.284**	**2.436**	2.770	3.950	5.810
	1925						**0.091**	**0.092**	**0.079**	**0.283**	**0.278**	**0.913**	**1.756**	2.300	2.840	4.020	5.880
	1930					**0.000**	**0.057**	**0.081**	**0.228**	**0.167**	**0.443**	**1.268**	1.520	2.350	2.880	4.060	5.920
	1935				**0.014**	**0.030**	**0.071**	**0.043**	**0.058**	**0.225**	**0.822**	1.020	1.530	2.350	2.890	4.070	5.930
	1940			**0.025**	**0.013**	**0.000**	**0.000**	**0.040**	**0.133**	**0.487**	0.570	1.020	1.530	2.360	2.890	4.070	5.940
	1945		**0.021**	**0.020**	**0.011**	**0.023**	**0.023**	**0.022**	**0.489**	0.395	0.612	1.070	1.570	2.400	2.930	4.110	5.980
	1950	**0.071**	**0.009**	**0.000**	**0.028**	**0.010**	**0.049**	**0.218**	0.267	0.398	0.614	1.070	1.580	2.400	2.940	4.120	5.980
	1955	**0.016**	**0.016**	**0.008**	**0.017**	**0.018**	**0.156**	0.137	0.264	0.395	0.611	1.060	1.570	2.400	2.930	4.110	5.980
	1960	**0.008**	**0.008**	**0.008**	**0.025**	**0.026**	0.085	0.125	0.252	0.383	0.599	1.050	1.560	2.390	2.920	4.100	5.970
	1965	**0.000**	**0.008**	**0.000**	**0.000**	0.011	0.074	0.114	0.241	0.372	0.589	1.040	1.550	2.380	2.910	4.090	5.950
	1970	**0.003**	**0.005**	**0.003**	0.011	0.016	0.078	0.118	0.245	0.376	0.592	1.050	1.550	2.380	2.910	4.090	5.960
	1975	**0.000**	**0.000**	0.003	0.011	0.016	0.078	0.118	0.245	0.376	0.592	1.050	1.550	2.380	2.910	4.090	5.960
	1980	**0.000**	0.005	0.003	0.011	0.016	0.078	0.118	0.245	0.376	0.592	1.050	1.550	2.380	2.910	4.090	5.960
ite Fema	1865																
	1870																
	1875																**7.924**
	1880															**3.466**	**4.935**
	1885														**1.964**	**3.034**	**3.904**
	1890													**1.369**	**1.372**	**2.626**	**3.772**
	1895												**0.799**	**1.247**	**1.665**	**1.906**	**2.154**
	1900											**0.472**	**0.781**	**0.933**	**1.736**	**1.449**	**2.221**
	1905										**0.355**	**0.591**	**0.754**	**1.154**	**1.085**	**2.168**	**1.964**
	1910									**0.311**	**0.235**	**0.505**	**0.825**	**0.810**	**1.265**	**1.492**	2.260
	1915								**0.113**	**0.194**	**0.263**	**0.612**	**0.616**	**1.015**	**1.410**	1.690	2.300
	1920							**0.087**	**0.110**	**0.241**	**0.306**	**0.388**	**0.656**	**1.234**	1.240	1.680	2.290
	1925						**0.075**	**0.064**	**0.113**	**0.232**	**0.249**	**0.470**	**0.813**	1.000	1.230	1.670	2.270
	1930					**0.053**	**0.041**	**0.039**	**0.110**	**0.081**	**0.204**	**0.278**	0.651	0.921	1.150	1.590	2.190
	1935				**0.014**	**0.028**	**0.000**	**0.000**	**0.126**	**0.073**	**0.278**	0.406	0.663	0.932	1.160	1.600	2.210
	1940			**0.013**	**0.025**	**0.013**	**0.025**	**0.013**	**0.039**	**0.069**	0.192	0.389	0.646	0.915	1.140	1.580	2.190
	1945		**0.011**	**0.021**	**0.022**	**0.000**	**0.011**	**0.054**	**0.056**	0.131	0.205	0.402	0.659	0.928	1.150	1.600	2.200
	1950	**0.056**	**0.000**	**0.009**	**0.000**	**0.019**	**0.020**	**0.066**	0.062	0.132	0.206	0.404	0.661	0.930	1.160	1.600	2.200
	1955	**0.050**	**0.000**	**0.000**	**0.009**	**0.026**	**0.017**	0.025	0.056	0.126	0.200	0.398	0.655	0.924	1.150	1.590	2.200
	1960	**0.008**	**0.017**	**0.000**	**0.009**	**0.000**	0.004	0.014	0.045	0.116	0.190	0.387	0.644	0.914	1.140	1.580	2.190
	1965	**0.009**	**0.009**	**0.009**	**0.018**	0.014	0.010	0.019	0.051	0.121	0.195	0.392	0.650	0.919	1.140	1.590	2.190
	1970	**0.023**	**0.009**	**0.003**	0.014	0.011	0.009	0.019	0.050	0.121	0.195	0.392	0.649	0.919	1.140	1.590	2.190
	1975	**0.011**	**0.000**	0.003	0.014	0.011	0.009	0.019	0.050	0.121	0.195	0.392	0.649	0.919	1.140	1.590	2.190
	1980	**0.023**	0.009	0.003	0.014	0.011	0.009	0.019	0.050	0.121	0.195	0.392	0.649	0.919	1.140	1.590	2.190

Note: The shaded areas represent actual information from the original EPA/NCI data. Unshaded areas represent projected mortality rates. This table can be read in two ways. First, the increase in mortality for the cohort born in a given year (e.g., 1960) can be read horizontally as the individuals in that cohort age. For example, a male born in 1965 would have a baseline mortality rate of 0.008 in 1972 (7 years old) and a 0.074 mortality rate in 1992 (27 years old). Second, mortality rates for a single age group can be tracked across birth cohorts by reading vertically from the selected age group (e.g., 20-24). Baseline mortality rates for females aged 40-44 can be observed to decrease from 0.311 to 0.121 for individuals born in 1910 and 1980, respectively. This is consistent with the decline in CMM mortality rates observed after the 1950s. It is important to note that the rows for these tables are presented in terms of "birth cohort mid-year." For example, "1980" represents birth years 1978, 1979, 1980, 1981, and 1982. Similarly, "1985" represents birth years 1983, 1984, 1985, 1986, and 1987.

Table 4: Estimated BCC Incidence Rates by Region, Sex, and Age Group (per 100,000)

	Age Groups																	
	0-4	**5-9**	**10-14**	**15-19**	**20-24**	**25-29**	**30-34**	**35-39**	**40-44**	**45-49**	**50-54**	**55-59**	**60-64**	**65-69**	**70-74**	**75-79**	**80-85**	**85+**
Male																		
40ºN to 50ºN	0.1	0.1	0.1	2.9	2.9	22.1	22.1	91.1	91.1	259.0	259.0	466.0	466.0	761.0	761.0	1160.0	1160.0	1310.0
30ºN to 40ºN	0.8	0.8	0.8	2.6	2.6	29.4	29.4	120.0	120.0	297.0	297.0	557.0	557.0	872.0	872.0	1150.0	1150.0	1140.0
20ºN to 30ºN	0.3	0.3	0.3	3.8	3.8	49.4	49.4	236.0	236.0	596.0	596.0	1080.0	1080.0	1790.0	1790.0	2330.0	2330.0	2300.0
Female																		
40ºN to 50ºN	0.5	0.5	0.5	5.6	5.6	22.2	22.2	91.0	91.0	202.0	202.0	287.0	287.0	466.0	466.0	638.0	638.0	754.0
30ºN to 40ºN	0.3	0.3	0.3	5.0	5.0	33.8	33.8	95.8	95.8	198.0	198.0	310.0	310.0	454.0	454.0	630.0	630.0	608.0
20ºN to 30ºN	0.5	0.5	0.5	5.8	5.8	49.8	49.8	175.0	175.0	365.0	365.0	561.0	561.0	815.0	815.0	1130.0	1130.0	1190.0

Source: U.S. EPA (1987) and Fears and Scotto (1983).

Table 5: Estimated SCC Incidence Rates by Region, Sex, and Age Group (per 100,000)

	Age Groups																	
	0-4	**5-9**	**10-14**	**15-19**	**20-24**	**25-29**	**30-34**	**35-39**	**40-44**	**45-49**	**50-54**	**55-59**	**60-64**	**65-69**	**70-74**	**75-79**	**80-85**	**85+**
Male																		
40ºN to 50ºN	0.2	0.2	0.2	0.3	0.3	1.6	1.6	7.4	7.4	32.6	32.6	87.4	87.4	147.0	147.0	350.0	350.0	432.0
30ºN to 40ºN	0.1	0.1	0.1	0.8	0.8	3.3	3.3	22.2	22.2	67.7	67.7	170.0	170.0	295.0	295.0	490.0	490.0	624.0
20ºN to 30ºN	0.0	0.0	0.0	0.3	0.3	11.2	11.2	43.0	43.0	169.0	169.0	377.0	377.0	640.0	640.0	966.0	966.0	696.0
Female																		
40ºN to 50ºN	0.0	0.0	0.0	0.1	0.1	1.4	1.4	4.1	4.1	10.5	10.5	27.5	27.5	54.8	54.8	113.0	113.0	168.0
30ºN to 40ºN	0.1	0.1	0.1	0.1	0.1	2.4	2.4	7.1	7.1	19.5	19.5	48.0	48.0	91.6	91.6	173.0	173.0	284.0
20ºN to 30ºN	0.0	0.0	0.0	0.1	0.4	4.3	4.3	15.3	15.3	55.7	55.7	121.0	121.0	254.0	254.0	383.0	383.0	537.0

Source: U.S. EPA (1987) and Fears and Scotto (1983).

3.5 U.S. Population Growth Rates

Data are needed on U.S. population estimates through 2100, disaggregated by 10-degree latitude band, as well as by age, sex, and race to provide the basis for developing population baselines for the AHEF. Population projections from the U.S. Census Bureau (U.S. Census Bureau Website 2000a, U.S. Census Bureau Website 2000b) were used to develop these estimates.

Specifically, the U.S. Census Bureau provided projections of the total U.S. population by age, sex, and race through 2025, as well as for the year 2050. However, because these data were only disaggregated by state through 2025, the following calculations were used to estimate future U.S. population by 10-degree latitude band (by age, sex, and race) through 2100:

- *Step 1*: State-by-state population projections through 2025 were grouped by latitude-based regions.

- *Step 2*: Populations by latitude-based region (by age, sex, and race) were projected for 2050 by distributing the Census Bureau's projected 2050 population by age, sex, and race to the three latitudinal regions, assuming that the distribution of the 2050 population by region, age, sex, and race will be the same as in 2025. This does not imply that, for example, the proportion of the total population that is female is the same in 2025 and 2050. Rather, it means that if there are proportionately more women in 2050 than in 2025, this greater number will be distributed across the regions in the same proportions as their representation in 2025.

- *Step 3*: Regional populations (broken out by latitude grouping) for years 2026 through 2049 were calculated assuming exponential growth for each age/sex/race group in each region from 2025 through 2050.

- *Step 4*: From 2050 through 2100, regional populations were assumed to remain constant.

4. Stratospheric Ozone Depletion Modeling

This section first reviews the approach used to model future stratospheric ozone concentrations based on past, current, and projected future ODS emissions. Next, it describes the ODS policy control scenarios underlying the simulations presented in this report. The section concludes by presenting projections of future ozone concentrations through 2100.

4.1 Approach for Stratospheric Ozone Concentration Modeling

ODS such as chlorofluorocarbons, halons, carbon tetrachloride, methyl chloroform, methyl bromide, and HCFCs are used in a variety of applications including refrigeration and air-conditioning, foam blowing, aerosols, fire suppression and explosion protection, solvent cleaning, sterilants, tobacco expansion, adhesives, coatings, inks, and agricultural uses.

Some of these sectors immediately emit the ODS used (e.g., fumigation and aerosols). Others emit the chemical as it performs a specific function over the course of a number of years. For example, the lifetime of some refrigeration equipment can be up to 25 years, some foams can continue emitting their blowing agent for up to 45 years, and fire suppression agents can remain in a total flooding system for years until discharged. As a result, new equipment production each year generates a stock of each chemical in those sectors with multi-year emission profiles. This creates a delay between initial use of some ODS and their subsequent emission into the atmosphere.

Because of this time lag between consumption and emissions, it is necessary to model emissions in two separate steps. First, the annual amount of ODS consumed in each of the end uses must be determined. Then, this consumption must be translated into emissions into the atmosphere over subsequent years. These two steps are examined individually below.

Step 1. Estimate Global Consumption of ODS

Annual consumption of ODS is based on historical estimates of ODS use, industry growth rates, and the allowable production of ODS for each region. Consumption for 1989 is considered the base year for each ODS in each end use for the United States, the rest of the developed world, and the developing world. Base year consumption is then allowed to grow for each ODS by end use using market growth rate assumptions to approximate a no-controls scenario (i.e., if consumption grew according to demand in the absence of regulation or international agreement). Consumption is then reduced from the base year by the specified phase-out percentages specific to each ODS and region for each year to model the policy scenario (see Appendix C for more detail on these percentages).

Step 2. Estimate Global Emissions of ODS

Once consumption has been projected for all years, emissions can be estimated using a series of emission profiles for each ODS sector, generated by EPA's Vintaging Model. The Vintaging Model is a tool developed for estimating the annual chemical use and emissions from industrial sectors that have historically used ODS in their products. In the context of the AHEF, the Vintaging Model provides emission profiles that translate consumption estimates into annual emission profiles for future years based on the lifetime and leak rates of each type of equipment.

To track this information, the Vintaging Model follows one "vintage" of new equipment through its lifetime and models emissions at each stage of the equipment lifecycle (i.e., manufacturing, lifetime, maintenance, and disposal). Equipment types are divided into two classes, either serviceable or non-serviceable. For non-serviceable equipment, emissions are assumed to take place at disposal and can be

either “instantaneous” emissions in the year of manufacture (for aerosols and solvents) or a “progressive disposal” (for foams) that allows for emissions to extend over a number of years. For serviceable equipment, such as refrigeration, air-conditioning, and fire-extinguishing equipment, the Vintaging Model applies information on annual leak rates, servicing emissions, and disposal emissions for each end use to model the lag between consumption of a chemical and its eventual emission to the atmosphere.

By aggregating the emission outputs, the Vintaging Model creates annual profiles of emissions for each end use. These profiles are then applied by end use to the United States and the rest of global consumption for each policy scenario to develop global ODS emission projections. Once emissions are estimated, the next step in the methodology is to predict the effect that these emissions will have on column ozone.

4.2 Stratospheric Ozone Depletion from ODS Emissions

The relationship between stratospheric ozone depletion and releases of ODS is modeled following the method implemented at the University of Illinois at Urbana-Champaign (UIUC) by Dr. Don Wuebbles et al. (WMO 1995). This approach uses atmospheric models and semi-empirical methods to best quantify the temporal evolution of ozone impacts associated with key ODS over specific time horizons relative to the reference gas, CFC-11. To measure the ozone-depleting capacity of a certain concentration of ODS while accounting for the time delay between consumption and emission of the ODS, the equivalent effective stratospheric chlorine (EESC) concentration is estimated.[11]

In computing EESC, an adjustment is required to quantify the greater efficiency of bromine in depleting ozone relative to chlorine. AHEF uses the UIUC method, which sets the bromine efficiency factor, alpha (α), at 55. Using α = 55 means that one bromine atom can deplete as much ozone as 55 chlorine atoms (Wuebbles 2003). The results that led to an alpha of 55 are found in a study published by the Independent Review Panel (2002) in its assessment of CH_3I for the U.S. Department of Defense.[12] In addition, the AHEF assumes a 3-year lag between tropospheric emissions of ODS and their migration to the stratosphere (percolation) where they cause ozone depletion (i.e., contribute to EESC).

Using the results of the Vintaging Model, modeled global values of annual EESC for the period 1978 to 1993 were compared to annually- and monthly-averaged stratospheric ozone concentrations at different latitudes, as measured by NASA's Nimbus-7 Total Ozone Mapping Spectrometer (TOMS), reported in McPeters et al. (1996a, 1996b). The empirical relationship between EESC and ozone was then estimated using linear regressions for the period 1978 to 1993 to derive column ozone estimates for each month of the year and for the following latitudinal regions: 20°N to 30°N, 30°N to 40°N, 40°N to 50°N, 50°N to 60°N, and 60°N to 70°N.[13]

---

[11] Atmospheric lifetimes (ALT) of ODS and the latitudinal location of the emissions are critical factors used in deriving EESC values. For example, short-lived ODS species emitted in higher latitudes will have a lower impact on EESC than will the same species emitted near the equator, whereas ODS species with longer atmospheric lifetimes will eventually reach the stratosphere and have the same EESC regardless of the latitude of release (Wuebbles 2003).

[12] Earlier work by Wuebbles et al. (1999) and Ko et al. (1998) used slightly different alpha values—of 60 and 58, respectively—based on their respective atmospheric models. Although the latest ozone assessment (WMO 2003) recommends an alpha value of 45 (Daniel at al. 1999) for long-lived gases, and higher values of 58 and 60 for short-lived gases, it is believed that an alpha value of 55 is most defensible and appropriate for use in the AHEF model. This decision is based on the results of state-of-the art atmospheric models, and is also the value used in a recent report prepared for the U.S. Department of Defense (Independent Review Panel 2002, Wuebbles 2003).

[13] The AHEF only uses ozone concentrations from the three latitude bands that cover the United States (i.e., 20ºN to 30ºN, 30ºN to 40ºN, and 40ºN to 50ºN).

The results of these regressions are then used to predict changes in column ozone resulting from changes in future EESC by month for the different latitude bands. ODS emission projections for the period 1985 to 2100 are based on past ODS use and various future ODS control scenarios, combined with end use-specific emission rates developed using the Vintaging Model. Future ozone concentrations are then calculated based on projected EESC and the month- and latitude-specific regression parameters. These calculations produce estimates of future column ozone concentrations (measured in Dobson units) for each latitude band and each month of future years for a given ODS control scenario.

Each ODS control scenario is compared to a baseline ozone level that assumes no further ozone depletion after 1980. Using the satellite measurements of atmospheric ozone, estimates of baseline monthly ozone levels for each latitude band are equal to the average of 1979 and 1980 ozone levels, which accounts for the observed natural biannual variability of ozone levels (WMO 1992).

4.3 Ozone Protection Policy Scenarios and Projections of Future Ozone Concentrations

Since the original Montreal Protocol was signed in 1987, amendments to expand and accelerate the controls on ODS have been approved by the nations that are Parties to the Protocol. The health effects impacts of four policy scenarios—the original Montreal Protocol, the London Amendments of 1990, the Copenhagen Amendments of 1992, and the Montreal Adjustments of 1997—are addressed in this analysis.[14] These policies are briefly described below. More detailed information on the specific restrictions for all ODS for each policy scenario is presented in Appendix C.

The original Montreal Protocol, signed in 1987, was the first step in international efforts to protect stratospheric ozone. Under this agreement, developed countries were required to begin phasing out CFCs in 1993 and achieve a 50% reduction relative to 1986 consumption levels by 1998. Under this agreement, CFCs were the only ODS addressed. Skin cancer incidence and mortality modeled under this policy reflect decreases in CFC emissions based on control measures adopted by signatories for developed and developing (Article 5) countries.

The London Amendments changed the ODS emission schedule by requiring the complete phaseout of CFCs, halons, and carbon tetrachloride by 2000 in developed countries, and by 2010 in developing countries. Methyl chloroform was also added to the list of controlled ODS, with phaseout in developed countries targeted in 2005, and in 2015 for developing countries. Thus, relative to the original Montreal Protocol, this policy scenario decreased U.S. skin cancer incidence and mortality.

The Copenhagen Amendments significantly accelerated the phaseout of ODS and incorporated an HCFC phaseout for developed countries, beginning in 2004. Under this agreement, CFCs, halons, carbon tetrachloride, and methyl chloroform were targeted for complete phaseout in 1996 in developed countries. The results show further reductions in health effects related to ozone depletion.

Finally, the Montreal Adjustments, the most stringent control policy accepted by the Parties thus far, includes the phaseout of HCFCs in developing countries, as well as the phaseout of methyl bromide in developed and developing countries in 2005 and 2015, respectively.

Projected column ozone concentrations for the four policy control scenarios examined in this paper relative to ozone levels prevalent in 1979-1980 (“baseline”) are presented in Figure 2 for the 30°N to 40°N degree latitude band. The figure shows that the initial international agreements to curtail ODS emissions

[14] The modular nature of the AHEF enables the model to be easily adapted to predict changes in skin cancer incidence and mortality, as well as cataract incidence, resulting from almost any scenario involving a change in ozone concentrations. For example, the AHEF was recently used in a peer-reviewed assessment to predict the human health impacts resulting from a proposed fleet of supersonic aircraft (U.S. EPA 2001).

(i.e., the original Protocol and the London Amendments) did much to reduce the risk of future UV radiation-induced health effects. The more recent policy scenarios—the Copenhagen Amendments and the Montreal Adjustments—provide additional risk reductions. Under these policies, atmospheric chlorine and bromine concentrations (expressed as EESC) are predicted to return to 1979-1980 levels in the mid-2040s and to maintain these levels indefinitely in the absence of additional ODS regulation—assuming full compliance with these mandated restrictions.[15]

Figure 2. Average Annual Ozone Concentration by ODS Scenario for the 30ºN to 40ºN Latitude Band

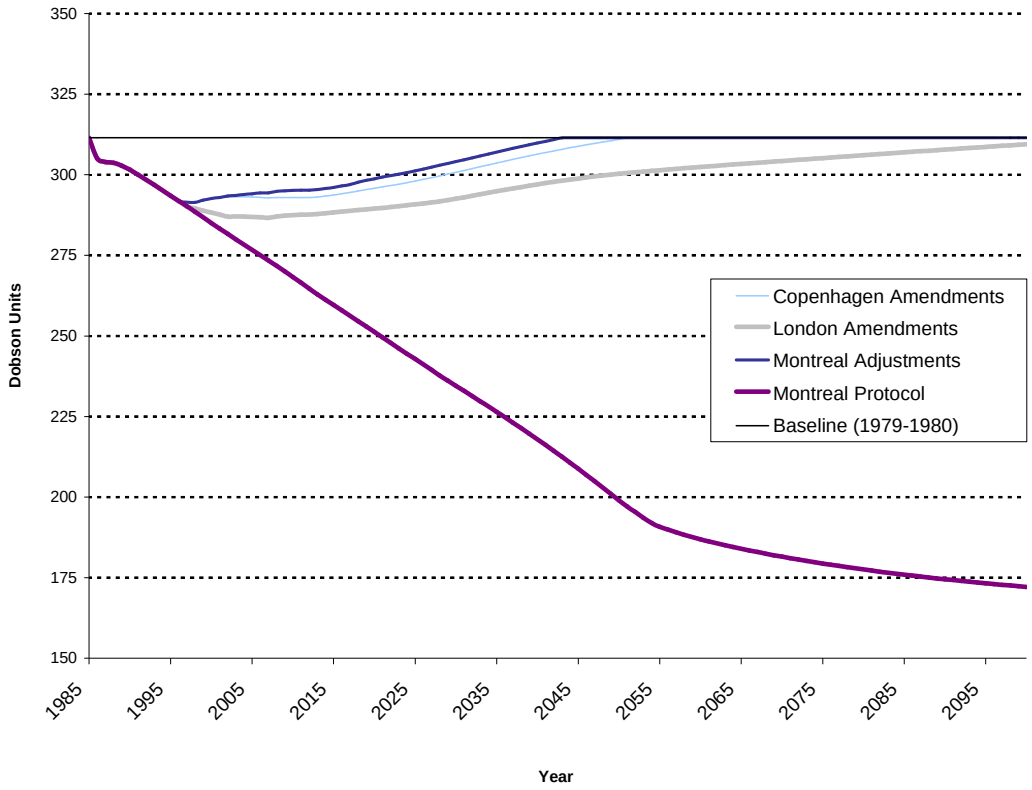

While not addressed in this analysis, the Beijing Amendment (2000) introduces further ODS production and consumption controls beyond those of the Montreal Adjustments. Specifically, the Beijing Amendment calls for a freeze on HCFC production, bans the import or export of HCFCs between non-Parties to the Copenhagen Amendments, and prohibits the non-essential production and consumption of bromochloromethane. However, because these additional policy requirements represent small incremental changes when compared to the overall ODS emission scenario (relative to those of the Montreal Adjustments), this policy scenario is not addressed further in this report or in the AHEF.

[15] The modeling projections assume no impacts from changes in non-ODS atmospheric perturbations (e.g., changes in global climate).

5. Modeling Changes in UV Exposure and Health Effects

This section describes the method for calculating future ground-level UV exposures and relating these values to changes in human health effects. Generally, this is done by first using the predicted future ozone concentrations under various policy scenarios as discussed in the previous section to model the change in UV radiation reaching the ground in the three latitude bands across the United States. Incremental changes in health effect incidence and/or mortality are then modeled based on those predicted changes in ground-level UV intensity.

5.1 The Tropospheric Ultraviolet-Visible Radiation (TUV) Model

The amount of UV radiation reaching the Earth's surface is computed using the TUV radiation model (Madronich 1992, 1993b; Madronich and de Gruijl 1993; Madronich et al. 1996, 1998). The TUV model provides "look-up tables" of biologically effective UV radiation as a function of the total ozone column and solar zenith angle. These tables are then used to calculate cumulative UV radiation (measured in Watts/m^2) by latitude, time of day, day of month, and amount of ozone measured in Dobson units. The AHEF has many different look-up tables, one for each different way of weighting the entire UV spectrum reaching the ground. The rationale for alternative ways to weight the UV spectrum is discussed fully in Section 5.2.

The TUV model is widely regarded as an accurate tool for calculating surface UV radiation levels and has been updated many times to reflect current science. The accuracy of the TUV model has been demonstrated in a number of comparisons to direct measurements of UV at the Earth's surface (e.g., Shetter et al. 1992, 1996; Kirk et al. 1994; Lantz et al. 1996; Gao et al. 2001; Bais et al. 2003). Since 1989, the TUV model has been used in the scientific evaluations of ozone depletion and related environmental consequences as mandated under the Montreal Protocol (WMO 1990, 1992, 1995, 1999; UNEP 1989, 1991, 1994, 1999).

The TUV model computes the radiation levels at any height in the atmosphere, including the Earth's surface. The spectral irradiance incident at the Earth's surface (i.e., the radiation at the Earth's surface measured across the UV spectrum), defined as $F(\lambda, x, t)$, at time t, location x, and wavelength λ, may be represented symbolically as the product of the solar spectral irradiance at the top of the atmosphere, $F_{toa}(\lambda)$, and an atmospheric transmission factor, T.

$$F(\lambda, x, t) = F_{toa}(\lambda)\, T(\lambda, x, t; \theta_o, O_3, \text{ clouds, aerosols, } \ldots)$$

Equation 1

Values of $F_{toa}(\lambda)$ are known from direct observations of the Sun by satellite-, balloon-, and ground-based instruments. The values of T depend on parameters such as the solar zenith angle (θ_o), atmospheric optical properties—specifically UV radiation absorption by ozone and possibly certain pollutant gases (e.g., NO_2, SO_2)—and UV scattering by air molecules (known as Rayleigh scattering). Atmospheric particles (e.g., clouds and aerosols) can contribute to both absorption (e.g., soot) and scattering (e.g., water mist) (mathematically described by the Mie theory) and may be used as inputs to the TUV. Surface reflections can contribute substantially to the radiation incident at the surface and are also included as inputs to the TUV (see, for example, McKenzie et al. 1998). Many of these factors are functions of location (i.e., latitude, surface elevation, altitude above the surface) and time (i.e., day, year, and long-term trends), so that $F(\lambda, x, t)$ is also a strong function of time and geographic site. The TUV model calculates T by first subdividing the atmosphere into vertical layers (typically 1 km thick), each having an

assumed uniform composition. The model uses vertical profiles of air density, temperature, and ozone from the United States Standard Atmosphere[16] (USSA 1976). The propagation of radiation through the atmosphere is then computed using a four-stream discrete ordinates method (Stamnes et al. 1988)—an approach that is widely accepted in the radiative transfer community as being accurate to within a few percentage points or better. The four-stream method is superior to most other models currently in operation, which use a two-stream discrete ordinates method.

5.2 Action Spectra

An action spectrum describes the relative effectiveness of energy at different UV wavelengths in producing a particular biological response, such as development of CMM, BCC, or SCC. The AHEF and the TUV rely on action spectra for each health effect because action spectra provide information regarding which wavelengths of the total UV spectrum are most effective at causing the particular health effect. For example, UV-B wavelengths (280-320 nm) are known to cause erythema, as well as the development of skin cancer, cataracts, and suppression of components of the immune system. UV-A radiation (320-400 nm) is not as readily absorbed by ozone (NOAA/National Weather Service 2002), and is not as potent as UV-B in the etiology of UV damage-related health effects. To ensure that the wavelengths are appropriately weighted when predicting each health effect, it is necessary to measure the extent to which wavelengths cause a particular health effect.

Prior to developing incidence and mortality estimates for health effects, an action spectrum must be selected for each health effect. Obtaining action spectra requires heavy investment, in terms of cost, labor, and time. Moreover, because it is unethical to expose human subjects to harmful UV radiation to test for the induction of skin cancers, action spectra for human health effects are only available for generalized DNA damage and a variety of animal subject experiments. Thus, the identification of an appropriate action spectrum for each health effect modeled by the AHEF required careful selection from the limited available action spectra. The following section describes the action spectra considered and selected for each health effect modeled in the AHEF, and explains the reasoning behind the ultimate selection.

5.2.1 Selection of Action Spectra for Modeling Skin Cancer

For modeling melanoma and NMSC incidence and mortality, three action spectra were considered:

- **DNA-h (1991):** This is a generalized DNA damage action spectrum (derived from studies on bacteria and other microorganisms), adjusted to account for transmission through untanned human skin.[17] This may be a good selection for predicting skin cancer incidence and mortality in humans, as theoretical analyses suggest that skin cancers result from damaged DNA (Pitcher and Longstreth 1991, Setlow 1974). In contrast to other action spectra, the DNA-h action spectrum is more tightly focused on the UV-B portion of solar UV irradiance, giving less weight to the UV-A portion of solar UV irradiance, which is not significantly altered by ozone depletion.

- **Erythema (1987):** This is an action spectrum derived on the basis of erythema (sunburn) induction in human volunteers (McKinlay and Diffey 1987). It has been observed in several

[16] The US Standard Atmosphere (USSA) provides average values for a number of atmospheric parameters at different altitudes.

[17] Absorbing molecules in the cell layers of human skin selectively filter out some wavelengths of UV light, reducing the effective energy that reaches human DNA. Microbial organisms may not have the same degree of protection from UV and thus are exposed to a greater amount of radiation.

epidemiologic studies that CMM risk is associated with intermittent intense UV exposure such as that acquired through sunburning.

- **SCUP-h (1993):** The SCUP spectrum was derived on the basis of the induction of SCC in hairless mice (denoted as SCUP-m). Because mouse skin and human skin have different absorption spectra for UV light, the action spectrum was corrected for human skin transmission by making adjustments to account for differences in epidermal thickness and the number of hair follicles per unit area. This adjusted action spectrum is denoted as SCUP-h (de Gruijl et al. 1993).

Figure 3 graphically presents the three action spectra described above. As can be seen, all of these action spectra show strong sensitivity at UV-B wavelengths (hence the sensitivity of skin cancer to ozone changes), and much less so to UV-A (which has a much lower sensitivity of skin cancer to ozone changes).

Figure 3. Action Spectra Considered for Modeling Skin Cancer

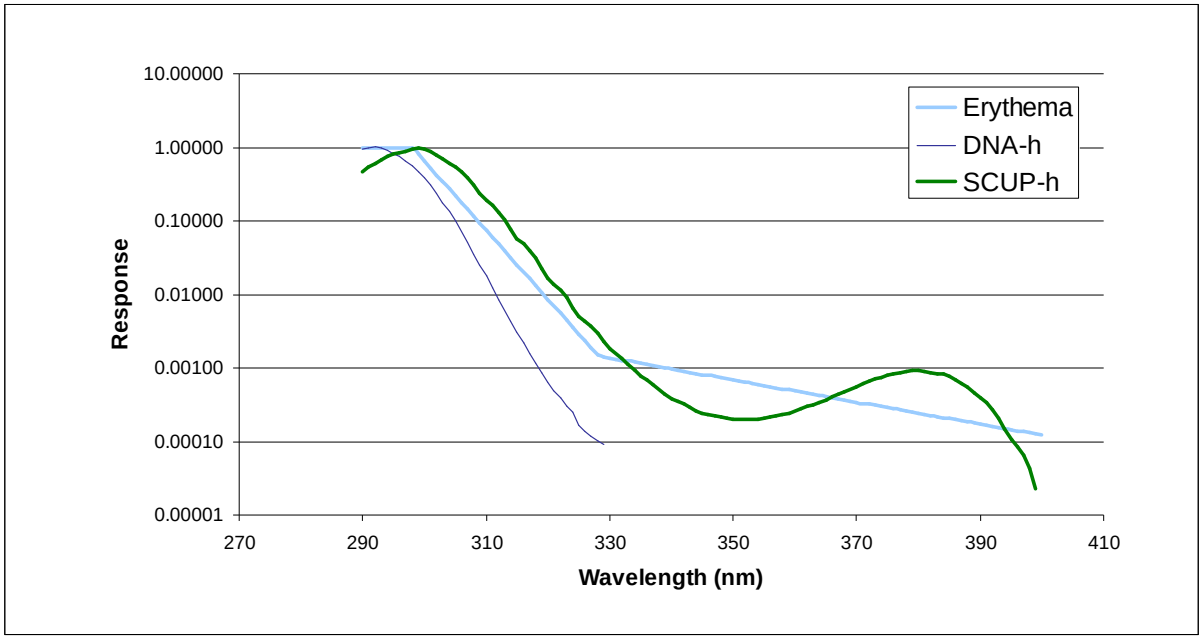

Note: The response (plotted on the Y-axis) is a log scale. At the normalizing wavelength, every 1 percent change in UV radiation causes a 1 percent change in the health effect.

Based on the available action spectra, the SCUP-h action spectrum was selected for modeling all types of skin cancers. Rationales for selecting this action spectrum for each type of skin cancer are as follows:

- ***SCC:*** The scientific community is largely in agreement that the SCUP-h is the appropriate action spectrum for SCC. Because there is sufficient scientific evidence to indicate that SCUP-h is the correct choice to predict SCC, the SCUP-h action spectrum was chosen to predict incidence of SCC in the AHEF.

- ***BCC:*** Because a biological action spectrum has not been developed for BCC, the SCUP-h was selected for use in the AHEF to predict incidence of this cancer, as it is the only available action spectrum based on the induction of skin cancer. SCUP-h is currently believed to be the most appropriate for modeling BCC (Longstreth *et al*. 1998). Nevertheless, because there is less scientific certainty in applying SCUP-h to predict BCC than SCC, this approach can be reconsidered if future studies investigating the action spectrum for BCC reveal that it is not congruent with the SCUP-h action spectrum for SCC.

- ***CMM:*** As is the case with BCC, the SCUP-h action spectrum was selected for use in the AHEF to predict CMM because action spectra specific to CMM have not yet been derived. However, this analysis may be reconsidered if future studies reveal that the action spectrum for CMM is not congruent with the SCUP-h action spectrum for SCC (i.e., if it does not have similar shape). To date, however, an action spectrum for CMM has not yet been developed.

5.3 Dose-Response Relationships

Once the appropriate action spectrum is selected for each health effect and the UV dose of biologically active radiation and morbidity or mortality across latitudes are identified, statistical regression analyses are used to estimate the dose-response relationship, known in technical terms as the biological amplification factor (BAF), for each health effect. The dose response relationship, or BAF, measures the degree to which changes in UV exposure weighted by the appropriate action spectrum (as measured in Watts/m^2) cause incremental changes in health effects (incidence or mortality), estimated after accounting for the influence of birth year and age, as necessary.

BAFs are defined as the percent change in a health effect resulting from a one-percent change in the intensity of UV radiation (weighted by the chosen action spectrum). For each health effect, the AHEF applies the BAF to predict future incidence and mortality. Estimated ground-level effective UV irradiance from the TUV model is combined with a selected BAF to translate changes in UV exposure to a percentage change in expected health effects.

The remainder of this section provides a description of how the available data and existing studies are utilized to develop BAFs for each health endpoint, as well as the uncertainties these estimated BAFs introduce to the AHEF's results.

5.3.1 Derivation of BAFs for CMM Incidence/Mortality and NMSC Mortality

BAFs for CMM incidence were not estimated separately from the BAFs for CMM mortality because, as described in Section 3.2, CMM incidence rates do not vary independently of CMM mortality rates in the model. The is due to the fact that CMM incidence rates were derived based on the EPA/NCI CMM mortality data set and the ratio of incidence to mortality for CMM. Therefore, BAFs used to predict the incidence of CMM are the same as those used to predict CMM mortality (i.e., the percentage change in CMM incidence is the same as for CMM mortality).

The general method for estimating BAFs for CMM incidence and mortality and NMSC mortality is as follows:

- Detailed EPA/NCI data on CMM and NMSC mortality provided raw mortality information by sex, age, and birth cohort year for a large set of locations across the United States. (Because the EPA/NCI data for NMSC do not provide a distinction between BCC and SCC, it is only possible to derive a BAF for total NMSC mortality using these data.)

- Combining CMM and NMSC incidence data with the associated total population by sex for each location, the rate of mortality per 100,000 people was computed for both CMM and NMSC.

- UV exposure at each location was then calculated based on latitude. Specifically, Serafino and Frederick's UV irradiance model was used to estimate ground-level UV exposures for each of the 639 U.S. sites surveyed by EPA/NCI, based on techniques, input data, and modeling methods described in Pitcher and Longstreth (1991).

- A statistical technique was then used to determine the influence of UV exposure and age on CMM and NMSC mortality rates. In the case of CMM, the influence of birth cohort year was also

determined, to account for the cohort effect.[18] The functional form of the regression equation used is expressed in Equation 2, below:

$$R_{ij} = e^{\left[B_0 + \sum B_{C_i} C_i + \sum B_{A_j} A_j + B_{UV} \ln\left(UV_{ij}\right)\right]} + \varepsilon_{ij}$$

Equation 2

where:

R_{ij}	=	mortality rate (CMM or NMSC) for the $_i$th cohort and the $_j$th age group[19]
UV_{ij}	=	percent change in UV radiation exposure for the $_i$th cohort and the $_j$th age group
C_i and A_j	=	cohort and age group categorical variables[20]
B_{Ci} and B_{Aj}	=	coefficients that control for the influence of cohort and age factors on CMM and NMSC mortality[21]
B_0	=	regression coefficient (intercept)
B_{UV}	=	BAF for either CMM or NMSC
ε_{ij}	=	Error term, used to measure how accurate the fitted curve is overall (i.e., how close on average the curve is to the observations).

The form of this equation is known as a power function, expressed as e^x, where *x* is the power. This is obtained by deriving a best-fit equation that describes the appropriate dose-response curve, where the dose is the yearly amount of weighted UV radiation, and the response is mortality for either CMM or NMSC. The BAF is equal to the slope of the dose-response curve for each of these health effects in percentage terms.

Because there are no significant cohort effects associated with NMSC mortality, the cohort term in Equation 2 is not estimated as part of the BAF derivation. In addition, although the derived BAFs for NMSC do not distinguish between SCC and BCC (given that the EPA/NCI data are not disaggregated into BCC and SCC), evidence suggests that 75 percent of the mortality from NMSC is attributable to SCC and 25 percent to BCC (Scotto et al. 1983).

Furthermore, new scientific research has enabled a more thorough understanding of the mechanisms of UV radiation-induced NMSC tumor induction that provides a theoretical foundation for the BAFs. Research suggests that a gene (p53) may play a significant role in suppressing NMSC skin cancer tumor

---

[18] More specifically, UV exposure estimates were combined with historical mortality data for both CMM and NMMSC mortality, as provided in the EPA/NCI data set. The resulting data set contained CMM and NMSC mortality rates per 100,000 people by sex, age, and cohort birth year for a large number of sites covering the United States, as well as estimated UV exposures at each location.

[19] As explained in Section 5.3, BAFs for CMM mortality and incidence and NMSC mortality were estimated directly from primary data sources. BAFs for NMSC and cataract incidence were estimated by other researchers using methods similar to those used to calculate BAFs for skin cancer mortality.

[20] Of the health effects of concern, cohort effects are only significant for CMM (i.e., statistics on incidence and mortality demonstrate an age-linked component).

[21] This regression is run using the maximum likelihood non-linear Poisson method because the error term is no longer normally distributed after the natural log is applied to both sides of the equation.

induction resulting from UV-B radiation (D'errico et al. 1996).[22] Certain portions of this gene appear to be more susceptible to UV-B-induced mutation than others. These "mutation hotspots" are easily affected by UV radiation, as evidenced by the more than 280 of the 393 amino acids sequenced on this gene that have been found to be mutated in tumors (Pfeifer and Denissenko 1998).

Uncertainty associated with the derived BAFs for CMM incidence and mortality and NMSC mortality are discussed in detail in Section 9.1.4.

5.3.2 Derivation of BAFs for BCC and SCC Incidence

The BAFs for both BCC and SCC incidence are based on analyses conducted by de Gruijl and Forbes (1995)—the most up-to-date estimates provided in the literature, derived using the SCUP-h action spectrum. In calculating BCC and SCC incidence, De Gruijl and Forbes assumed that humans are steadily exposed to UV radiation throughout their lifetimes, and that various skin sites of humans are exposed to specific fractions of annual ambient UV exposure. The uncertainty associated with the derived BAFs for BCC and SCC incidence is discussed in Section 9.1.4.

5.4 Resulting BAFs by Health Effect

The resulting BAFs for all health effects are presented in Table 6, as well as the key inputs used to derive each one. For CMM incidence and mortality and NMSC mortality, BAFs for light-skinned males and females are shown for both annual exposures with typical cloud conditions and for a peak clear day exposure (i.e., June 21). Generally, peak clear day BAFs are substantially greater than annual dose BAFs because the annual value is based on exposure across the entire year, while the peak day is only for exposure on the sunniest day of the year. Because the variation in UV radiation across latitudes is greater on an annual basis than it is on June 21st (when all latitudes across the United States are in the summer season and UV radiation is relatively high everywhere), underlying variations in UV radiation are much less for peak clear days than for cumulative annual exposure. Therefore, BAFs are larger on peak clear days, as they must account for the underlying fixed variation in cancer and mortality across latitudes. In both cases, the results will be similar in magnitude: if the peak day UV exposure metric is used, a relatively smaller variation in UV exposure across latitudes will be multiplied by a relatively higher BAF, while the reverse is true if the cumulative annual UV exposure metric is used. Because annual dose BAFs better reflect underlying UV radiation variations across latitudes, they are considered to be more representative of actual exposures and are, therefore, used in the AHEF. It should be noted, however, that the AHEF is capable of using peak clear day exposures as well.

For most health effects, BAFs are higher for males than for females, implying that skin cancer incidence and mortality in males are typically more affected by a given change in the intensity of UV radiation. This may be due to differences in UV exposure patterns between men and women.

[22] Mice lacking one functional copy of gene p53 were shown to be more susceptible to skin cancer induction than those with two functional copies. Mice without a functional copy of this gene were even more susceptible to tumor induction on both the skin and the eyes (Jiang et al. 1999).

Table 6. Summary of Calculated BAFs and Key Inputs

Health Effect	Data Sources[a]	Selected Action Spectrum	BAF: Used in AHEF (Annual Exposures)		BAF: Not Used in AHEF (Peak Clear Day Exposures)	
			Males	Females	Males	Females
CMM Incidence/ Mortality	*Incidence*: Ratios from SEER data set (see Section 3.2) *Mortality*: EPA/NCI data set (see Section 3.1) *BAF*: Developed using econometric analysis (described in Section 5.3.1)	SCUP-h (1993)	0.5846	0.5047	1.444	1.310
BCC Incidence	*Incidence:* Based on methods used in U.S. EPA (1987) and Fears and Scotto (1983) (see Section 3.4) *BAF:* de Gruijl and Forbes (1995)	SCUP-h (1993)	1.5	1.3	NA	NA
SCC Incidence	*Incidence:* Based on methods used in U.S. EPA (1987) and Fears and Scotto (1983) (see Section 3.4) *BAF:* de Gruijl and Forbes (1995)	SCUP-h (1993)	2.6	2.6	NA	NA
NMSC Mortality	*Mortality:* EPA/NCI data set (see Section 3.3) *BAF*: Developed using econometric analysis (described in Section 5.3.1)	SCUP-h (1993)	0.7094	0.4574	2.068	1.565

NA = Not available.

[a] For all health effects, the Serafino and Frederick model (1987) was used by independent researchers to derive the BAFs used in the AHEF. The Serafino and Frederick model is a radiative transfer model that translates ozone measurements from the Nimbus-7 satellite into ground-level solar UV irradiance, similar to the TUV model used in the AHEF.

6. Projecting Future Health Effects Under ODS Control Policies

The final step in the modeling framework integrates baseline estimates of health effects, estimates of future changes in ozone concentration, and the associated changes in solar UV irradiance, appropriate UV spectrum weighting functions, and BAFs to project future additional skin cancer incidence and mortality for any ODS emission control scenario. Scenario estimates are then compared to the incidence and mortality estimates expected under 1979-1980 ozone conditions.

For example, suppose that it is necessary to estimate the absolute increase in BCC incidence for light-skinned males aged 50-54 living in the southern latitude band of the United States. The BAF for light-skinned male BCC incidence is 1.4 (see Section 5.3.2) and the future percentage change in cumulative lifetime SCUP-h-weighted UV exposure of the age 50-54 group is 1 percent (a hypothetical estimate). Multiplying these two numbers together indicates that the increase in BCC incidence among this population group is estimated to be 1.4 percent for a 1 percent change in weighted UV exposure. When this percentage change in incidence is multiplied by the baseline light-skinned male BCC incidence for the 50-54 age group (suppose this is 100,000 cases), the result is an estimate of the absolute number of additional future cancers of this type among this population group attributable to a 1 percent change in UV radiation dose. These calculations are summarized in Equation 3:

(Cumulative Percentage Increase in UV Exposure) x (BAF for BCC) x (Baseline Incidence of BCC for the Population Group) = Absolute Increase in BCC Incidence:

$$(0.01) \times (1.4) \times (100{,}000) = 1{,}400 \text{ cases}$$

Equation 3

Performing these calculations for each health effect and for each future population group produces predictions of the additional health effects for a particular ODS emission scenario relative to those prevalent during the baseline (1979-1980).

7. Modeling Results

This section presents the projected changes in incidence and/or mortality for each of the health effects and policy scenarios examined.

7.1 Results Presented by Policy Scenario and by Health Effect

Table 7 presents the incremental number of skin cancer cases/deaths in excess of the baseline (i.e., those associated with changes in column ozone concentrations from levels observed in 1979-1980) that are projected to occur under each ODS control scenario. Decreasing incidences/mortalities that result as more stringent control scenarios are implemented illustrates the benefits of each further amendment and/or adjustment to the Montreal Protocol. Table 8 presents the *avoided* health effects realized in moving from one ODS policy scenario to the next (e.g., from the Montreal Protocol to the London Amendments). Figure 4 illustrates that as ODS controls are tightened, additional incidence and mortality estimates for each health effect relative to baseline move closer to zero on the y-axis (i.e., closer to the incidence and mortality that would be expected if 1979-1980 ozone concentrations had been maintained throughout the time period modeled).

Table 7. Summary of Incremental Skin Cancer Incidence/Mortality for ODS Policy Scenarios Relative to Baseline

Cohort Group/ Scenario	CMM Incidence (Cases)	CMM Mortality (Deaths)	BCC Incidence (Cases)	SCC Incidence (Cases)	NMSC Mortality (Deaths)
Montreal Protocol					
1890-1980	301,687	44,582	8,814,835	5,050,875	30,859
1985-2010	794,121	109,352	21,250,450	11,517,066	66,829
2015-2050	2,042,358	265,759	50,978,569	26,627,765	147,554
2055-2100	3,228,517	409,876	78,708,574	40,793,037	220,452
London Amendments					
1890-1980	101,523	13,774	2,785,732	1,514,657	7,960
1985-2010	113,885	13,854	2,688,789	1,375,322	6,926
2015-2050	80,379	9,527	1,830,867	924,516	4,602
2055-2100	31,569	3,831	734,634	377,381	1,946
Copenhagen Amendments					
1890-1980	76,048	10,118	2,047,391	1,096,153	5,593
1985-2010	66,922	7,815	1,495,278	743,682	3,634
2015-2050	18,026	2,023	379,285	186,009	906
2055-2100	0	0	0	0	0
Montreal Adjustments					
1890-1980	68,816	9,076	1,834,142	974,827	4,923
1985-2010	54,940	6,356	1,210,046	599,467	2,925
2015-2050	10,308	1,155	216,245	105,993	517
2055-2100	0	0	0	0	0

Note: The numbers presented above indicate the number of cases in excess of the baseline (1979-1980) for each scenario.

Table 8. Incremental Number of Avoided Skin Cancer Incidence/Mortality Under ODS Policy Scenarios with Increasingly Stringent Controls

Cohort Group/Scenario	CMM Incidence (Cases)	CMM Mortality (Deaths)	BCC Incidence (Cases)	SCC Incidence (Cases)	NMSC Mortality (Deaths)
Incremental Number of Avoided Cases/Deaths: From Montreal Protocol to London Amendments					
1890-1980	200,164	30,809	6,029,103	3,536,217	22,898
1985-2010	680,236	95,498	18,561,661	10,141,745	59,903
2015-2050	1,961,979	256,232	49,147,703	25,703,249	142,952
2055-2100	3,196,948	406,045	77,973,940	40,415,656	218,506
Total	**6,039,327**	**788,584**	**151,712,406**	**79,796,866**	**444,258**
Incremental Number of Avoided Cases/Deaths: From London Amendments to Copenhagen Amendments					
1890-1980	25,475	3,655	738,342	418,504	2,368
1985-2010	46,963	6,038	1,193,511	631,640	3,292
2015-2050	62,353	7,504	1,451,582	738,507	3,697
2055-2100	31,569	3,831	734,634	377,381	1,946
Total	**166,360**	**21,028**	**4,118,068**	**2,166,033**	**11,303**
Incremental Number of Avoided Cases/Deaths: From Copenhagen Amendments to Montreal Adjustment					
1890-1980	7,232	1,042	213,249	121,326	670
1985-2010	11,982	1,459	285,232	144,215	708
2015-2050	7,718	868	163,040	80,017	389
2055-2100	0	0	0	0	0
Total	**26,932**	**3,369**	**661,520**	**345,557**	**1,767**

Note: The numbers presented above indicate the number of avoided cases from one policy scenario to another.

Based on data presented in Table 7, Figure 4 through Figure 7 graphically present the incremental health benefits for successively more stringent scenarios for CMM incidence, CMM mortality, NMSC incidence, and NMSC mortality.[23] As shown in Figure 4, the curve representing impacts associated with the Montreal Adjustments most closely approaches the baseline (1979-1980) ozone concentration (at zero on the y-axis) after a number of years, but there remain significant opportunities for further reducing health effects. Because the recovery of ozone (i.e., the return to pre-depletion levels prevalent in the 1979-1980 timeframe) is projected to occur around 2050, no exposures attributable to ozone depletion will accrue for people born after this recovery date. Incremental UV exposures for people born before 2050, however, will continue to result in health effects incidence and mortality after 2050, albeit at a lower rate than in earlier years. By approximately 2150, it is predicted that there will be no living population that experienced incremental exposure associated with depleted ozone levels, and hence, no additional health effects incidence or mortality above those expected to occur under "normal" conditions (i.e., 1979-1980 ozone levels).

[23] These estimates do not include effects on ozone from climate variation and other factors. How climate may ultimately affect the recovery of stratospheric ozone is unclear and beyond the scope of the AHEF.

Figure 4. Annual Incremental U.S. CMM Incidence through 2100 Under Different ODS Control Policies (SCUP-h Action Spectrum)

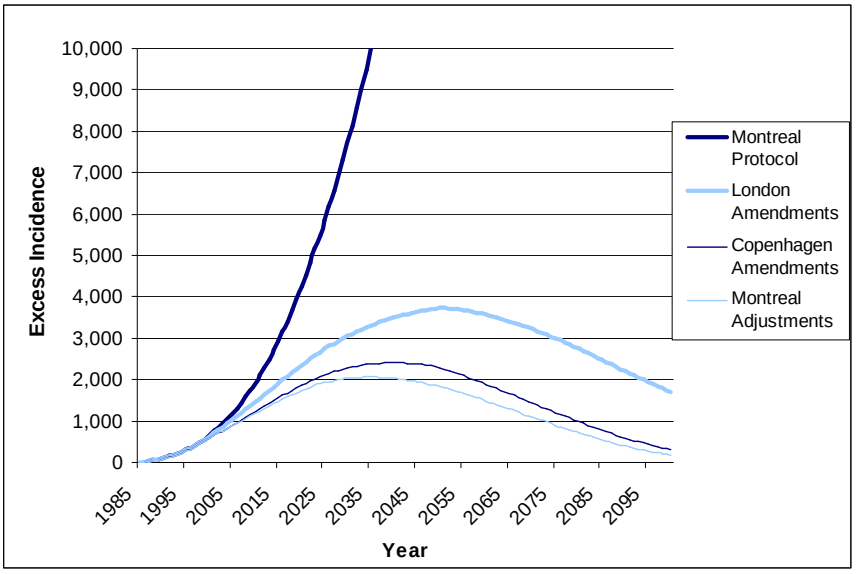

Note: Because this graph shows the incremental CMM incidence relative to the 1979-1980 baseline, the level of CMM incidence in the baseline is represented by zero on the y-axis.

Figure 5. Annual Incremental U.S. CMM Mortality through 2100 Under Different ODS Control Policies (SCUP-h Action Spectrum)

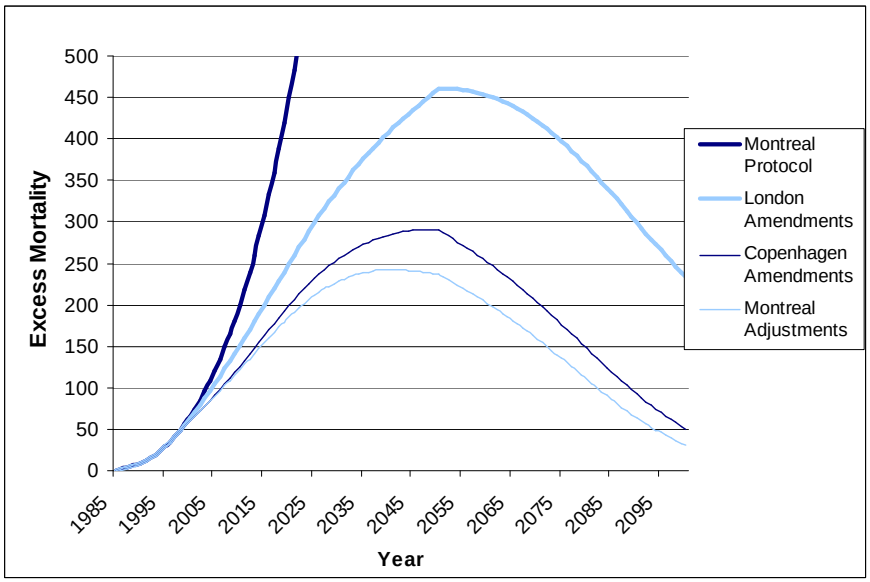

Note: Because this graph shows the incremental CMM mortality relative to the 1979-1980 baseline, the level of CMM mortality in the baseline is represented by zero on the y-axis.

Figure 6. Annual Incremental U.S. NMSC Incidence through 2100 Under Different ODS Control Policies (SCUP-h Action Spectrum)

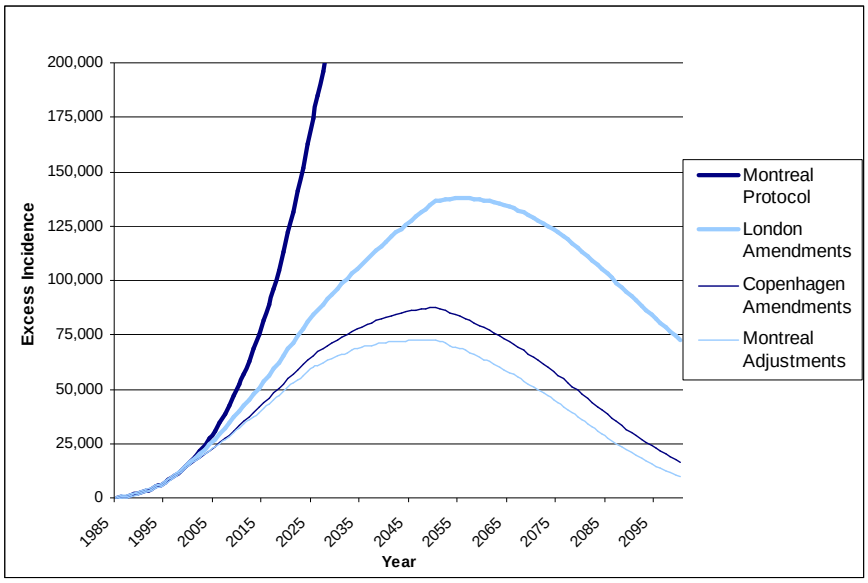

Note: Because this graph shows the incremental NMSC incidence relative to the 1979-1980 baseline, the level of NMSC incidence in the baseline is represented by zero on the y-axis.

Figure 7. Annual Incremental U.S. NMSC Mortality through 2100 Under Different ODS Control Policies (SCUP-h Action Spectrum)

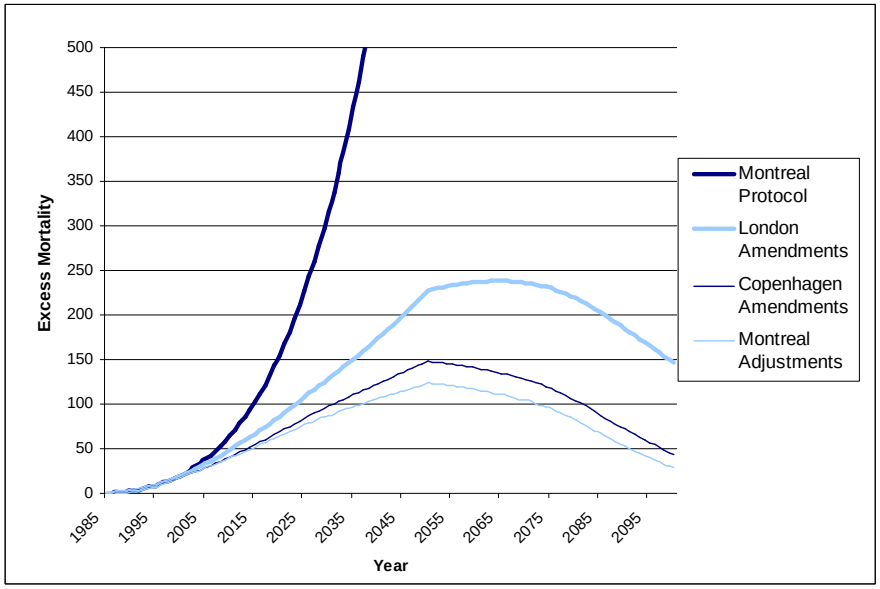

Note: Because this graph shows the incremental NMSC mortality relative to the 1979-1980 baseline, the level of NMSC mortality in the baseline is represented by zero on the y-axis.

8. Sensitivity Analyses

This section describes the results of sensitivity analyses conducted concerning the selection of action spectra for CMM incidence and CMM and NMSC mortality and the effects of modeling early life exposure on CMM mortality.

8.1 Action Spectra and Exposure/Dose Metrics Sensitivity Analyses

Because there are uncertainties associated with selecting an appropriate UV action spectrum and dose metric for induction of the UV radiation -induced health effects discussed in this paper, it is important to explore the impacts of alternative action spectra and dose metrics on these estimates. Table 9 presents results of simulations performed under the Montreal Adjustments policy scenario to estimate CMM incidence and mortality and NMSC mortality using three different action spectra (i.e., erythema, DNA-h, and SCUP-h).

The incremental health effects are comparable for all action spectra, with the DNA-h action spectrum having somewhat higher values for the selected health effect end-points. As discussed in Section 5.2.1, the DNA-h action spectrum is tightly focused on the UV-B portion of solar UV irradiance. In contrast, the other action spectra give more weight to the UV-A portion of solar UV irradiance, which is not altered by ozone depletion. Thus, BAFs generated from the DNA-h action spectrum are likely to be different from those generated by the more UV-A-focused action spectra, resulting in differences in estimates of predicted skin cancer cases. For reasons outlined in Section 5.2.1, selection of the SCUP-h action spectrum to model CMM and NMSC is the most scientifically valid choice. It also yields estimated health benefits that are lower than would be modeled using the DNA-h action spectrum, for a more conservative modeling approach.

Table 9. Summary of Results for Selected Health Effects by Action Spectrum Under the Montreal Adjustments Scenario

Action Spectrum	Cohort Group	Health Effect		
		CMM Incidence (Cases)	CMM Mortality (Deaths)	NMSC Mortality (Deaths)
DNA-h	1890-1980	98,914	13,025	7,342
	1985-2010	78,922	9,106	4,354
	2015-2050	14,658	1,636	760
	2055-2100	0	0	0
Erythema	1890-1980	68,289	8,983	4,865
	1985-2010	54,652	6,295	2,892
	2015-2050	10,258	1,143	510
	2055-2100	0	0	0
SCUP-h	1890-1980	68,816	9,076	4,923
	1985-2010	54,940	6,356	2,925
	2015-2050	10,308	1,155	517
	2055-2100	0	0	0

8.2 CMM: Effects of Emphasizing Early Life Exposures

Another area of uncertainty for which sensitivity was modeled involves the weight that is given to UV exposures at different points in an individual's life. Cumulative UV exposure over a lifetime is thought to be the most important risk factor for NMSC. However, early life exposure has been identified as a potentially important risk factor associated with increased susceptibility to CMM (Harrison *et al*. 1994, Zanetti *et al*. 1992). It has been estimated that people receive 50 percent of their cumulative lifetime UV exposure before the age of 18 (Bergfeld 1997).

Because there is a long latency period associated with the onset of CMM, disease manifestation for exposure to UV may not be seen for decades (Geller *et al*. 1998). While the current simulation for CMM does not model latency, it does offer the option of weighting UV exposures by age and by type of exposure (e.g., peak day exposure and annual exposure) summed over the lifetime of the individual. Figure 8 presents the results of these simulations for CMM mortality using annual and peak day exposures, each computed either by weighting all exposures equally over a person's lifetime, or by weighting only the exposures received between age one and age twenty. More specifically, the following approach was used for estimating whole-life versus early-life exposures:

- *For whole life exposure*: exposures throughout the individual's lifetime are given equal weighting (i.e., each year's exposure is counted in the results).

- *For early life exposure*: only exposures received between the ages of one and 20 are considered (i.e., later life exposures do not contribute to the results).

Figure 8. Excess CMM Mortality for the Montreal Adjustments Scenario for Equal Age Exposure Weighting and Weighting of Exposures Only for Ages 1-20: Annual and Peak Day Exposures

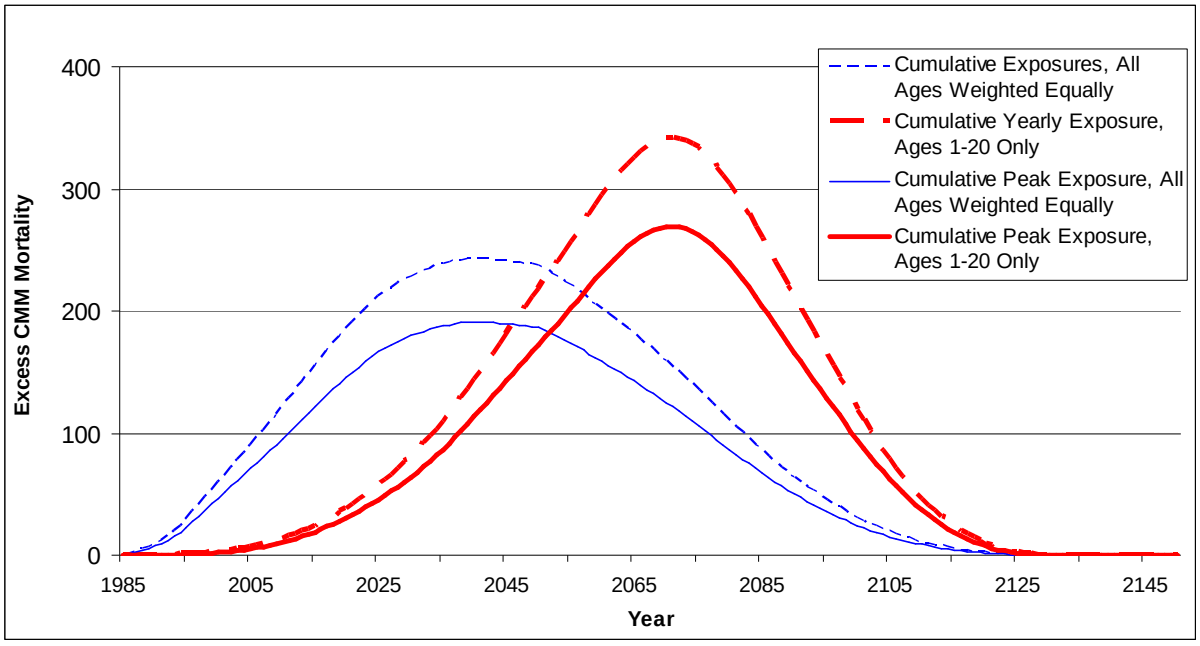

Table 10 tabulates excess CMM mortality using the SCUP-h action spectrum for both whole lifetime exposure and early life exposure assumptions for the Montreal Adjustments policy scenario, assuming peak and annual dose exposure scenarios. The table indicates that CMM mortality changes by up to 11 percent when the age-weighting exposure assumptions are changed.

Table 10. Incremental CMM Mortality Under Different Dose and Exposure Weighting Assumptions[a] (SCUP-h Action Spectrum)

Cohort Group	CMM MORTALITY			
	Annual Dose		Peak Dose	
	Whole Life Exposure	Early Life Exposure	Whole Life Exposure	Early Life Exposure
1890-1980	9,100	2,100	7,100	1,700
1985-2010	6,400	12,600	5,000	9,900
2015-2050	1,200	3,500	900	2,800
2055-2100	0	0	0	0
Total	16,700	18,200	13,000	14,400
Change	9%		11%	

[a] Results are rounded to the nearest 100.

The timing of the health effects changes, however, is more dramatic. Using the age 1-20 cumulative exposure scenario shifts the incremental skin cancer risk substantially forward in time from current generations to future ones. Therefore, uncertainty concerning the appropriate exposure dose manifests itself less in the total incremental risks predicted, than in when those incremental effects are predicted to occur and, thus, who will bear them (i.e., this shifts the risk to children born after 1980). More specifically, for the whole life exposure assumption, the risks of ozone depletion are borne primarily by the present population of adults who will experience these health effects as they age. It is children and future generations that will experience increased early life UV exposures and the associated incremental health effects later in their lives. It should be noted that this shift of health risks does not reflect a formal modeling of CMM latency, which would involve an elaborate method for assigning different weights to exposures incurred at different ages or some other yet-to-be-developed approach.

9. Uncertainty Analysis

The AHEF, like any complex modeling framework, uses inputs and computational procedures that introduce uncertainty to the results. These inputs come from various existing sources and are combined with other inputs and procedures derived specifically for this analytical framework. Proper interpretation and use of the human health effects results generated by the AHEF requires some understanding of the nature and magnitudes of the major sources of uncertainty involved. This section uses a combination of empirical analyses and theoretical reasoning to roughly characterize the quantifiable and unquantifiable uncertainties associated with the AHEF's incidence and mortality predictions.

The remainder of this section is organized as follows:

- Section 9.1 focuses on four major sources of uncertainty in the AHEF's estimates of health effects that are considered to be central to its structure, and that have been quantified to the extent possible;
- Section 9.2 presents a discussion of other unquantified sources of uncertainty that affect the AHEF's results, but that are not considered to be central to its structure; and
- Section 9.3 summarizes the quantified and unquantified sources of uncertainty.

9.1 Major Sources of Uncertainty

The AHEF uses past and future ODS emissions to generate equivalent effective stratospheric chlorine (EESC) concentrations, which in turn are used to estimate stratospheric column ozone changes. These column ozone changes then are used to compute changes in ground-level UV radiation, from which estimated changes in human health effects can be calculated. Figure 9 illustrates these model inputs.

Figure 9. Central Computational Procedures Associated with Uncertainty in the AHEF

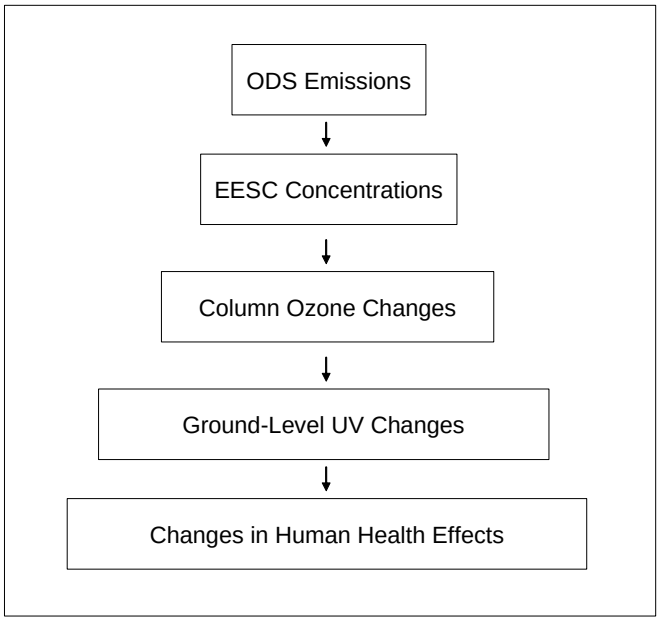

Each of the linkages identified in the figure is the source of some degree of uncertainty. Although some might attempt to combine these different sources using statistical techniques, it is best to consider each source separately for two reasons. First, the quantitative estimates of the levels of uncertainty of the AHEF's many inputs and modeling components were derived using different techniques of varying levels of precision. Second, and perhaps more important, is that uncertainties concerning some of the inputs and computations might be inversely related. For example, if the TUV's estimated ground-level UV radiation is biased upward, so that variations in UV exposures are too high, then the estimated BAFs (which are derived based on correlation with ground-level UV radiation variation) will be biased downward.

From a purely statistical standpoint, the largest source of uncertainty in the AHEF is the EESC-to-column ozone component, with standard errors around the mean effects ranging from about 25 to over 100 percent. However, as will be discussed in Section 9.1.2, this is a product of the limited data available for the regression analysis and likely does not reflect the true uncertainty that would be revealed with substantially more data.

By contrast, the TUV's estimates of changes in ground-level UV radiation due to changes in column ozone impart statistical uncertainty of up to 10 percent. Similarly, the choice of action spectrum for each health endpoint yields very small variations in the health effects results, with the exception of the DNA-h action spectrum (which is not used in the AHEF), as explained in more detail in Section 9.1.4. The last two sources of quantified uncertainty—the age-weighted exposure scenario assumption and the estimated BAFs—also introduce relatively modest variation in the estimated health effects, of about 11 percent and up to 30 percent, respectively.

Thus, as is true of any complex modeling framework with multiple inputs and computational procedures, the AHEF does contain uncertainties. Perhaps over time, these can be reduced as additional data and research become available. At present, however, the AHEF embodies the best inputs, assumptions, and computational procedures that are known. The remainder of this section discusses the five major areas of uncertainty in greater detail.

9.1.1 Translating ODS Emissions into EESC Concentrations

One source of uncertainty in the AHEF methodology is that the magnitude of ozone depletion and recovery based on ODS emissions could be different from those predicted under the international controls in place now or scheduled for the future. This could occur because ODS use might be less than allowed under the various current and future phaseout requirements, or ODS use could be higher in the future if ODS use exceeds allowable amounts due to non-compliance with the phaseout targets. However, to date, countries have reportedly tended to over-comply with Montreal Protocol obligations (i.e., they have generally undertaken ODS phaseout efforts before the limits imposed by the Protocol take effect), as described in WMO (2003). For example, in 1999, reports of CFC production indicated that production of CFCs was 20,000 ODP-tons less than allowable consumption in that year (WMO 2003).[24] Thus, the scenario of total compliance used in the AHEF may potentially represent the maximum ODS emissions scenario.

Similarly, the parameters that characterize the process of how ODS emissions translate into EESC are also taken to be given, despite the fact that the reaction kinetics of these transitions and the composition

[24] Although scientific measurements of actual CFC-11 and CFC-12 emissions have indicated that mixing ratios were 5 to 10 percent higher than ratios that would have been expected if production levels were identical to those reported, the discrepancy between measurements and reported values could be related to differences in measured and reported values that have occurred throughout the entire measurement period for CFC-11 and CFC-12, rather than as a result of under-reporting in 1999. Supporting this hypothesis, measurement and production values have been closer in recent years (WMO 2003).

of the future atmosphere are also subject to uncertainty (as discussed in more detail in Section 9.2). These inputs are as up-to-date as the available complex atmospheric models can provide. Moreover, undertaking a sensitivity analysis for all of the relevant parameters that translate ODS emissions at the ground into EESC would be prohibitively resource intensive. Hence, the uncertainties in ODS use/emissions to EESC portion of the AHEF's structure are noted, but not quantitatively examined.

9.1.2 Translating EESC Concentrations into Stratospheric Column Ozone

From a statistical standpoint, the largest source of uncertainty in the AHEF is introduced by the limited data points available for use in predicting changes in column ozone resulting from changes in EESC. The reason these factors are statistically uncertain is that they are estimated from a very limited data set of satellite-measured stratospheric ozone concentrations and estimated EESC for the years that stratospheric ozone data are available from NASA's Nimbus-7 Total Ozone Mapping Spectrometer (TOMS) (i.e., 1978 to 1993). Relatively few observations in a data set can lead to large standard errors in any statistical analysis.

Furthermore, UV radiation changes resulting from ozone depletion and ground level pollution (i.e., tropospheric ozone generation) are more accurately measured by spectrally resolved ground-based monitors than by satellite measurements on which the AHEF currently relies (this is discussed further in Section 10.5). Satellite data are not as accurate for measuring ozone concentrations at ground-level as they are at higher altitudes because of the coupling between UV absorption by ozone and UV scattering by aerosols and particulate matter. These considerations are important when the ozone perturbations occur in the lower-to-middle troposphere, where soot and other aerosols are prevalent. When ozone perturbations occur in the stratosphere (i.e., well above the region where scattering occurs), absorption predominates. Thus, the altitude at which ozone perturbations occur can affect UV radiation at the ground level. These effects are not well captured by satellite data and hence, ground level UV monitoring data could help to improve modeling estimates, particularly in urban areas.

Table 11 presents the estimated mean impacts of EESC on column ozone, along with the standard errors, for four different months and for each of the three latitude bands modeled by the AHEF. Because the AHEF estimates EESC by year and then estimates column ozone by month and latitude based on regression analyses using TOMS data, the variation in the AHEF's predicted ozone by month and latitude is attributable in large part to the data source and not the regressions that estimate the impact of EESC on column ozone. EESC is measured in parts per billion and column ozone is measured in Dobson units. Table 11 illustrates that an EESC increase of 1,000 parts per billion (ppb) results in an estimated reduction of 16 Dobson Units of column ozone in January in the 30°N to 20°N latitude band.

Table 11. Means and Standard Errors of EESC to Column Ozone Coefficients for Select Months and Latitudes (Change in Dobson Units for a 1 ppb Change in EESC)

Month	30°N-20°N Latitude Band		40°N-30°N Latitude Band		50°N-40°N Latitude Band	
	Mean	Standard Error	Mean	Standard Error	Mean	Standard Error
January	-0.0160	0.0104 (65%)	-0.0344	0.0124 (36%)	-0.0431	0.0122 (28%)
April	-0.0142	0.0096 (68%)	-0.0268	0.0108 (40%)	-0.0400	0.0107 (27%)
July	-0.0032	0.0055 (172%)	-0.0080	0.0060 (75%)	-0.0103	0.0074 (72%)
October	-0.0077	0.0053 (69%)	-0.0076	0.0045 (59%)	-0.0122	0.0045 (37%)

Standard errors of roughly 25 to over 150 percent indicate large statistical uncertainty of the column ozone coefficients. Until additional data on column ozone from satellite or ground-level measurements are obtained to refine these estimates, such uncertainty cannot be reduced. For additional discussion on the uncertainty associated with the AHEF's column ozone estimates, see Appendix D, which compares AHEF and WMO (1999) predicted ozone concentrations.

9.1.3 Translating Column Ozone into Ground-Level UV Radiation

Uncertainty in the estimation of weighted UV exposure at the Earth's surface was not explicitly quantified. Experts generally agree that the uncertainty contributed by the column ozone-to-UV calculations is relatively small compared to those introduced by other inputs and components of the analysis. Uncertainties in translating column ozone to ground-level UV radiation are dominated by uncertainties in the following:

- *Clear sky radiation model*. The accuracy of the TUV model has been evaluated extensively by comparisons with other models (e.g., Koepke et al. 1998) and with direct measurements of UV radiation (e.g., Shetter et al. 1992, 1996; Kirk et al. 1994; Lantz et al. 1996; Gao et al. 2001; Bais et al. 2003). For spectrally resolved radiation, the agreement is 10% or better for all wavelengths of biological relevance (e.g., Kirk et al. 1994, Bais et al. 2003). For integrated quantities (e.g. biologically effective UV and atmospheric photolysis coefficients), agreement improves to roughly 5% or better due to averaging over the relevant wavelength ranges. These small errors are believed to result primarily from uncertainties in the extraterrestrial irradiance (approximately 5-10% in the UV-B band), the ozone absorption cross-section (less than 2% in the UV-B, De More et al. 1997), and from incomplete knowledge of the atmosphere (e.g., exact aerosol amount) at the time of the measurements.

- *UV perturbations due to clouds and air pollutants*. Clouds and air pollutants generally reduce the UV radiation incident at the Earth's surface. However, as long as cloud cover and pollutant levels remain constant, the relative (percent) changes in UV radiation due to changes in stratospheric ozone are expected to be identical to those computed for cloud-free, pollution-free conditions (WMO 1990). This is because the absorption of photons by stratospheric ozone occurs at altitudes far above those of clouds and air pollutants. Any future systematic changes in cloud cover (e.g., related to climate change) or air pollutants are highly uncertain and speculative, and are not included in the AHEF at the present time. It is recognized, however, that such putative changes could either increase or decrease the average UV radiation levels incident at the Earth's surface.

9.1.4 Translating UV Exposures into Human Health Effects

The final major modeling step in the AHEF's structure that introduces some uncertainty to the estimated health effects is the translation of changes in ground-level UV exposure into incremental skin cancers. This step involves multiplying the percentage change in estimated UV exposure by the BAF for a particular action spectrum, exposure scenario (discussed in Section 5), and health effect. Specifically, three sources of uncertainty come into play: (i) uncertainty associated with choice of action spectrum, (ii) uncertainty regarding exposure period, and (iii) uncertainty in the BAF. Each of these sources of uncertainty is explored further below.

9.1.4.1 Uncertainty associated with choice of action spectrum

An important source of uncertainty in the AHEF's estimates of UV-related health effects is related to a lack of complete understanding regarding the correct weighting for the portions of the UV spectrum that are most effective in causing health effects. Several candidate action spectra have been developed based on both human observations (e.g., erythema) and from laboratory experiments on animals (e.g., SCUP-h), but precisely which spectrum weighting causes particular human health effects remains unknown.

Despite some uncertainty regarding selection of an appropriate action spectrum for each health effect, it is possible to choose among the available spectra based on certain parameters. For example, as Table 12 illustrates for various health effects endpoints under the Montreal Adjustments ODS control scenario,

there is a range of expected incidence and mortality estimates for CMM and NMSC based on which action spectrum is selected. Both the SCUP-h and erythema spectrum have good correlation (within a few percentage points) for the examined health effects, while the DNA-h spectrum has wider variability. This divergence is because the DNA-h action spectrum is more tightly focused on the UV-B portion of the spectrum. Furthermore, there is a poor understanding of the correction factors needed to adjust between viral/bacterial DNA (for which the spectrum was originally developed) and human DNA (i.e., DNA-h).

Table 12. Incremental CMM Incidence and Mortality and NMSC Mortality for Three Action Spectra

Action Spectrum/ All Cohorts	CMM Incidence		CMM Mortality		NMSC Mortality	
	Excess Incidence	Difference from SCUP-h	Excess Mortality	Difference from SCUP-h	Excess Mortality	Difference from SCUP-h
DNA-h	192,494	41.5%	23,767	41.3%	12,457	79.8%
Erythema	133,199	-1.2%	16,421	-1.4%	8267	-2.7%
SCUP-h	134,064	-	16,587	-	8,365	-

As additional data become available on the dose-response relationship for CMM and NMSC, use of the SCUP-h action spectrum may be re-evaluated.

9.1.4.2 Uncertainty regarding exposure period

Another source of uncertainty in the AHEF's health effects estimates is associated with the exposure period over a person's lifetime that is most likely to be the cause of UV-related health effects. This is especially relevant for CMM, since it has been hypothesized that CMM is largely the product of intense exposures early in life (e.g., through age 20) rather than cumulative lifetime exposure. As discussed on page 32 (see Table 10), CMM mortality changes by ±11 percent when the exposure assumptions are changed, with uncertainty concerning the appropriate exposure dose manifesting itself less in the total incremental risks predicted, than in *when* those incremental effects are predicted to occur, and *who* will bear them (i.e., shifting the risk to children born after 1980).

9.1.4.3 Uncertainty in the BAFs

Uncertainty in the BAFs is associated with (1) the accuracy of the BAFs themselves, as measured by the uncertainty ranges, and (2) whether or not the BAF can be appropriately calculated for the health effect of concern, which depends on the selection of the action spectrum. As described in detail below, the uncertainty in the AHEF's predicted excess UV-related human health effects is 6 percent for CMM mortality, 5 percent for NMSC mortality, and 30 percent for NMSC incidence. These uncertainty ranges are small and not significant compared to the levels of uncertainty that are common in health effects assessments for other hazards.

CMM Incidence/Mortality

The BAFs used by the AHEF for CMM incidence and mortality were estimated econometrically by correlating data on latitudinal variations in UV exposure and skin cancer mortality. As with any statistical estimate, these estimated BAFs have standard errors. The estimated BAFs for CMM mortality and their standard errors for the SCUP-h UV action spectrum using the cumulative lifetime UV exposure assumption are shown in Table 13. At a 95 percent confidence interval, the BAF for light-skinned males based on annual exposures ranges from 0.55 to 0.62. This yields an uncertainty range of approximately ±6 percent around the central value (median).

Table 13. Estimated Mean, Standard Errors, and Confidence Intervals for the BAFs for CMM Mortality for the SCUP-h Action Spectrum and Exposure Scenarios, by Sex

	Annual With Clouds				Peak Clear Day (June 21)			
	Light-Skinned Males		Light-Skinned Females		Light-Skinned Males		Light-Skinned Females	
Mean	0.5846		0.5047		1.444		1.310	
Standard Error	0.02		0.02		0.05		0.06	
95% Confidence Limit	*Upper Bound*	*Lower Bound*	*Upper Bound*	*Lower Bound*	*Upper Bound*	*Lower Bound*	*Upper Bound*	*Lower Bound*
	0.62	0.55	0.55	0.46	1.55	1.34	1.43	1.19
97.5% Confidence Limit	*Upper Bound*	*Lower Bound*	*Upper Bound*	*Lower Bound*	*Upper Bound*	*Lower Bound*	*Upper Bound*	*Lower Bound*
	0.63	0.54	0.56	0.45	1.56	1.33	1.45	1.17

Although researchers' understanding of the biology and pathogenesis of CMM tumors has improved in recent years (Nesbit et al. 1998, Fidler 1998), uncertainty remains about the etiology and mechanism(s) of induction of these tumors (Longstreth 1998). While most researchers agree that the primary environmental risk factor for CMM is exposure to sunlight, there is uncertainty about three important aspects of this relationship:

- *Effects of Early Life Exposure.* Some studies indicate that exposures early in life could increase the risk of adult cases of CMM, although preliminary results suggest that high childhood exposures are only important in the context of high adult exposures (Harrison *et al*. 1994, Zanetti *et al*. 1992, Autier and Dore 1998). It has also been hypothesized that chronic low-level UV exposure may even be protective (Holman and Armstrong 1984). Depending on how and if early childhood exposure does indeed influence CMM incidence, and on whether chronic low-level UV exposure may be protective, CMM incidence rates may be under- or over-projected in the AHEF. However, the overall impacts on results are not expected to be great (i.e., up to 11 percent, as explained in Section 8.2).

- *Choice of Appropriate Action Spectrum.* There are no studies on CMM induction in test animals and, as such, an action spectrum specific to CMM has not yet been developed. However, recent studies suggest that the appropriate action spectrum to predict tumor induction may be more dependent on UV-A radiation than previously suspected (Setlow et al. 1993, Ley 1997). The lack of adequate experimental data from which to derive an action spectrum for CMM is one of the greatest sources of uncertainty in estimating UV-induced health impacts. Due to this lack of information, the AHEF predicts CMM cases and deaths based on the SCUP-h action spectrum for SCC. However, this analysis should be reconsidered if future studies aimed at developing an action spectrum for CMM reveal that its shape is not similar to the SCUP-h action spectrum for SCC (DeFabo 2001).

- *Effects of UV-B on Tumor Suppression.* One important variable confounding the dose-response relationship is the effect of UV-B on human tumor suppression genes. It is hypothesized that UV-B may inactivate tumor suppression genes (i.e., the p21 gene), making humans more susceptible to UV-related cancers. More specifically, research indicates that UV light targets the retinoblastoma (RB) pathway of the p21 genetic locus, which contains genes that encode kinase inhibitors and act as tumor suppressors (Kannan *et al*. 2003, Chin *et al*. 1997, Hutchinson 2003). This introduces uncertainty into the AHEF, as the model does not consider how UV independently affects tumor suppression genes and how this may lead to increased UV-related health impacts. Thus, because it is not possible to separate the effects of UV radiation on DNA and the p21 gene, there is some uncertainty regarding the dose-response relationship derived from incidence and

mortality data. Although the degree of uncertainty is not quantified, it is not expected to be significant.

NMSC Mortality

The BAFs used by the AHEF for NMSC mortality were estimated econometrically by correlating data on latitudinal variations in UV exposure and skin cancer mortality. The estimated BAFs for NMSC mortality and their standard errors for the SCUP-h UV action spectrum using the cumulative lifetime UV exposure assumption are shown in Table 14. At a 95 percent confidence interval, the BAF for light-skinned males based on annual exposures ranges from 0.65 to 0.77. This yields an uncertainty range of approximately ±5 percent around the central value (median).

Table 14. Estimated Mean, Standard Errors, and Confidence Intervals for the BAFs for NMSC Mortality for the SCUP-h Action Spectrum and Exposure Scenarios, by Sex

	Annual With Clouds				Peak Clear Day (June 21)			
	Light-Skinned Males		Light-Skinned Females		Light-Skinned Males		Light-Skinned Females	
Mean	0.7094		0.4574					
Standard Error	0.03		0.03		0.07		0.09	
95% Confidence Limit	*Upper Bound*	*Lower Bound*	*Upper Bound*	*Lower Bound*	*Upper Bound*	*Lower Bound*	*Upper Bound*	*Lower Bound*
	0.77	0.65	0.52	0.40	2.21	1.93	1.74	1.39
97.5% Confidence Limit	*Upper Bound*	*Lower Bound*	*Upper Bound*	*Lower Bound*	*Upper Bound*	*Lower Bound*	*Upper Bound*	*Lower Bound*
	0.78	0.64	0.53	0.39	2.22	1.91	1.77	1.36

SCC and BCC Incidence

Table 15 presents the mean BAF values and associated standard errors for SCC and BCC incidence, which were derived by de Gruijl and Forbes (1995) using similar statistical techniques. Sources of uncertainty associated with the BAFs calculated by de Gruijl and Forbes include confounding factors, such as migration, patient reporting delay, high early life exposure, and potential exposure to other carcinogens. Relative error for carcinogenicity caused by wavelengths over 340 nm was still very substantial in 1995. In addition, the model was unable to account for epidermal thickening and pigmentation that alter spectral sensitivity of the skin, although corrections for thicker human epidermises could be applied. Also, differences between mice and humans (e.g., better adaptation of humans to increases in UV exposure) may have influenced the results of applying the hairless mouse model to humans. This yields an upper uncertainty range of approximately 30 percent for the BCC and SCC incidence AHEF estimates.

Table 15. BAFs and Standard Errors for BCC and SCC Incidence

SCC		**BCC**	
U.S. Males	***U.S. Females***	***U.S. Males***	***U.S. Females***
2.6 ± 0.7	2.6 ± 0.8	1.5 ± 0.5	1.3 ± 0.4

Source: de Gruijl and Forbes 1995.

9.2 Other Unquantified Sources of Uncertainty

There are a number of other sources of uncertainty in the AHEF's health effects predictions. Some of these sources of uncertainty are possible to quantify, but are not central to the structure of the AHEF. Others cannot be quantified because any assumptions or estimates would be simply speculative. These other sources of uncertainty include:

- Composition of the future atmosphere;
- Future conditions of the ozone layer;
- Effect of climate change on ozone depletion;
- Global compliance with modeled policy scenarios;
- Laboratory techniques and instrumentation for deriving action spectra;
- Demographic and human behavioral changes; and
- Baseline information.

Accurate prediction of future changes in human health effects would require consideration of the net effect of all of the factors described above. Although this challenge is beyond the ability of the current state of atmospheric and epidemiological science, these uncertainties are described qualitatively in more detail below. This section concludes with a summary of these uncertainties.

9.2.1 Composition of the Future Atmosphere

The exact composition of the future atmosphere as a result of compliance with different ODS phaseout policies is unknown. As levels of atmospheric chlorine are reduced, the impact of ozone depletion from chlorine and bromine radical species generated from ODS would change. In addition, long-term systematic changes in atmospheric opacity (e.g., clouds, aerosols, other pollutants) will also impact the AHEF's ability to model changes in ozone. Likewise, future changes in climate could result in changes in the atmospheric circulation patterns and therefore could change cloud cover. The impacts of such changes on the predicted recovery of the ozone layer are unknown. All of these uncertainties could influence the AHEF's ability to model atmospheric processes accurately.

9.2.2 Future Conditions of the Ozone Layer

Uncertainties also can be contributed by assumptions regarding the future conditions of the ozone layer in response to the phaseout of ODS. Some computer models predict that the phaseout of ODS will slow and eventually stop the rate of ozone depletion, and suggest that natural ozone-making processes will enable stratospheric ozone to return to 1979-1980 ozone conditions. These models also predict that the recovery will eventually result in increased concentrations beyond 1979-1980 levels[25] (see Chapter 12 in WMO 1999 for more detail). Because there is incomplete knowledge about the behavior of ozone prior to the satellite measurements taken in 1979-1980, the AHEF imposes a limit on future ozone recovery to the conditions observed in 1979-1980.

9.2.3 Effect of Climate Variations on Ozone Depletion

The effects of global climate variations on stratospheric temperature and, in turn, on ozone depletion, are not well understood, and have therefore not been modeled in the AHEF. While this effect is not incorporated into any other international models used to assess future global ozone depletion, it does represent a modeling constraint that should be noted.

[25] Whether this recovery scenario, called "ozone superabundance," is likely to occur is open to debate, particularly because of the potential for complex interactions between global climate change and stratospheric ozone dynamics. Model computations have predicted both higher and lower amounts of ozone in the future.

9.2.4 Global Compliance with Modeled Policy Scenarios

This analysis assumes global compliance with each of the modeled policy scenarios. To the extent that these limitations are not adhered to, future ODS emissions could be different in both composition and quantity.

9.2.5 Laboratory Techniques and Instrumentation

Additional uncertainty can be contributed by the laboratory techniques and instrumentation used for deriving the action spectra used to weight UV exposure. Discrepancies between the wavelengths of UV radiation intended to be administered and the wavelengths actually received by the test organism can result in orders of magnitude differences in the measured response. In addition, many action spectra are derived using monochromatic light sources that do not fully simulate the polychromatic light received directly from the sun.

9.2.6 Demographic and Behavior Changes

Future demographic and behavior changes that could affect the accuracy of the AHEF include:

- *Changes in human UV exposure behavior*: This evaluation assumes that human exposure behavior remains constant through time, and does not take into account innovations in sun protection technology (e.g., improved sunglasses and sunscreens), increased public awareness of the effects of overexposure to UV, and increased sensitization to the need for early treatment of suspicious lesions.

- *Improvements in medical care/increased longevity*: Improvements in medical care and predictions of increased longevity for many population subgroups could affect estimates of future skin cancer incidence and mortality significantly.

- *Changes in socioeconomic profiles*: Socioeconomic profiles can impact a variety of factors, ranging from demand for air travel to areas where high UV exposure is expected (i.e., the beach), to the types of skin cancer most commonly observed.

- *Changes in population composition and size*: Population composition changes such as the expected increase in Hispanic populations, whose more pigmented skin is thought to decrease skin cancer risk, could have significant effects on future U.S. skin cancer rates.

The above factors are either not easily quantified (e.g., human behavior), or they are not central to the analysis (e.g., improvements in medical care), and are therefore not addressed further in this evaluation.

9.2.7 Accuracy of Baseline Information

It is possible that error is introduced to the AHEF's results through misreporting of skin cancer incidence and mortality data (i.e., the AHEF's baseline estimates). With disease data, under-, over-, and mis-reporting are not uncommon. For example, a recent study revealed that the incidence of CMM has been systematically under-reported in the SEER data (Clegg *et al*. 2002).[26] The original SEER data indicated that CMM rates in white males were relatively flat or even falling (ranging from -11.1 percent to 3.3 percent annually after 1996). However, after adjusting for underreporting, CMM rates were actually found

[26] There is little reason to believe that the SEER CMM incidence under-reporting extends to the NCI-based CMM mortality input information.

to have increased between 3.8 to 4.4 percent annually since 1981 (Clegg *et al*. 2002). Underreporting of CMM incidence is largely attributable to diagnosis in doctors' offices, as opposed to hospitals and other treatment centers with better reporting accuracy. However, the AHEF results are not significantly affected by this underreporting because CMM incidence estimates in the AHEF are not based directly on SEER incidence data. Rather, because the AHEF estimates CMM incidence based on the *ratio* of SEER incidence data to projected annual mortality estimates, and because underreporting would affect both baseline and scenario estimates, the effects on *incremental* changes in CMM incidence would be second order.

9.3 Summary of Quantified and Unquantified Sources of Uncertainty

Of the major sources of uncertainty associated with the AHEF, the total quantified uncertainty is roughly 60 percent, as summarized in Table 16:

Table 16. Major Sources of Quantified Uncertainty

Source of Uncertainty	Quantified Uncertainty
Translating column ozone to ground-level UV	
TUV Model	≈ 5%
Translating UV exposure to human health effects	
Uncertainty in the BAFs	≤ 30%
• CMM mortality (6%)	
• NMSC mortality (5%)	
• NMSC incidence (30%)	
Uncertainty with choice of action spectrum	≈ 50%
Early life exposure vs. whole life exposure	≈ 10%
Total $\sqrt{(5^2 + 30^2 + 50^2 + 10^2)}$	**≈ 60%**

In addition to the major quantified sources of uncertainty listed above, the atmospheric component of the AHEF (i.e., translation of ODS emissions into (a) EESC concentrations and (b) changes in column ozone concentrations) is also a source of uncertainty, though not quantitatively examined in this analysis. It should be noted, however, that this uncertainty associated with the atmospheric parameters used in the AHEF is inherent in all atmospheric models, including those used by WMO in its Scientific Assessment of Ozone Depletion reports (WMO 1990, 1992, 1995, 1999, 2003).

Other unquantified sources of uncertainty discussed above relate to different parts of the AHEF that estimate changes in ozone, changes in UV radiation, and changes in health effects. Table 17 summarizes these unquantified uncertainties.

Table 17. Factors with Unknown Contributions to Uncertainty

Factor	Parameter
Change in Ozone Estimates	▪ Composition of Future Atmosphere ▪ Ability to Model Atmospheric Processes Accurately ▪ Response of Ozone Layer to Changing ODS Concentrations ▪ Effect of Climate Change on Ozone Depletion ▪ Global Compliance with Modeled Policy Scenarios ▪ Changes in Composition and Quantity of ODS Emissions
Change in UV Radiation Estimates	▪ Long-term Systematic Changes in Atmospheric Opacity (e.g., clouds, aerosols, other pollutants)
Change in Health Effect Estimates	▪ Changes in Human UV Exposure Behavior ▪ Laboratory Techniques and Instrumentation for Deriving an Action Spectrum ▪ Improvements in Medical Care/Increased Longevity ▪ Changes in Socioeconomic Factors (e.g., demographics and human behavioral changes) ▪ Baseline Information (e.g., misreporting of skin cancer incidence and mortality data) ▪ Changes in Population Composition and Size

10. Topics for Future Research

Because research on the health effects of UV exposure is ongoing, no model or set of results quantifying health effects impacts can be considered final. Indeed, new information and research results on skin cancer and UV radiation continue to flow from the academic community. Many important issues such as the inclusion of data on UV responsiveness on darker-skinned populations, new information on UV-induced cataract incidence, incorporation of research on other human health endpoints (e.g., immune suppression), and investigation of the feasibility of predicting non-human endpoints must continue to be investigated. As significant new findings are incorporated into the AHEF, the accuracy of predictions and the implications for protecting stratospheric ozone will be enhanced. This section discusses some of the major topics where future research could improve the ability to accurately predict UV-related impacts.

10.1 Prediction of Impacts on Different Skin Types

The AHEF is not completely comprehensive in its assessment of UV effects in the population because it only accounts for light-skinned individuals in the United States. Although "light-skinned" individuals in the United States account for nearly 90 percent of the population,[27] data are needed to account for additional population skin-types, in order to complete a more comprehensive assessment of health effects resulting from UV changes.

10.2 Research on Dose-Response Relationship of Cataract Incidence and UV Exposure

Although recent analysis of the dose-response relationship between UV exposure and cataract incidence in the United States were not able to establish a strong correlation, a more rigorous disaggregated analysis could be performed to ensure that this lack of correlation is not the result of data limitations. Similarly, if a dose-response relationship or BAF for cataract becomes available through independent research, this health effect should be reconsidered for inclusion in the AHEF. (For more information on modeling cataract incidence, see Appendix E.)

10.3 Inclusion of Other Human Health Endpoints

In addition to the health effects featured in the AHEF, UV-B has been associated with other human health consequences that are as yet unquantified, as discussed in Section 9.2. For example, UV-B exposure can produce immunosuppression in humans that may be associated with increases in the incidence and severity of some infectious diseases or result in an increased failure rate of vaccination programs (Longstreth et al. 1998). Numerous studies with animals have shown that UV-B exposure depresses immune responses to viruses and in microorganisms (principally those that enter via the skin), and results in more severe infections. Infectious diseases where such an effect has been shown using animal models include herpes, tuberculosis, leprosy, trichinosis, leishmaniasis, listeriosis, and Lyme disease (Longstreth et al. 1998). In addition, immunosuppression may be associated with increased cancer incidence, including UV-induced cancers.

Although action spectra have been derived for immunosuppression (e.g., De Fabo and Noonan 1983), certain key data gaps make it difficult to develop estimates of health effects changes for this endpoint. For example, sufficient epidemiological data do not presently exist that would allow quantification of the number of affected individuals necessary to estimate baseline incidence. Further, the scientific community

[27] "Light skinned" populations include those defined in the U.S. Census (1990) as *whites*, *Amer Indians*, *Asian or Pacific Islanders*, and *Other* (including the majority of Hispanic populations).

is not in agreement as to which dose metric should be used to assess the consequences of immunosuppression. However, adding this endpoint could be reconsidered for inclusion in the AHEF if future studies fill these data gaps.

In addition to the uncertainty surrounding the number of individuals affected by immunosuppression, the levels of immunosuppression experienced by cancer-afflicted individuals, and the dose metric, the relative strength of UV-B-induced immunosuppression compared to other cellular mutagenic effects remains unclear. UV-B simultaneously suppresses cellular immunity and damages specific DNA and anti-cancer pathways in cells that are important for mutagenesis. Much recent work has attempted to explain the differential effects of immunosuppression and other UV-B sensitive cellular changes using murine models (Noonan et al. 2003, Kannan et al. 2003, Moodycliffe et al. 2000). Furthermore, while additional information is needed to define the relationship between UV-B and immunosuppression, the role of UV-A in this relationship is also uncertain (de Fabo 2003).

10.4 Inclusion of Impacts of Climate Variations on Ozone Depletion

Future research may shed light on the relationship between global climate and stratospheric ozone depletion, which could eventually be modeled in the AHEF.

10.5 Improved Ground-Level UV Measurements

Ground level UV monitoring is essential for advancing human health effects research and should be linked to epidemiological observations to improve our understanding of UV-related health effects. While satellites provide an excellent means of measuring the UV radiation reflected from the atmosphere and estimating some atmospheric properties, such as clouds and total ozone column, they cannot directly measure ground level UV radiation. Additionally, satellites are insensitive to pollution in the lower atmosphere. Therefore, while satellite data compare fairly well to ground level UV measurements in clean locations, this is not so in polluted areas, such as cities. This produces a systematic effect such that ground level UV measurements are 10 to 20 percent lower than satellite measurements in urban areas. Because urban areas are where U.S. populations are concentrated, it is in these areas that monitoring is most important. But monitoring data must be robust in order to be useful to epidemiologists. In particular, long term monitoring is essential because of high inter-annual variability in UV radiation levels, and because many health effects are the result of long term accumulated exposure to UV radiation. With continued ground level UV monitoring, human health effects associated with changes in UV exposures can be better understood and, ultimately, incorporated into the AHEF.

10.6 Prediction of UV Impacts on Non-Human Endpoints

Many economic, ecological, and environmental effects are also associated with increased UV radiation. Economic impacts include damage to agricultural crops, effects on ecosystems, and degradation of polymeric materials. Each of these has far-reaching impacts on construction and manufacturing industries (Andrady et al. 1998).

Enhanced UV radiation levels have varied repercussions on terrestrial ecosystems, ranging from decreased photosynthesis rates to changes in competitive balance and increased susceptibility to disease (Caldwell et al. 1998).

Effects on aquatic ecosystems include decreased species diversity and reduced larval survival rates (Häder et al. 1998). Because UV radiation is able to penetrate tropical ocean waters to depths of more than 20 meters, many species of coral may also be affected by increased ozone depletion. For example, the death of organisms and the inhibition of skeletal growth and bleaching have been observed both in

laboratory tests and in situ (e.g., Brown et al. 2000). In addition, UV radiation may indirectly damage coral reefs by causing the formation of oxidative radicals that can in turn damage organismal DNA, enzymes, lipids, and other molecules associated with cell function. Studies have shown that the fluorescent pigments in coral that regulate light for the zooxanthellae—symbiotic algae on which coral reefs depend for photosynthetic functions—may react to increased radiation from sunlight by scattering radiation of wavelengths not essential to photosynthesis (Salih *et al*. 2000). Although fluorescent pigments in coral may provide buffering action against increased UV radiation levels, studies have also indicated that increased UV radiation may play a role in coral bleaching by increasing DNA lesions (called thymine dimers) in corals and the zooxanthellae algae living within coral structures. Experiments showed that thymine dimers increased with increasing UV radiation, although the increase was not proportional (Anderson et al. 2001).

Increased UV radiation intensity caused by ozone depletion may also cause negative impacts in amphibians, and may be responsible in part for the observed decreases in the size of amphibian populations. The egg stage is believed to be the period of life in which amphibians are most susceptible to UV radiation because eggs are often deposited in full sunlight. Researchers speculate that current levels of UV-B alone are not sufficient to explain the decrease in amphibian numbers. However, additional research is required to better understand the impact of UV radiation on susceptible species (Licht and Grant 1997).

11. References

Anderson, Susan, Richard Zepp, Jana Machula, Debbie Santavy, Lara Hansen, and Erich Mueller 2001. "Indicators of UV exposure in corals and their relevance to global climate change and coral bleaching." *Hum. Ecol. Risk Assess.* 7:1271-1282.

Andrady, D.L., S.H. Hamid, X. Hu, and A. Torikai (1998), "Effects of increased solar ultraviolet radiation on materials," *Photochemistry and Photobiology B: Biology* 46:93-103.

Anduze, Alfred L., M. D. (1993), "Ultraviolet radiation and cataract development in the U.S. Virgin Islands," *J. Cataract Refract. Surg.* 19:298-300.

Autier, P., and J.F. Dore (1998), "Influence of sun exposures during childhood and during adulthood on melanoma risk," *Int. J. Cancer* 77:533-537.

Bais, A.F., S. Madronich, J. Crawford, S. R. Hall, B. Mayer, M. van Weele, J. Lenoble, J. G. Calvert, C. A. Cantrell, R. E. Shetter, A. Hofzumahaus, P. Koepke, P. S. Monks, G. Frost, R. McKenzie, N. Krotkov, A. Kylling, S. Lloyd, W. H. Swartz, G. Pfister, T. J. Martin, E. -P. Roeth, E. Griffioen, A. Ruggaber, M. Krol, A. Kraus, G. D. Edwards, M. Mueller, B. L. Lefer, P. Johnston, H. Schwander, D. Flittner, B. G. Gardiner, J. Barrick, R. Schmitt (2003), "International Photolysis Frequency Measurement and Modelling Intercomparison: Spectral Actinic Flux Measurements and Modelling," Accepted in *J. Geophys. Res*.

Bergfeld, W.F. (1997), "The aging skin," *International Journal of Fertility*, 42:57-66.

Brown, B.E., R.P. Dunne, M.S. Goodson, and A.E. Douglas 2000. "Marine ecology: bleaching patters in reef corals." *Nature* 404:142-143.

Caldwell M.M., L.O. Bjorn, J.F. Bornman, S.D. Flint, G. Kulandaivelu, A.H. Teramura, and M. Tevini (1998), "Effects of increased solar ultraviolet radiation on terrestrial ecosystems," *Photochemistry and Photobiology B: Biology* 46:40-52.

CIESIN (Consortium for International Earth Science Information Network) website. Accessed December 2003. "Overview of Health Effects from Increased Ultraviolet-B Exposure due to Ozone Depletion." Available at <http://www.ciesin.org/TG/HH/ozover.html>.

Chin, Lynda, Jason Pomerantz, David Polsky, Mark Jacobson, Carlos Cohen, Carlos Cordon-Cardo, James W. Horner II, and Ronald A. DePinho (1997), "Cooperative effects of *INK4a* and *ras* in melanoma susceptibility in vivo," *Genes & Development* 11:2822-2834.

Clegg, Limin X., Eric J. Feuer, Douglas N. Midthune, Michael P. Fay, and Benjamin F. Hankey (2002), "Impact of reporting delay and reporting error on cancer incidence rates and trends," *J. Natl. Cancer Inst.* 94:1537-1545.

Daniel, J. D., S. Solomon, R. W. Portmann, and R. R. Garcia (1999), "Stratospheric ozone destruction: the importance of bromine relative to chlorine," *J. Geophys. Res*. 104:23871-23880, 1999.

De Fabo, E.C. (2003), *Peer Reviewer Comments on the Health Module of the Human Health Benefits of Stratospheric Ozone Protection*, submitted to ICF Consulting in September 2003.

De Fabo, E.C. (2001), *Peer Reviewer Comments on Human Health Effects of Ozone Depletion from Stratospheric Aircraft*, submitted to ICF Consulting on April 26.

De Fabo, E.C. and F.P. Noonan (1983), “Mechanism of immune suppression by ultraviolet irradiation *in vivo*. I. Evidence for the existence of a unique photoreceptor in skin and its role in photoimmunology,” *J.Exp.Med.* 158:84-98.

de Gruijl, F.R. and P.D. Forbes (1995), "UV-induced skin cancer in a hairless mouse model," *BioEssays* 17:651-660.

de Gruijl, F.R., H.J.C.M. Sterenborg, P.D. Forbes, R.E. Davies, C. Cole, G. Kelfkens, H. van Weelden, H. Slaper, and J.C. van der Leun (1993), "Wavelength dependence of skin cancer induction by ultraviolet irradiation of albino hairless mice," *Cancer Research* 53:53-60.

de Gruijl, F.R, and J.C. Van der Leun (1993), “Influence of ozone depletion on the incidence of skin cancer: quantitative prediction,” in *Environmental UV Photobiology*, A.R. Young, L.O. Bjorn, J. Moan, and W. Nultsch (eds.), Plenum Press, New York:1-39.

De More, W. B., S. P. Sander, D. M. Golden, R. F. Hampson, M. J. Kurylo, C. J. Howard, A. R. Ravishankara, C. E. Kolb, and M. J. Molina (1997), Chemical Kinetics and Photochemical Data for Use in Stratospheric Modeling, JPL Publication 97-4, Jet Propulsion Laboratory, National Aeronautics and Space Administration, Pasadena.

D’errico, M., A. Calcagnile, and E. Dogliotti (1996), “Genetic alterations in skin cancer,” *Ann. Ist. Super Sanita* 32:53-63.

Elterman, L. (1968), “UV, visible, and IR attentuation for altitudes to 50 km,” *Air Force Cambridge Research Laboratories (AFCRL) Report-68-0153*, Bedford, MA.

Fears, T.R., and J. Scotto (1983), "Estimating increases in skin cancer morbidity due to increases in ultraviolet radiation exposure," *Cancer Investigation* 1:119-126.

Fidler, I.J. (1998), “Biology of melanoma metatasis,” in *Cutaneous Melanoma*, C.M. Balch, A.N. Houghton, A.J. Sober, and S-J. Soong (eds.), St. Louis: Quality Medical Publishing, Inc.

Gao, W., J.R. Slusser, J.H. Gibson, G. Scott, D.S. Bigelow, J. Kerr and B. McArthur (2001), “Direct-sun column ozone retrieval by the ultraviolet multi-filter rotating shadow-band radiometer and comparison with those from Brewer and Dobson spectrophotometers,” *Applied Optics* 40:3149-3155.

Geller, A.C., et. al. (1998), “Do pediatricians counsel families about sun protection?” *Archives of Pediatric and Adolescent Medicine* 152: 372-76.

Häder, D.P., H.D. Kumar, R.C. Smith, and R.C. Worrest (1998), “Effects on aquatic ecosystems,” *Photochemistry and Photobiology B: Biology* 46:53-68.

Harrison, S.L., R. MacLennan, R. Speare, and I. Wronski (1994), “Sun exposure and melanocytic naevi in young children in Townsville, Queensland,” *Lancet* 344:1529-1532.

Hiller, R., R. Sperduto, and F. Ederer (1983), "Epidemologic associations with cataracts in the 1971-1972 National Health and Nutrition Examination Survey," *American Journal of Epidemiology* 118:239-249.

Holman, C.D.J., and B.K. Armstrong (1984), “Cutaneous malignant melanoma and indicators of total accumulated exposure to the sun: an analysis separating histogenetic types,” *J. Nat. Cancer Inst.* 73:75-82.

Hutchinson, Ezzie (2003), “Sunburn effects dissected,” *Nature Reviews – Cancer*: 151.

Independent Review Panel (2002), *Suitability of CF_3I to Replace Halon 1301 as the Inerting Agent in Wing Fuel Tanks on the F-16 Aircraft*. Report prepared for the U.S. Department of Defense, Washington, D.C.

IPCC (Intergovernmental Panel on Climate Change) 2001. *Climate Change 2001: The Scientific Basis.* Contribution of Working Group I to the Third Assessment Report of the Intergovernmental Panel on Climate Change. Edited by J.T. Houghton, Y. Ding, D.J. Griggs, M. Noguer, P.J. van der Linden, X. Dai, K. Maskell, and C.A. Johnson. Cambridge, UK.

Jiang, W., H.N. Ananthaswamy, H.K. Muller, and M.L. Kripke (1999), "p53 protects against skin cancer induction by UV-B radiation," *Oncogene* 18:4247-53.

Kannan, K., N.E. Sharpless, J. Xu, R. O'Hagan, M. Bosenberg, and L. Chin (2003), "Components of the Rb pathway are critical targets of UV mutagenesis in a murine melanoma model," *PNAS* 100:1221-1225.

Kirk, J. T. O., B. R. Hargreaves, D. P. Morris, R. Coffin, B. David, D. Fredrickson, D. Karentz, D. Lean, M. Lesser, S. Madronich, J. H. Morrow, N. Nelson, and N. Scully (1994), "Measurements of UV-B radiation in two freshwater lakes: an instrument intercomparison," *Archiv für Hydrobiologie* 43:71-99.

Ko, M.K.W., N.D. Sze, C. Scott, J.M. Rodríguez, and D.K. Weisenstein (1998), "Ozone depletion potential of CH_3Br," *J. Geophys. Res.* 103:28187-28195.

Koepke, P., A. Bais, D. Balis, M. Buchwitz, H. De Backer, X. de Cabo, P. Eckert, P. Eriksen, D. Gillotay, A. Heikkila, T. Koskela, B. Lapeta, Z. Litynska, J. Lorente, B. Mayer, A. Renaud, A. Ruggaber, G. Schauberger, G. Seckmeyer, P. Seifert, A. Schmalwieser, H. Schwander, K. Vanicek, and M. Weber (1998), "Comparison of Models Used for UV Index Calculations," *Photochemistry and Photobiology (B:Photobiology)* 67:657-662.

Lantz, K. O., R. E. Shetter, C. A. Cantrell, S. J. Flocke, J. G. Calvert, and S. Madronich (1996), "Theoretical, actinometric, and radiometric determinations of the photolysis rate coefficient of NO_2 during MLOPEX II," *J. Geophysical Research* 101:14613-14629.

Ley, R.D. (1997), "Ultraviolet radiation A-induced precursors of cutaneous melanoma in Monodelphis domestica," *Cancer Research* 57:3682-3684.

Licht, L.E. and K.P. Grant (1997), "The effects of ultraviolet radiation on the biology of amphibians," *American Zoologist* 37:137-145.

Longstreth J.D. (1998), "Melanoma genesis: putative causes and possible mechanisms," in *Cutaneous Melanoma*, C.M. Balch, A.N. Houghton, A.J. Sober, and S-J. Soong (eds.), St. Louis: Quality Medical Publishing, Inc.

Longstreth, J., F.R. de Gruijl, M.L. Kripke, S. Abseck, F. Arnold, H.I. Slaper, G. Velders, Y. Takizawa, and J.C. van der Leun (1998), "Health risks," *Journal of Photochemistry and Photobiology B: Biology* 46:20-39.

Madronich, S. (1993a), "The atmosphere and UV-B radiation at ground level," in *Environmental UV Photobiology*, A.R. Young, L.O. Bjorn, J. Moan, and W. Nultsch (eds.), Plenum Press, New York, 1-39.

Madronich, S. (1993b), "UV radiation in the natural and perturbed atmosphere," in *UV-B Radiation and Ozone Depletion: Effects on Humans, Animals, Plants, Microorganisms, and Materials*, M. Trevini (ed.), Lewis Publisher, Boca Raton, 17-69.

Madronich, S. (1992), “Implications of recent total atmospheric ozone measurements for biologically active ultraviolet radiation reaching the Earth's surface,” *Geophysical Research Letters* 19:37-40.

Madronich, S. and F. R. de Gruijl (1994), “Stratospheric ozone depletion between 1979 and 1992: Implications for biologically-active ultraviolet-B radiation and non-melanoma skin cancer incidence,” *Photochemistry and Photobiology* 59:541-546.

Madronich, S. and F. R. de Gruijl (1993), “Skin cancer and UV radiation,” *Nature* 366:23.

Madronich, S., R.L. McKenzie, L.O. Bjorn, and M.M. Caldwell (1998), “Changes in ultraviolet radiation reaching the earth’s surface,” *J. Photochem. Photobiol. B* 46:5-19.

Madronich, S., E. Weatherhead, and S. Flocke (1996), “Trends in UV radiation,” *Int. J. Environ. Sci*. 51:183-198.

McKenzie, R. L., K. J. Paulin, and S. Madronich (1998), “Effects of snow cover on UV irradiances and surface albedo: A case study,” *Journal of Geophysical Research* 103:28785-28792.

McKinlay, A.F. and B.O. Diffey (1987), “A reference action spectrum for ultraviolet-induced erythema in human skin,” in *Human Exposure to Ultraviolet Radiation: Risks and Regulations*. W.R. Passchier and Bosnjakovic, B.F.M. (Eds); Elsevier, Amsterdam.

McPeters, R.D., Pawan K. Bhartia, Jay R. Herman, and A. Oaks (1996a), “Nimbus-7 total ozone mapping spectrometer (TOMS) data products user's guide,” NASA Reference Publication.

McPeters, R.D., S.M. Hollandsworth, L.E. Flynn, J.R. Herman, and C.J. Seftor (1996b), “Long-term ozone trends derived from 16-year combined Nimbus 7/Meteor 3 TOMS Version 7 Record," *Geophysical Research Letters* 23:3699-3702.

Merriam, J. C., S. Lofgren, R. Michael, P. Soderberg, J. Dillon, L. Zheng, and M. Ayala (2000),” An action spectrum for UV-B radiation and the rat lens,” *Invest. Opthalmol. Vis. Sci.* 41:2642-2647.

Moodycliffe, Angus, Dat Nghiem, Gavin Clydesdale, and Stephene Ullrich. 2000. “Immune suppression and skin cancer development: regulation by NKT cells.” Nature Immunology 1:521-525.

NEI/BPA (National Eye Institute/Prevent Blindness America) 2002. *Vision Problems in the U.S.: Prevalence of Adult Vision Impairment and Age-Related Eye Disease in America*. Available at http://www.nei.nih.gov/eyedata/pdf/VPUS.pdf

NASA/EPA 2001. *Human Health Effects of Ozone Depletion From Stratospheric Aircraft*. NASA/CR-2001-211160, September 2001.

NASA (National Aeronautics and Space Administration) 1999. *Models and Measurements Intercomparison II*, Langley Research Center, Hampton, VA, NASA/TM-1999-209554.

Nesbit, M., V. Setaluri, and M. Herlyn (1998), “Biology of melanocytes and melanoma,” in *Cutaneous Melanoma*, C.M. Balch, A.N. Houghton, A.J. Sober, and S-J. Soong (eds.), St. Louis: Quality Medical Publishing, Inc.

NOAA/National Weather Service (2002). “UV Index: Information,” Climate Prediction Center, web page last modified December 18, 2002. Available at http://www.cpc.ncep.noaa.gov/products/stratosphere/uv_index/uv_nature.html.

Noonan, Frances, Juan Recio, Hisashi Takayama, Paul Duray, Miriam Anvers, Walter Rush, Edward de Fabo, and Glenn Merlino. 2003. “Neonatal sunburn and melanoma in mice.” Nature 413:271-272.

Oriowo, Olanreqju M., Anthony P. Cullen, B. Ralph Chou, and Jacob G. Sivak (2001), “Action spectrum recovery for in vitro UV-induced cataract using whole lenses,” *Investigative Ophthalmology & Visual Science*, October 42:2596- 2602.

Pitcher, H.M., and J.D. Longstreth (1991), "Melanoma mortality and exposure to ultraviolet radiation: An empirical relationship," *Environment International* 17:7-21.

Pitts, D.G., A.P. Cullen, and P.D. Hacker (1977), “Ocular effects of ultraviolet radiation from 295 to 365 nm,” *Invest. Ophthalmol. Visual Sci.*16:932-939.

Pfeifer, G.P. and M.F. Denissenko (1998), “Formation and repair of DNA lesions in the p53 gene: relation to cancer mutations?” *Environ. Mol. Mutagen*, 31:197-205.

Ries, L.A.G., C.L. Kosary, B.F. Hankey, B.A. Miller, and B.K. Edwards (Eds.) (1999), *SEER Cancer Statistics Review, 1973-1996,* National Cancer Institute, Bethesda, MD.

Salih, Anya, Anthony Larkum, Guy Cox, Michael Kühl, and Ove Hoegh-Guldberg 2000. “Fluorescent pigments in corals are photoprotective.” *Nature* 408:850-853.

Scotto, J., H. Pitcher, and J.A.H. Lee (1991), "Indications of future decreasing trends in skin-melanoma mortality among whites in the United States," *Int. J. Cancer* 49:490-497.

Scotto, J., T.R. Fears, and J.F. Fraumeni Jr. (1983), "Incidence of nonmelanoma skin cancer in the United States," U.S. Department of Health and Human Services, (NIH) 82-2433, Bethesda, MD.

Serafino, G. and J. Frederick (1987), “Global modeling of the ultraviolet solar flux incident on the biosphere,” in *Assessing the Risks of Trace Gases that Can Modify the Stratosphere, Vol. VII*, U.S. Environmental Protection Agency, Washington, D.C.

Setlow, R.B. (1974), “The wavelengths in sunlight effective in producing skin cancer: A theoretical analysis,” *Proc. Natl. Acad. Sci. USA* 71:3363-3366.

Setlow, R.B., E. Grist, K. Thompson, and A.D. Woodhead (1993), "Wavelengths effective in induction of malignant melanoma," *Proc. Natl. Acad. Sci. USA* 90:6666-6670.

Shetter, R.E., C.A. Cantrell, K.O. Lantz, S.J. Flocke, J.J. Orlando, G.S. Tyndall, T.M. Gilpin, S. Madronich, and J. G. Calvert (1996), “Measurements and calculations of the photodissociation rate coefficient for $O_3 + h\nu \rightarrow O(^1D) + O_2$ during the MLOPEX II field campaign,” *J. Geophys. Res*. 101:14631-14641.

Shetter, R. E., A. H. McDaniel, C. A. Cantrell, S. Madronich, and J. G. Calvert (1992), “Actinometer and Eppley radiometer measurements of the NO_2 photolysis rate coefficient during MLOPEX,” *Journal of Geophysical Research 97*:10349-10359.

Stamnes, K., S. Tsay, W. Wiscombe, and K. Jayaweera (1988), “A numerically stable algorithm for discrete-ordinate-method radiative transfer in multiple scattering and emitting layered media,” *Appl. Opt*. 27:2502-2509.

Tang, X., S. Madronich, T. Wallington, and D. Calamari (1998), “Changes in tropospheric composition and air quality,” *Journal of Photochemistry and Photobiology B: Biology* 46:83-95.

Taylor HR, West SK, Rosenthal FS, Munoz B, Newland HS, Abbey H, Emmett EA. " Effect of ultraviolet radiation on cataract formation." N Engl J Med. 1988 Dec 1;319(22):1429-33.

UNEP (United Nations Environment Programme) (1989, 1991, 1994, 1998), "Environmental effects of ozone depletion," *UNEP Environmental Effects Panel Report*, United Nations Environmental Programme, Nairobi, Kenya.

U.S. Census Bureau Website (2000a), "(NP-D1-B) Quarterly Projections of the Resident Population by Age, Sex, Race, and Hispanic Origin: Middle Series, January 1, 1999 to January 1, 2101," http://www.census.gov/population/www/projections/natdet-D1B.html, accessed 2/24/2000.

U.S. Census Bureau Website (2000b), "Detailed State Projections by Single Year of Age, Sex, Race, and Hispanic Origin: 1995 to 2025," http://www.census.gov/population/www/projections/stproj.html, accessed 2/24/2000.

U.S. Census Bureau Website (1990), "1990 Census of Population and Housing," available at <http://factfinder.census.gov/servlet/DTTable?_ts=89647172958>.

U.S. EPA (2001), *Human Health Effects of Ozone Depletion from Stratospheric Aircraft*, In Publication, United States Environmental Protection Agency, Washington, D.C.

U.S. EPA (1999). Class I Ozone Depleting Substances and Class II Ozone Depleting Substances. EPA website. Available at http://www.epa.gov/ozone/ods.html and http://www.epa.gov/ozone/ods2.html.

U.S. EPA (1987), *Regulatory Impact Analysis: Protection of Stratospheric Ozone*, United States Environmental Protection Agency, Washington, D.C.

USGCRP (US Global Change Research Program) 1998. "Depletion and Recovery of the Ozone Layer: An Update of the Scientific Understanding." USGCRP Seminar, 23 September 1998. Available at <http://www.usgcrp.gov/usgcrp/seminars/980916FO.html> Accessed December 2003.

USSA (1976), "U.S. Standard Atmosphere," National Oceanic and Atmospheric Administration (NOAA), National Aeronautics and Space Administration (NASA), United States Air Force, Washington, D.C.

Weinstock, M. A. (1993), "Ultraviolet radiation and skin cancer: epidemiological data from the United States and Canada," in *Environmental UV Photobiology*, A.R. Young, L.O. Bjorn, J. Moan, and W. Nultsch (eds.), Plenum Press, New York, 1-39.

WMO (1990), *Scientific Assessment of Ozone Depletion: 1989*. World Meteorological Organization Global Ozone Research and Monitoring Project -- Report No. 20.

WMO (1992), *Scientific Assessment of Ozone Depletion: 1991*. World Meteorological Organization Global Ozone Research and Monitoring Project -- Report No. 25.

WMO (1995), *Scientific Assessment of Ozone Depletion: 1994*. World Meteorological Organization Global Ozone Research and Monitoring Project -- Report No. 37.

WMO (1999), *Scientific Assessment of Ozone Depletion: 1998*. World Meteorological Organization Global Ozone Research and Monitoring Project -- Report No. 44.

WMO (2003). *Scientific Assessment of Ozone Depletion: 2002*. WMO Global Ozone Research and Monitoring Project - Report No. 47, Geneva, 2002.

Wuebbles, D.J., R. Kotamarthi, and K.O. Patten (1999), “Updated evaluation of Ozone Depletion Potentials for Chlorobromomethane (CH2ClBr) and 1-bromo-propane (CH2BrCH2CH3),” *Atmospheric Environment* 33:1641-1643.

Wuebbles (2003), Personal Communication with Dr. Don Wuebbles, Department of Atmospheric Sciences, University of Illinois, Urbana, IL, March 6, 2003.

Zanetti, R., S. Franceschi, S. Rosso, S. Colonna, and E. Bidoli (1992), *Eur. J. Cancer* 28A:1172-1176.

12. Glossary

Action spectrum — Experimentally-derived plots describing the relative effectiveness of each wavelength of UV-A and UV-B radiation in the induction of a specific health effect (e.g., skin cancer, sunburn). Action spectra are used as weighting functions in order to estimate the potential of a particular UV exposure to induce adverse health effects.

BAF (biological amplification factor) — BAFs are equal to slope of the dose-response curve (see "dose-response relationship").

Basal cell carcinoma (BCC) — BCC is the most common type of skin cancer. It is caused primarily by exposure to ultraviolet radiation, and occurs most frequently among light-skinned persons over age 45. Although BCC has a very high cure rate, in rare instances it can be lethal.

Baseline — The AHEF defines the "baseline" incidence and/or mortality for skin cancer as what would be expected to occur in the future if the concentration of stratospheric ozone remained fixed at 1979-1980 levels.

Birth cohorts — Individuals assigned by year of birth into groups for further study. The AHEF uses the results of these birth cohort studies to create and project a baseline estimate of skin cancer incidence and/or mortality.

Column ozone — The amount of ozone (measured in Dobson units) contained in a vertical column of air extending from the Earth's surface to an orbiting satellite designed to measure ozone concentrations. Roughly 90 to 95% of column ozone is in the stratosphere with small amounts (5-10%) in the troposphere.

Cutaneous malignant melanoma (CMM) — CMM is the most serious type of skin cancer. It occurs most frequently in light-skinned persons over age 40 with light complexions and hair color.

Dobson unit — A measure of the thickness of the ozone. For a vertical column of ozone compressed at 0 degrees Celsius and 1 atmosphere pressure, a Dobson unit is defined to be 0.01 millimeter thick.

Dose metrics — Measures used to express the amount of UV radiation received over a specific time period (i.e., the dose). Examples are peak hour dose, daily dose, or cumulative doses for a month or for an entire year.

Dose-response relationship — The relationship between an effect (e.g., skin cancer) and the exposure (e.g., UV radiation) producing that effect. If plotted on a log-log scale, BAFs are equal to the slope of the dose-response curve.

Econometric — A statistical technique that enables analysts to determine to what degree one specific variable (e.g., UV exposure) may be responsible for a specific effect (e.g., skin cancer) thought to be caused by the interaction of several related variables. For example, it is hypothesized that age, birth year, and UV exposure all play a role in the etiology of CMM. Because ODS control policies can only reduce one of these risk factors (i.e., the amount of UV-B reaching the ground can be reduced by a thicker ozone layer), econometric estimation is used to isolate and quantify the contribution of UV exposure to CMM incidence and mortality.

Equivalent effective stratospheric chlorine (EESC) — An expression of the ozone-depleting capability of a substance and its degradation products, expressed in terms of chlorine molecules. The EESC of substances that contain bromine instead of chlorine can be calculated by using a bromine efficiency factor ("alpha factor") that defines the number of chlorine molecules needed to deplete one molecule of

ozone as efficiently as one bromine molecule. The AHEF assumes that 55 chlorine molecules are needed to deplete a molecule of ozone as efficiently as one bromine molecule.

Incidence — For the purposes of this paper, the incidence is defined as the number of new cases of a given health effect that develop each year.

Isotropic ground reflectivity — The assumption that all wavebands of UV radiation striking the Earth's surface are reflected equally in all directions.

Latency — The length of time between the exposure to a stressor (e.g., UV-B radiation) and the response to that stressor (e.g., skin cancer).

No further ozone depletion — The total column ozone observed in the 1979-1980 timeframe is defined as the baseline against which the impacts of future ozone changes are measured. These column ozone levels are assumed in the AHEF to remain constant in the baseline projections.

Ozone-depleting substances (ODS) — A group of chemicals containing chlorine and/or bromine atoms that destroy ozone molecules in the stratosphere. Emissions of these chemicals are the chief cause of anthropogenic stratospheric ozone depletion and have been targeted for phaseout by the Montreal Protocol and its amendments.

Prevalence — Refers to the total number of existing cases of a given health effect, at a specific time, as opposed to new cases ("incidence").

Solar UV irradiance — UV radiation from the sun reaching the Earth's surface.

Solar zenith angle — The solar zenith angle is the angle of the sun's direction with respect to the local upward vertical, measured in degrees from 0^o (overhead sun) to 90^o (sun at the horizon).

Spectral irradiance – The radiation at the Earth's surface measured across the full UV spectrum.

Squamous cell carcinoma (SCC) — SCC is the second most common form of NMSC in humans. It is thought to be primarily caused by exposure to ultraviolet radiation. SCC may grow quickly and spread to other parts of the body, making it a dangerous form of skin cancer.

Total Ozone Mapping Spectrometer (TOMS) — A satellite-based instrument to measure the total vertical column of ozone in the atmosphere. The method is based on detecting UV radiation backscattered by the lower atmosphere after it passes through stratospheric ozone. The amount of ozone is determined by comparing the backscattered radiation at several pairs of wavelengths, selected for different sensitivity to absorption by ozone. The TOMS instrument aboard the Nimbus-7 satellite provided nearly continuous global ozone data from late 1978 to early 1993. Shorter data records from more recent satellites (Meteor-3, Earth Probe) are also available.

Ultraviolet (UV) radiation — Ultraviolet radiation is a portion of the electromagnetic spectrum with wavelengths shorter than visible light. The sun produces UV radiation, which is commonly split into three arbitrarily-defined bands: UV-A, UV-B, and UV-C. Because the AHEF relies on action spectra equations to estimate health effects, it is not necessary to define the exact wavelengths that make up each band. UV-A is not absorbed by ozone. UV-B is mostly absorbed by ozone, although some reaches the Earth. UV-C is completely absorbed by ozone and normal oxygen. The AHEF uses the percentage change in UV exposure multiplied by the appropriate BAF and the age-specific baseline incidence or mortality rate to predict future changes in human health effects. Although the AHEF considers only solar UV radiation, UV radiation from artificial sources (e.g., tanning beds, welding, mercury lamps) are also associated with adverse health effects.

UV-A — A band of ultraviolet radiation with wavelengths from 320-400 nanometers produced by the sun. UV-A is not absorbed by ozone. This band of radiation has wavelengths just shorter than visible violet light.

UV-B — A band of ultraviolet radiation with wavelengths from 280-320 nanometers produced by the sun. UV-B has been associated with human health impacts and is particularly effective at damaging DNA. UV-B has been identified as a cause of melanoma and other types of skin cancer as well as cataract and suppression of the immune system. It has also been linked to damage to some materials, crops, and marine organisms. The ozone layer protects the Earth against most solar UV-B radiation.

UV-C — A band of ultraviolet radiation with wavelengths shorter than 280 nanometers. UV-C is extremely dangerous, but it is completely absorbed by ozone (at wavelengths between 240 and 280 nm) and normal oxygen (O_2) (at wavelengths between 200 and 280 nm), and hence does not reach the Earth's surface.

Appendix A. Updates Made to the Original AHEF

Since its inception in the early 1980s, the AHEF has undergone a series of updates to ensure that it reflects the current state of knowledge about the relationships between ozone depletion, UV exposure, and human health endpoints. Thirteen revisions or updates have been performed since 1985. Of these, four involve significant changes to the results predicted by the model:

- The bromine alpha factor was changed from 40 to 55 to account for recent findings that bromine emissions are more potent in depleting ozone than previously thought.
  - Impact: Medium-sized increase in results (roughly 30%).

- For projecting CMM mortality and incidence, BAFs were developed using the SCUP-h action spectrum in place of the DNA-h action spectrum. Since action spectra specific to CMM have not yet been developed, the SCUP-h was also chosen for modeling CMM, as it is the only action spectrum derived based on the induction of skin cancer. Peer reviewed articles and studies support this.
  - Impact: Large decreases in estimated health effects. CMM incidence and mortality rates estimated using the SCUP-h action spectrum are approximately 40% lower than those developed using the DNA-h action spectrum.

- NMSC mortality rates were revised based on NCI NMSC mortality data and well-established statistical techniques for estimating BAFs. Previous versions of the AHEF used a 1 percent incidence-to-mortality assumption to predict mortality for NMSC because mortality data for NMSC was lacking. Also, the BAF for modeling MNSC mortality is now based on the SCUP-h action spectrum, and not the DNA-h action spectrum that was used in previous versions of the AHEF. Developments in the skin cancer literature suggest that SCUP-h is the most accurate action spectrum available for NMSC, because it covers a broader spectral range and is more appropriate than use of the DNA-h action spectrum.
  - Impact: The combined impact of these two changes is a large decrease in NMSC mortality estimates (by approximately 80%). These lower NMSC mortality estimates reflect more accurate data on NMSC mortality instead of relying on unfounded assumptions regarding the correlation of NMSC incidence and mortality.

- Cataract incidence was removed as a health effect assessed by the AHEF. This decision was based on recent analyses that showed weak dose-response relationship between cataract incidence and UV exposure in the U.S. population based on readily available data.
  - Impact: Small decrease in projected health effects. When cataract incidence was included in the AHEF projections, cataracts accounted for only about 5% of the monetized benefits.

A number of minor updates also ensure that the AHEF uses the most recent data and reflects state-of-the-art knowledge about issues related to stratospheric ozone depletion and the prediction of UV-mediated human health effects. These updates include the following:

- The BAF used to project SCC incidence was updated from 2.5 to 2.6, based on new research conducted by de Gruijl and Forbes (1995). The new BAF is derived based on the SCUP-h action spectrum instead of the SCUP-m action spectrum, which was used in previous studies (e.g., Van der Leun and De Gruijl 1994, de Gruijl and Van der Leun 1994). The SCUP-m spectrum was derived on the basis of the induction of SCC in hairless mice. The SCUP-h spectrum is an adjusted spectrum, corrected for human skin transmission to account for differences in epidermal thickness and the number of hair follicles per unit area.

- Impact: Small increase in estimated NMSC incidence and mortality. Projected SCC incidence rates estimated using the SCUP-h action spectrum are approximately 4% higher than those developed using the SCUP-m action spectrum.

- Methyl bromide baseline usage estimates were updated, as current and future methyl bromide uses are lower than had been originally projected in the older version of the AHEF (due to both a decline in baseline use and to future controls).
  - Impact: Small to very small decrease in total cancer incidence and mortality.

- Population projections through 2050 were updated for the United States by state, race, and sex to reflect more recent information (i.e., 1990 data and 1998 mid-level projections from the U.S. Census Bureau).
  - Impact: Negligible change in results.

- The NCI CMM mortality data were tied to the SEER CMM incidence and mortality data instead of relying on data from the 1970s, to produce more consistent CMM incidence estimates.
  - Impact: Negligible change in results.

- Satellite measurements of stratospheric ozone were updated, based on new data provided by NASA.
  - Impact: Negligible change in results.

- The AHEF's TUV inputs (which provide ground-level irradiance through time and by latitude) were updated to reflect updates and refinements made directly to the TUV model, all of which have been published in peer reviewed journals (Madronich 1992, 1993; Madronich and de Gruijl 1993, Madronich et al. 1996, 1998). In addition, the accuracy of the TUV has been demonstrated in a number of comparisons to direct measurements of UV radiation at the Earth's surface (e.g., Shetter et al. 1992, 1996; Kirk et al. 1994; Lantz et al. 1996). In addition, since 1989, the TUV model has been used in the scientific evaluations of ozone depletion (WMO 1990, 1992, 1995, 1999) and related environmental consequences (UNEP 1989, 1991, 1994, 1998) as mandated under the Montreal Protocol.
  - Impact: Two to four percent change in absolute UV irradiance used to estimate health effects. Because these changes apply to both the baseline and policy scenarios, there are only second order (i.e., negligible) impacts on incremental health effects estimates.

- The capability to use age-weighted UV exposures was added to the AHEF, to place a greater emphasis on exposures received early in an individual's life. This weighting changes the total number of predicted cases or deaths by up to 11 percent. This improvement allows an evaluation of the manner in which cases or deaths are distributed across age cohorts and generations, for comparison purposes. This is particularly useful for exploring the hypothesis that early life and intense UV exposures are disproportionately responsible for CMM incidence and mortality.
  - Impact: Adds flexibility to the model; only changes results if age-weighting is being evaluated (i.e., for whole-life exposure, results are unchanged).

- The modular structure and design of the AHEF's input data files and routines were refined, to efficiently handle future enhancements and additions. For example, adding a new action spectrum has been greatly simplified. Similarly, when relationships between UV exposure and other benefit categories—human and non-human—are available, these can be easily added to the new AHEF once the appropriate data become available. Possible enhancements and additions to the new AHEF include human immune system impairment, and effects on agricultural, terrestrial, and aquatic ecosystems.
  - Impact: Increases model flexibility by allowing new impacts to be evaluated; no impacts on current results.

- The design of the AHEF's output data files and routines were refined to produce more detailed outputs that easily summarize results from a variety of perspectives, such as total health effects, incremental effects over time, at finer levels of resolution (resolution increased from a 100 cases level to a one case level).
    - Impact: Increased model resolution (i.e., allows smaller impacts to be evaluated); no impacts on results.

Appendix B: Supplementary Tables for Baseline Incidence and Mortality Projections

This appendix presents supplementary information for the determination of baseline incidence and mortality projections for both cutaneous malignant melanoma (CMM) and non-melanoma skin cancer NMSC, as discussed in Section 3 of the report.

Table B-1. Regional Definitions for Mortality Data Set

40^{o} N to 50^{o} N	30^{o} N to 40^{o} N	20^{o} N to 30^{o} N
Alaska	California (North)*	Alabama
Connecticut	Colorado	Arizona
Idaho	Delaware	Arkansas
Maine	District of Columbia	California (South)*
Massachusetts	Illinois	Florida
Michigan	Indiana	Georgia
Minnesota	Iowa	Hawaii
Montana	Kansas	Louisiana
New Hampshire	Kentucky	Mississippi
New York	Maryland	New Mexico
North Dakota	Missouri	South Carolina
Oregon	Nebraska	Texas
Rhode Island	Nevada	
South Dakota	New Jersey	
Vermont	North Carolina	
Washington	Ohio	
Wisconsin	Oklahoma	
	Pennsylvania	
	Tennessee	
	Utah	
	Virginia	
	West Virginia	
	Wyoming	

* Counties in California were segregated into either the South or Middle region. The population was split based upon county population data from the Demographic Research Unit of the California Department of Finance.

Table B-2. CMM Mortality Rates (per 100,000) for White Males by Cohort and Year of Death, U.S. Totals

Cohort Mid Birth Year	Year of Death						
	1950-54	1955-59	1960-64	1965-69	1970-74	1975-79	1980-84
1865	6.324						
1870	5.802	8.006					
1875	4.879	7.079	10.273				
1880	3.861	5.833	7.344	10.522			
1885	3.379	4.408	5.968	8.917	12.992		
1890	3.144	3.921	5.560	8.264	9.861	15.229	
1895	2.434	3.311	4.511	6.078	9.050	12.475	17.863
1900	1.895	2.618	3.745	5.218	6.784	10.513	14.613
1905	1.705	2.583	3.491	4.389	6.530	9.297	12.934
1910	1.347	2.111	3.051	3.959	5.424	7.793	11.424
1915	1.359	1.771	2.496	3.684	4.667	7.047	9.659
1920	0.987	1.472	2.277	3.243	4.243	6.137	7.537
1925	0.780	1.227	1.867	2.658	3.759	5.354	6.996
1930	0.419	0.779	1.555	2.294	2.672	4.435	5.547
1935	0.117	0.377	0.883	1.482	2.047	2.995	4.062
1940	0.015	0.131	0.526	0.886	1.509	2.423	3.608
1945	0.003	0.018	0.159	0.433	0.998	1.690	2.546
1950	0.013	0.013	0.020	0.175	0.598	1.151	1.866
1955		0.007	0.007	0.009	0.150	0.475	0.987
1960			0.012	0.009	0.025	0.138	0.382
1965				0.005	0.007	0.013	0.071
1970					0.006	0.008	0.008
1975						0.009	0.009
1980							0.003

Table B-3. CMM Mortality Rates (per 100,000) for White Females by Cohort and Year of Death, U.S. Totals

Cohort Mid Birth Year	Year of Death						
	1950-54	1955-59	1960-64	1965-69	1970-74	1975-79	1980-84
1865	5.528						
1870	3.856	6.281					
1875	3.853	4.838	7.106				
1880	3.077	4.257	5.126	7.226			
1885	2.200	3.223	4.374	6.111	7.322		
1890	2.244	2.934	3.949	5.107	6.480	9.065	
1895	1.822	2.435	3.417	4.051	5.707	7.735	10.521
1900	1.490	2.020	2.637	3.425	4.491	5.999	8.973
1905	1.294	1.811	2.270	2.917	3.908	5.559	6.565
1910	1.183	1.770	1.917	2.686	3.264	4.653	5.763
1915	1.005	1.370	1.901	2.335	2.944	3.700	4.413
1920	0.858	1.286	1.665	1.991	2.650	3.225	4.120
1925	0.611	0.971	1.469	1.987	2.382	2.979	3.482
1930	0.404	0.732	1.109	1.486	2.167	2.794	3.171
1935	0.098	0.330	0.719	1.116	1.435	2.082	2.721
1940	0.015	0.092	0.267	0.646	0.998	1.625	2.156
1945	0.006	0.018	0.118	0.336	0.725	1.051	1.502
1950	0.014	0.011	0.016	0.107	0.304	0.730	1.155
1955		0.017	0.005	0.019	0.101	0.387	0.648
1960			0.007	0.002	0.010	0.097	0.294
1965				0.005	0.000	0.011	0.079
1970					0.003	0.000	0.006
1975						0.009	0.003
1980							0.012

Appendix C. Supplementary Tables for Stratospheric Ozone Depletion Modeling

Tables C-1 through C-4b of this appendix present the ODS controls for both non-Article 5 and Article 5 countries under each of the policy scenarios examined (i.e., the original Montreal Protocol, the London Amendments of 1990, the Copenhagen Amendments of 1992, and the Montreal Adjustments of 1997) as discussed in Section 4.3 of the report. Table C-5 lists the types of CFCs and HCFCs that are included in the phaseout schedules.

Table C-1. Original Montreal Protocol (1987)

Controls for Non-Article 5 Nations			Controls for Article 5 Nations		
	CFCs	Halons		CFCs	Halons
Base Year:	1986	1986	Base Year:	1996	1996
Controls			Controls		
Year	Percent of Base Year	Percent of Base Year	Year	Percent of Base Year	Percent of Base Year
July 1, 1989	100%	---	July 1, 1999	100%	---
1990	100%	---	2000	100%	---
1991	100%	---	2001	100%	---
1992	100%	100%	2002	100%	100%
1993	80%	100%	2003	80%	100%
1994	80%	100%	2004	80%	100%
1995	80%	100%	2005	80%	100%
1996	80%	100%	2006	80%	100%
1997	80%	100%	2007	80%	100%
1998	50%	100%	2008	50%	100%

Table C-2. London Amendments (1990)

Controls for Non-Article 5 Nations					Controls for Article 5 Nations				
	CFCs	Halons	Carbon Tet. (CCl_4)	Methyl Chlor. (CH_3CCl_3)		CFCs	Halons	Carbon Tet. (CCl_4)	Methyl Chlor. (CH_3CCl_3)
Base Year:	1986	1986	1989	1989	Base Year:	1996	1996	1999	1999
Controls					Controls				
Year	Percent of Base Year	Percent of Base Year	Percent of Base Year	Percent of Base Year	Year	Percent of Base Year	Percent of Base Year	Percent of Base Year	Percent of Base Year
July 1, 1989	100%	---	---	---	July 1, 1999	100%	---	---	--
1990	100%	---	---	---	2000	100%	---	---	---
1991	100%	---	---	---	2001	100%	---	---	---
1992	100%	100%	---	---	2002	100%	100%	---	---
1993	100%	100%	---	100%	2003	100%	100%	---	100%
1994	100%	100%	---	100%	2004	100%	100%	---	100%
1995	50%	50%	15%	70%	2005	50%	50%	15%	70%
1996	50%	50%	15%	70%	2006	50%	50%	15%	70%
1997	15%	50%	15%	70%	2007	15%	50%	15%	70%
1998	15%	50%	15%	70%	2008	15%	50%	15%	70%
1999	15%	50%	15%	70%	2009	15%	50%	15%	70%
2000	0%	0%	0%	30%	2010	0%	0%	0%	30%
2001	0%	0%	0%	30%	2011	0%	0%	0%	30%
2002	0%	0%	0%	30%	2012	0%	0%	0%	30%
2003	0%	0%	0%	30%	2013	0%	0%	0%	30%
2004	0%	0%	0%	30%	2014	0%	0%	0%	30%
2005	0%	0%	0%	0%	2015	0%	0%	0%	0%

Table C-3a. Copenhagen Amendments (1992) – Controls for Non-Article 5 Nations

	CFCs	Halons	Carbon Tetrachloride (CCl_4)	Methyl Chloroform (CH_3CCl_3)	HCFCs*	Methyl Bromide (CH_3Br)**
Base Year:	1986	1986	1989	1989	1989 (3.1%)	1991
Controls						
Year	Percent of Base Year	Percent of Base Year	Percent of Base Year	Percent of Base Year	Percent of Base Year	Percent of Base Year
July 1, 1989	100%	---	---	---	---	---
1990	100%	---	---	---	---	---
1991	100%	---	---	---	---	---
1992	100%	100%	---	---	---	---
1993	80%	100%	---	100%	---	---
1994	25%	0%	---	50%	---	---
1995	25%	0%	15%	50%	---	100%
1996	0%	0%	0%	0%	100%	100%
1997	0%	0%	0%	0%	100%	100%
1998	0%	0%	0%	0%	100%	100%
1999	0%	0%	0%	0%	100%	100%
2000	0%	0%	0%	0%	100%	100%
2001	0%	0%	0%	0%	100%	100%
2002	0%	0%	0%	0%	100%	100%
2003	0%	0%	0%	0%	100%	100%
2004	0%	0%	0%	0%	65%	100%
2005	0%	0%	0%	0%	65%	100%
2010	0%	0%	0%	0%	35%	100%
2015	0%	0%	0%	0%	10%	100%
2020	0%	0%	0%	0%	0.5%	100%
2030	0%	0%	0%	0%	0%	100%

* The baseline HCFC consumption, or HCFC cap, was calculated as the total ODP-weighted HCFC consumption in 1989 plus 3.1 percent of the ODP-weighted CFC consumption in 1989.

** The methyl bromide freeze did not apply to post-harvesting uses (i.e., quarantine and pre-shipment).

Table C-3b. Copenhagen Amendments (1992) - Controls for Article 5 Nations

	CFCs	Halons	Carbon Tetrachloride (CCl_4)	Methyl Chloroform (CH_3CCl_3)
Base Year:	1996	1996	1999	1999
Controls				
Year	Percent of Base Year	Percent of Base Year	Percent of Base Year	Percent of Base Year
July 1, 1999	100%	---	---	---
2000	100%	---	---	---
2001	100%	---	---	---
2002	100%	100%	---	---
2003	80%	100%	---	100%
2004	80%	100%	---	100%
2005	50%	50%	15%	70%
2006	50%	50%	15%	70%
2007	15%	50%	15%	70%
2008	15%	50%	15%	70%
2009	15%	50%	15%	70%
2010	0%	0%	0%	30%
2011	0%	0%	0%	30%
2012	0%	0%	0%	30%
2013	0%	0%	0%	30%
2014	0%	0%	0%	30%
2015	0%	0%	0%	0%

Note: The Copenhagen Amendments did not change the Article 5 control schedule.

Table C-4a. Montreal Adjustment (1997) - Controls for Non-Article 5 Nations

	CFCs	Halons	Carbon Tetrachloride (CCl_4)	Methyl Chloroform (CH_3CCl_3)	HCFCs*	Methyl Bromide (CH_3Br)**
Base Year:	1986	1986	1989	1989	1989 (2.8%)	1991
Controls						
Year	Percent of Base Year	Percent of Base Year	Percent of Base Year	Percent of Base Year	Percent of Base Year	Percent of Base Year
July 1, 1989	100%	---	---	---	---	---
1990	100%	---	---	---	---	---
1991	100%	---	---	---	---	---
1992	100%	100%	---	---	---	---
1993	80%	100%	---	100%	---	---
1994	25%	0%	---	50%	---	---
1995	25%	0%	15%	50%	---	100%
1996	0%	0%	0%	0%	100%	100%
1997	0%	0%	0%	0%	100%	100%
1998	0%	0%	0%	0%	100%	100%
1999	0%	0%	0%	0%	100%	75%
2000	0%	0%	0%	0%	100%	75%
2001	0%	0%	0%	0%	100%	50%
2002	0%	0%	0%	0%	100%	50%
2003	0%	0%	0%	0%	100%	30%
2004	0%	0%	0%	0%	65%	30%
2005	0%	0%	0%	0%	65%	0%
2010	0%	0%	0%	0%	35%	0%
2015	0%	0%	0%	0%	10%	0%
2020	0%	0%	0%	0%	0.5%	0%
2030	0%	0%	0%	0%	0%	0%

* The baseline HCFC consumption, or HCFC cap, is calculated as the total ODP-weighted HCFC consumption in 1989 plus 2.8 percent of the ODP-weighted CFC consumption in 1989.

** The methyl bromide freeze does not apply to post-harvesting uses (i.e., quarantine and pre-shipment).

Table C-4b. Montreal Adjustment (1997) - Controls for Article 5 Nations

	CFCs	Halons	Carbon Tetrachloride (CCl_4)	Methyl Chloroform (CH_3CCl_3)	HCFCs	Methyl Bromide (CH_3Br)*
Base Year:	1996	1996	1999	1999	2015	Average of 1995-1998
Controls						
Year	Percent of Base Year	Percent of Base Year	Percent of Base Year	Percent of Base Year	Percent of Base Year	Percent of Base Year
July 1, 1999	100%	---	---	---	---	---
2000	100%	---	---	---	---	---
2001	100%	---	---	---	---	---
2002	100%	100%	---	---	---	100%
2003	80%	100%	---	100%	---	100%
2004	80%	100%	---	100%	---	100%
2005	50%	50%	15%	70%	---	80%
2006	50%	50%	15%	70%	---	80%
2007	15%	50%	15%	70%	---	80%
2008	15%	50%	15%	70%	---	80%
2009	15%	50%	15%	70%	---	80%
2010	0%	0%	0%	30%	---	80%
2011	0%	0%	0%	30%	---	80%
2012	0%	0%	0%	30%	---	80%
2013	0%	0%	0%	30%	---	80%
2014	0%	0%	0%	30%	---	80%
2015	0%	0%	0%	0%	---	0%
2016	0%	0%	0%	0%	100%	0%
2040	0%	0%	0%	0%	0%	0%

* The methyl bromide freeze does not apply to post harvesting uses (i.e., quarantine and pre-shipment).

Table C-5. Class I and Class II Ozone-Depleting Substances

Class I					
Group I (CFCs)*					
CFC-11	CFC-12	CFC-113	CFC-114	CFC-115	
Group II (halons)*					
halon-1211	halon-1301	halon-2402			
Group III (other CFCs)*					
CFC-13	CFC-111	CFC-112	CFC-211	CFC-212	CFC-213
CFC-214	CFC-215	CFC-216	CFC-217		
Group IV					
carbon tetrachloride					
Group V					
methyl chloroform					
Group VI					
methyl bromide					
Group VII					
$C_3H_2F_3Br_3$	$C_3H_3FBr_4$	C_2H_4Br	$C_3H_3F_3Br_2$	$C_2HF_3Br_2$	$C_3H_2F_5Br$
$C_2H_2F_3Br$	$C_3H_4FBr_3$	C_3HFBr_6	$C_3H_4F_3Br$	$C_3H_3F_2Br_3$	C_2HFBr_4
$C_3H_4F_2Br_2$	$C_3H_5F_2Br$	$C_3HF_2Br_5$	CH_2FBr	$C_2H_3F_2Br$	$C_2H_2FBr_3$
$C_2H_2F_2Br_2$	$C_2HF_2Br_3$	$C_2H_3FBr_2$	C_2HF_4Br	C_3H_6FBr	$C_3HF_3Br_4$
$C_3HF_4Br_3$	$CHFBr_2$	C_3HF_6Br	$C_3HF_5Br_2$	$C_3H_2FBr_5$	
$C_3H_2F_2Br_4$	CHF_2 Br (HBFC-22B1)	$C_3H_2F_4Br_2$	$C_3H_5FBr_2$	$C_3H_3F_4Br$	
Class II (HCFCs)					
HCFC-21	HCFC-22	HCFC-31	HCFC-121	HCFC-122	HCFC-123
HCFC-124	HCFC-131	HCFC-132	HCFC-133	HCFC-141	HCFC-142
HCFC-221	HCFC-222	HCFC-223	HCFC-224	HCFC-225	HCFC-226
HCFC-231	HCFC-232	HCFC-233	HCFC-234	HCFC-235	HCFC-241
HCFC-242	HCFC-243	HCFC-244	HCFC-251	HCFC-252	HCFC-253
HCFC-261	HCFC-262	HCFC-271			

Isomers of the listed chemicals are also included in the ODS phaseout.
Source: U.S. EPA Website 1999.

Appendix D: Comparison of AHEF and WMO Predicted Ozone Concentrations

To validate the AHEF's projections of stratospheric ozone concentrations, the AHEF ozone level predictions under the Montreal Adjustments (see Figure D- 1) were compared to measurements and modeling reported in Figure 11-14 of the *Scientific Assessment of Ozone Depletion, 1998* by the World Meteorological Organization's (WMO 1999) Global Ozone Research and Monitoring Project (see Figure D- 2). The WMO graph of ozone levels also applied the Montreal Adjustments policy scenario in predicting chlorine and bromine levels in the atmosphere and resulting stratospheric ozone column levels. Both the AHEF and WMO projections are based on annually- and monthly-averaged stratospheric ozone concentrations for different latitudes as measured by NASA's Nimbus-7 Total Ozone Mapping Spectrometer (TOMS) satellite. The most recent ozone assessment conducted by the WMO (2003) does not provide similar predictions of column ozone concentration that are comparable to AHEF output (in terms of format and type of data reported), therefore, direct comparison with the AHEF was not possible.[28]

Figure D- 1. Stratospheric Ozone Column Levels at 40-50°N: AHEF Predictions, Montreal Adjustments

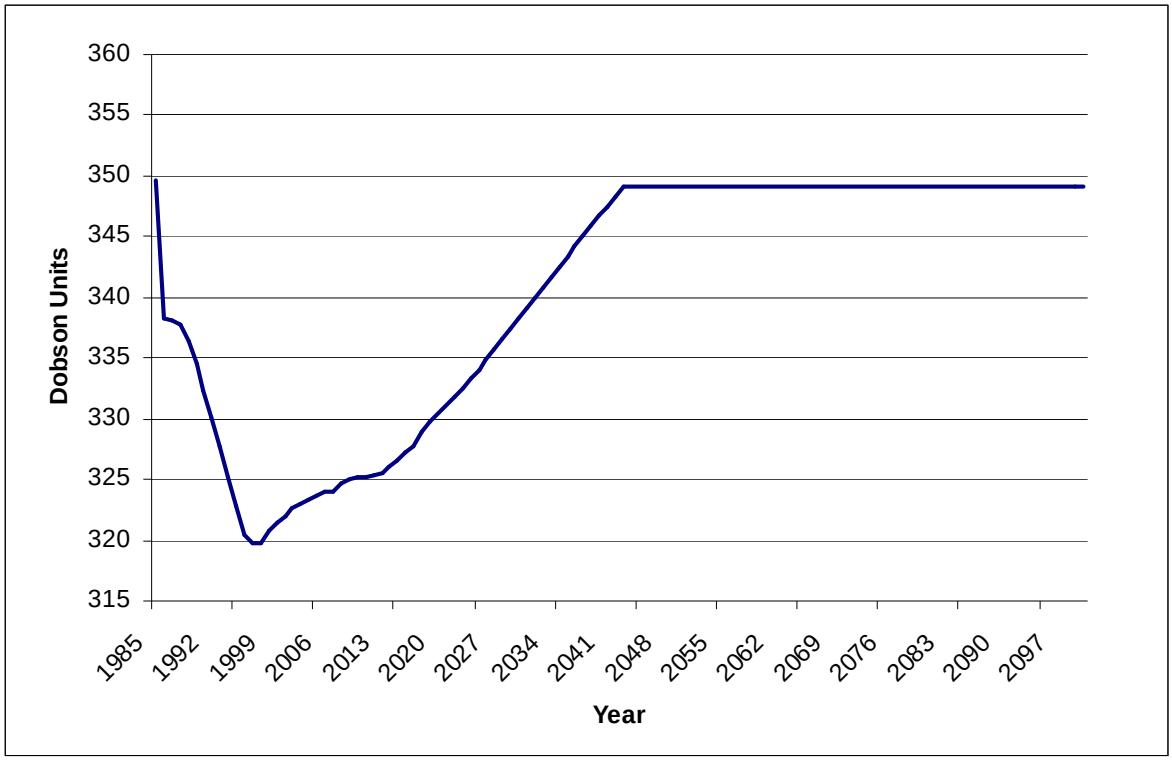

[28] The WMO (2003) report does provide updated estimates of projected EESC levels (Figure 1-23), but does not provide updated ozone depletion estimates associated with these EESC projections. Therefore, the 2003 WMO projections are insufficient for use in conducting a comparative analysis with the AHEF. Further, the 2003 assessment incorporated revised assumptions regarding HCFC production levels. Thus, the WMO (2003) EESC projections are lower than those projected in WMO (1999). Without the revised ozone concentrations projections associated with this lower EESC scenario, it is unclear how the latest WMO projections compare to the AHEF in terms of ozone concentration predictions—and/or how these changes in ozone concentrations would impact changes in incremental health effects.

Figure D- 2. Stratospheric Ozone Column Levels at 45°N: WMO Measurements/Predictions

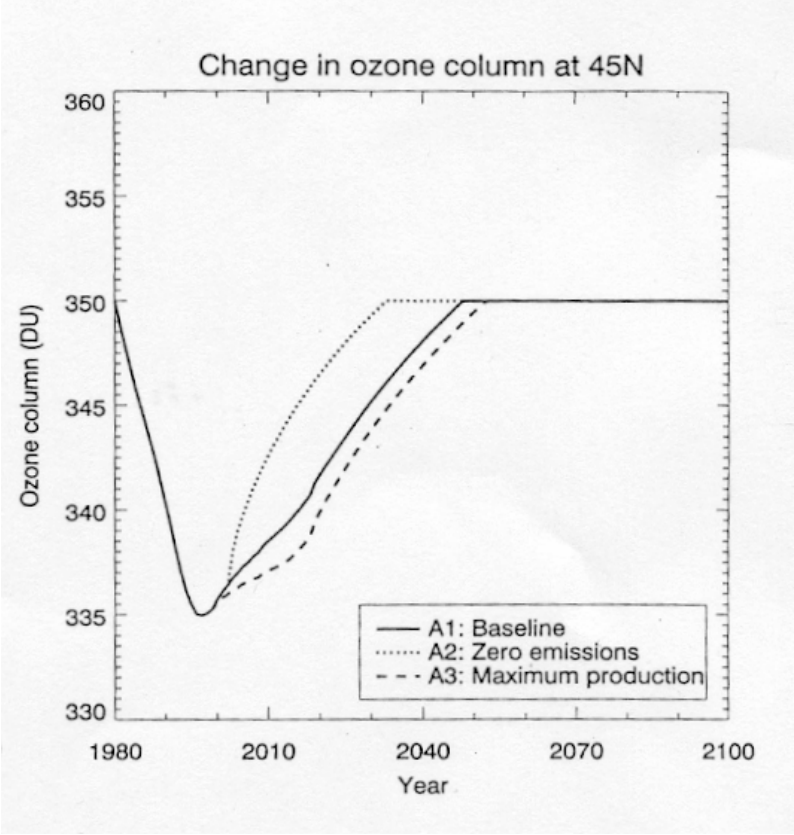

Source: World Meteorological Organization 1999.

As illustrated by Figures D-1 and D-2, the AHEF and WMO projections agree that year of minimum stratospheric ozone concentration would be in the late 1990s to early 2000s. This finding agrees with the U.S. Global Change Research Program estimate, which projected that concentrations of ODS in the atmosphere would peak before the year 2000 (USGCRP 1998). Figure D- 1 and Figure D- 2 also show that AHEF and the 1999 WMO assessment are in agreement regarding the speed of ozone recovery, both projecting full recovery around 2045.

The major difference between the two models is the absolute minimum predicted ozone concentration. The AHEF predicts that the minimum value reaches approximately 320 Dobson Units (DU) for the 40-50 degree latitude band, while WMO estimates indicate an absolute minimum of approximately 335 DU at 45 degrees of latitude.

This primary reason for this difference is believed to be variations between the models' estimated equivalent effective stratospheric chlorine (EESC), particularly in the earlier years modeled (Figure D- 3). Factors that influence EESC estimates include the estimated ODS emissions, the degree of dissociation of each ODS species, and the rate of transport to the stratosphere. In the estimation of ODS emissions alone, for example, there exists significant opportunity for variation. For example, the AHEF estimates annual ODS emissions by generating annual emission profiles for each ODS end use, by chemical, for all ODS-consuming countries. This is performed through a complex, bottom-up model that estimates the stock and growth rates of all types of ODS-containing equipment, as well as their average lifetimes, annual leak rates, service rates, and disposal rates. Conversely, WMO estimates are based on measured values of EESC extrapolated into the future by compound. WMO projections are based on emission functions acting on the banks of material yet-to-be emitted from end-use categories with similar emissions patterns. The WMO assumes that the banks by end-use categories are replenished by sales, where sales are based on future production and consumption estimates. Thus, given the difference in modeling

approaches, and the uncertainty associated with the assumptions used by both approaches, variation across models is to be expected.

Figure D- 3. Comparison of AHEF and WMO (1999) EESC Estimates

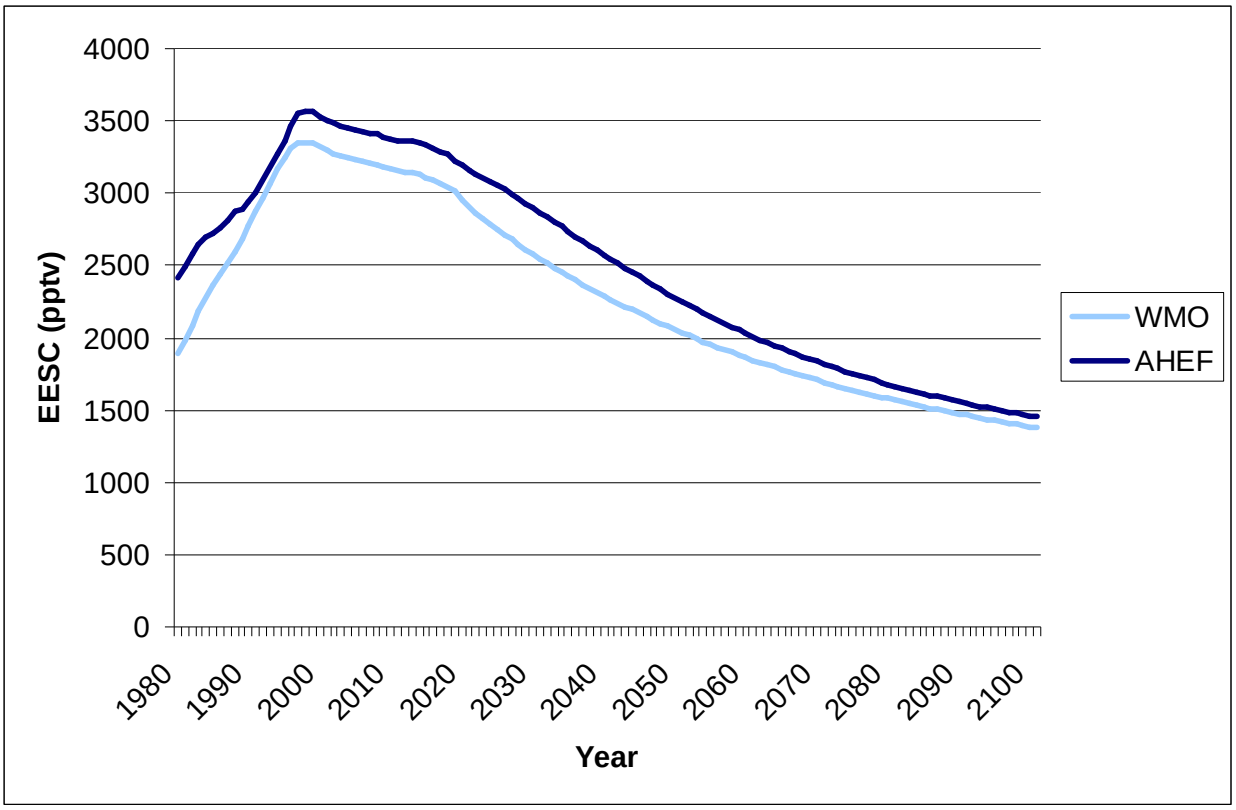

However, in a peer reviewed report titled *Human Health Effects of Ozone Depletion from Stratospheric Aircraft* (2001), it was found that the difference between the AHEF and WMO model predictions of the maximum ozone depletion is well within the acceptable range of variation. This report, co-authored by NASA and EPA, compared and evaluated six different atmospheric models capable of projecting ozone concentrations. These six models generated ozone estimates that varied by a factor of five, as presented in Figure D- 4. Indeed, the estimated ozone levels of the six models had an uncertainty range of +0.9% to -2.1% around the central value of -0.6% in 2050. If this range is taken to define the uncertainty arising wholly from variability within the models, the AHEF and WMO predictions can be considered to be statistically similar.

Similarly, the 2003 WMO Scientific Assessment supports the assertion that the AHEF and WMO column ozone estimates are within an acceptable range of variation. As shown in Figure D- 5, the differences in column ozone predictions from different computer models used for the GHG scenario MA2[29] in the 2003 WMO report are roughly the same order of magnitude as those between the AHEF and WMO (1999) estimates.

Thus, the general agreement of the decline and recovery estimates, the shapes of the curves, and the use of identical data sets indicate that the similarities between the AHEF and WMO approaches outweigh

[29] WMO GHG scenario MA2 is taken from IPCC (2001) scenario A2. In this scenario, by 2050, atmospheric levels of CO_2 concentrations reach 532 ppmv, CH_4 concentrations reach 2,562 ppbv, and N_2O concentrations reach 373 ppbv.

the differences—which are themselves within an acceptable range of variation for atmospheric models of this kind.

Figure D- 4. Sensitivity and Uncertainty Envelopes Used in HSCT Analysis

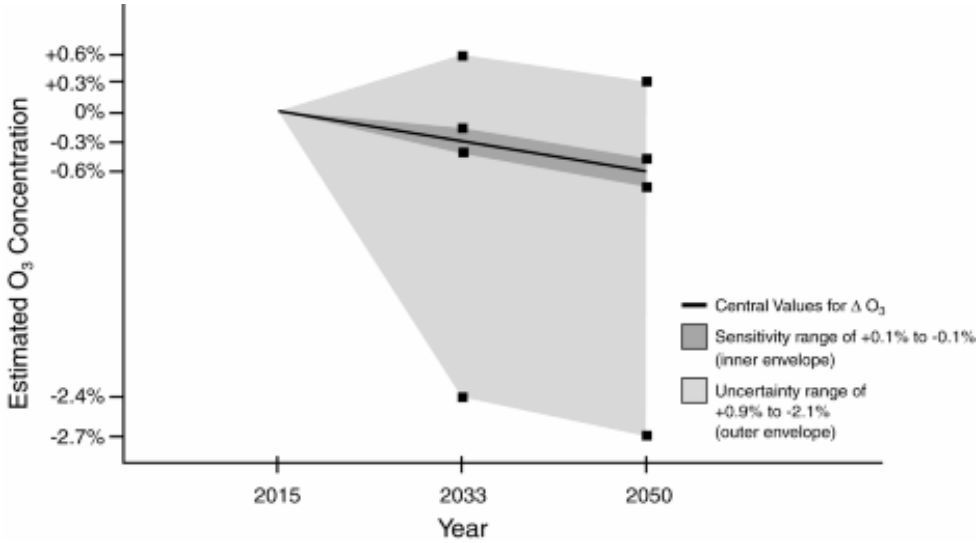

Source: NASA/EPA 2001.

Figure D- 5. Variations in Column Ozone Projections from Different Atmospheric Models*

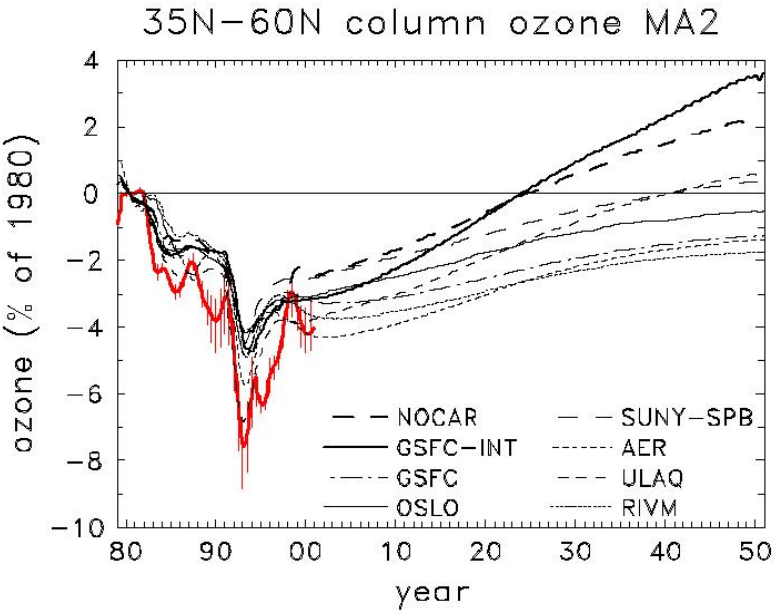

*Predicted future evolution of column ozone is shown for WMO GHG scenario MA2 from eight 2-D models. The plot also includes observations of past trends (red lines) prior to 2000.
Source: WMO 2003.

Appendix E: Modeling Cataract Incidence

In previous versions of the AHEF, cataract incidence attributable to increased UV exposure has been modeled. This health effect was handled in much the same way as the other health effects, with baseline cataract incidence rates estimated using cataract incidence data reported in U.S. EPA (1987). These cataract incidence rates were derived from prevalence data presented in Hiller et al. (1983), which in turn were based on a subset of the National Health and Nutrition Examination Study (NHANES) data.[30] The subset consisted of 2,225 subjects between the ages of 45 and 74 at 35 different locations across the United States. Incidence rates were stratified by location, based on the three latitudinal bands (i.e., 20°N to 30°N, 30°N to 40°N, and 40°N to 50°N). Future cataract incidence for particular ozone depletion scenarios was estimated in the same way that skin cancer incidence and mortality are computed—i.e., by multiplying incidence rates by population projections by age, sex, and latitude band. Table E-1 reports baseline cataract incidence rates developed by age group.

Table E-1. Baseline Cataract Incidence Rates by Age Category (Used in Previous Versions of the AHEF)

Age Category	Incidence Rates Assuming 1979-1980 Ozone Levels (per 100,000)
55-64	450
65-70	1,350
75-84	2,750
85+	0[a]

[a] Because the prevalence (existing cases) of cataract in the 85+ group is the same for the age 75-84 category, incidence (new cases) for the 85+ group is assumed to be zero

In deriving the dose-response relationship for cataracts, BAFs were developed based on a study conducted by Taylor et al. (1988), which looked at exposure histories for a sample population in a single location (i.e., the Chesapeake Bay in Maryland). The resulting BAF was 0.225 for males and females.

However, while the Taylor study was able to show that high cumulative levels of UV-B exposure significantly increased the risk of cortical cataract in a controlled population, the study was not appropriate for deriving a BAF for cataract incidence because it is based on only one location in the United States, as opposed to latitudinal averages, like the other health effects that are modeled.

Thus, a recent effort was made to revise the BAFs for cataract incidence based on available action spectra and the latest data on U.S. cataract incidence. All available action spectra were reviewed, including:

- **Erythema (1987):** This is an action spectrum derived on the basis of erythema (sunburn) induction in human volunteers (McKinlay and Diffey 1987). This action spectrum was used to predict cataract incidence in the original AHEF developed in the 1980s.

- **Merriam *et al*. (2000)**: This action spectrum was generated based on induction of cataracts in rats. The action spectrum spans the UV spectrum from 295 nm to 315 nm, covering only the UV-B spectrum.

- **Pitts *et al*. (1977)**: This action spectrum was generated as an average of action spectra values based on the ocular effects of UV radiation on the corneas of humans, primates, and rabbits, as well as human conjunctiva and rabbit uveitis.

[30] NHANES analyzed all three forms of cataract, but only cortical cataract is clearly associated with UV exposure, while much uncertainty exists with regard to the role of UV-B and the other forms of cataract. Thus, in terms of using the NHANES data in developing baseline cataract incidence in the AHEF, cataract incidence may be overestimated.

- **Oriowo *et al*. (2001)**: This action spectrum was generated based on induction of cataracts in pigs using whole cultured lenses. The action spectrum spans from 270 nm to 370 nm, thus extending into the UV-A spectrum.

Figure E-1 graphically presents the identified action spectra for cataract induction. As can be seen, these action spectra show strong sensitivity at UV-B wavelengths (hence the sensitivity of cataracts to ozone changes), and much less to UV-A (which is not significantly affected by ozone changes).

Figure E-1. Action Spectra Considered to Model Cataracts

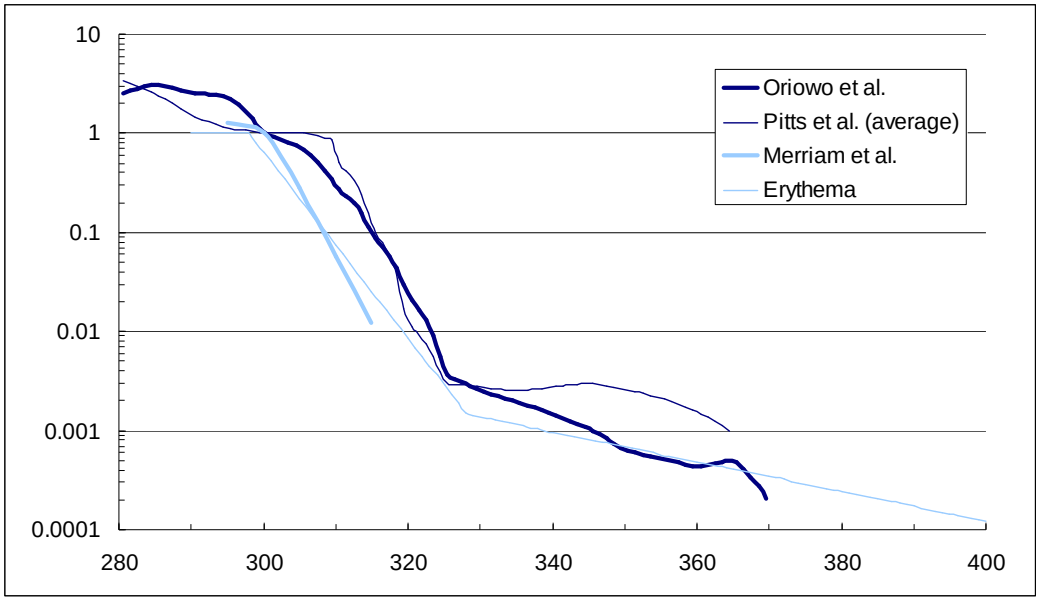

Note: The Response (plotted on the Y-axis) is a log scale. At the normalizing wavelength, every 1 percent change in UV radiation causes a 1 percent change in the health effect.

While the shapes of these four action spectra are very similar, the Oriowo action spectrum was selected for use in the AHEF because it is believed to be the most appropriate for modeling cataracts in humans due to the following:

- The Oriowo action spectrum is based on the induction of cataracts in pigs, which is more appropriate for modeling cataract incidence than the Erythema action spectrum, which is based on the induction of erythema (sunburn) in humans.
- Of all action spectra developed based on the induction of cataracts in animals, the pig lens is believed to be most physiologically similar to the human eye—as opposed to the rat or rabbit lenses used in the Merriam et al. (2000) and Pitts et al. (1977) action spectra.
- The Oriowo action spectrum is not an averaged action spectrum, like the Pitts et al. action spectrum, and is therefore less likely to be complicated by inconsistencies arising from attempts to combine data from different studies.
- The Oriowo action spectrum appeared in a peer-reviewed journal (*Investigative Ophthalmology & Visual Science*), and is the most recently developed action spectrum of the three action spectra considered.

Then, in an attempt to calculate the BAFs, estimated average UV exposures by state were correlated with cataract incidence data reported by the National Eye Institute/Prevent Blindness America (NEI/PBA) (2002)—the most recent and comprehensive cataract incidence data available—of populations aged 40 and above. The results of this analysis suggested that cataract incidence is directly correlated with age. However, it was not possible to develop a good correlation between the intensity of UV exposure and cataract incidence. Therefore, it was not possible to predict changes in cataract incidence based on

changes in ODS emission scenarios with a high level of confidence. Consequently, this health effect was omitted from the AHEF.

The lack of correlation between UV radiation intensity and cataract incidence may be due to confounding factors that prevent accurate assessment of UV exposure within the population. Such confounding factors include changes in behavior (i.e., wearing protective sunglasses or actively avoiding the sun) or changes in demographics (i.e., travel or relocation). For example, the actual cumulative UV exposure of someone who has moved to a new state may not be well represented by the averaged UV radiation values in their new location.

Despite this, it may be possible to discern differences in population-based effects if state UV radiation intensity values become available in a more disaggregated form. If additional research or data become available, this health effect can be reconsidered for development of a dose-response relationship and inclusion in the AHEF.